MORPHOLOGICAL INVESTIGATIONS INTO THE DEVELOPMENT OF THE MAMMALIAN CORNEAL ENDOTHELIUM USING THE MOUSE MODEL

Thandiswa Mgwebi

Thesis presented for the degree of
Doctor of Philosophy (Medicine) in the
Department of Human Biology
University of Cape Town

May 2004

I, Thandiswa Mgwebi, hereby declare that the work on which this thesis is based is my original work (except where acknowledgements indicate otherwise) and that neither the whole work nor any part of it has been, is being, or is to be submitted for another degree in this or any other University. I empower the University to reproduce for the purpose of research either the whole or any portion of the contents in any manner whatsoever.

May 2004

I greatly acknowledge:

Professor Sue Kidson, my mentor, for support, undying patience and the passion for science she has instilled in me. Most of all, for the encouragement through the worst of times and for helping me understand that we learn much more from failure than we do from success.

Colleagues in the Kidson lab: Hugh Napier[chicken] , Natalya Nikitina and Paula Sommer for many fruitful discussions and for providing support and friendship.

Toni Wiggins: for support, friendship and much more. Special thanks also goes to Miranda Waldon, Mohamed Jaffer, Liz van der Merwe and Sharon Marshall for technical assistance. Thanks to the Ray Fortuin for the clean mugs and readily available boiling water every morning.

Dr Anthony Graham, for allowing me to spend two months in his laboratory at King's College, London. I would like to thank him and the Company of Biologists (Pty. Ltd) for funding this visit. Special thanks goes to Dr Maria Balda of University College, London, for taking interest in my research life ever since we met.

My family and friends: for encouragement and support.

The Medical Research Council (MRC) and the University of Cape Town for providing financial support throughout the course of this study, and particularly, the MRC for support of my overseas visits.

Dedication

To my late mother, Lettie Ntuthu Tshontoni Mgwebi

Table of Contents

List of figures

Glossary of terms

Alx4 = Aristaless 4
ARA = Axenfeld-Rieger anomaly
ATP = adenosine tri-phosphate
BMP = Bone morphogenetic protein
BSA = Bovine serum albumin
CE = corneal endothelium
CHED = congenital hereditary dystrophy
CYP1B1 = cytochrome P450, family 1, subfamily B, polypeptide 1
DAPI = diamidino-2-phenylidole
ECM = Extracellular matrix
EGF = Epidermal Growth factor
EMT = Epithelial-mesenchymal transformation
ER = Endoplasmic reticulum
Eya1 = Eyes absent 1
Foxc1 = Forkhead BoxC1 transcription factor
GAGs = Gylcoaminoglycans
Gdnf1 = Growth derived neutrotrophic factor 1
GFP = Green fluorescent protein
GLC1A = trabecular meshwork induced glucocorticoid response gene
IRD1 = irodogoniodysgenesis type 1
ISH = in situ hybridisation
JAM = Junctional adhesion molecules
KS = keratan sulphate
MAG-1 = membrane-associated guanylate kinase inverted
MDCK = Martin Darby canine kidney cells
Msx2 = msh (Drosophila) homeobox homolog 2
N-cadherin= neural-cadherin
PAR =partitioning defective
Pax6 = paired homeobox 6
PBS = Phosphate buffered saline
Pdgfra = Platelet derived growth factor receptor alpha
Pitx2 = paired-like homeodomain transcription factor 2
PKC = protein kinase C
PP2A = Protein phosphatase 2A
PTEN = Phosphatase and tensin homologue
SEM = Scanning electron microscopy
TER = trans-electrical resistance
TG = thapsigargin
Tgfb2 = transforming growth factor-2
ZO-1 = zonula occludens-1
ZONAB = zonula occludens-1 nucleic acid binding protein

Abstract

Morphological investigations into the development of the mammalian corneal endothelium using the mouse model

The corneal endothelium (CE), a mesenchyme-derived tissue, is a monolayer of squamous cells on the inner corneal surface. In *Foxc1*$^{-/-}$ mice, the CE fails to form. The understanding of the cause of this defect has implications for the study of human eye disorders that are related to FOXC1 mutations.

To understand the basis of CE defects in *Foxc1*$^{-/-}$ mice, an analysis of normal CE development was performed using scanning electron microscopy. Results showed that in normal mice the transformation from mesenchyme to endothelium was initiated at embryonic day (E) 12.5 and was characterised by a change from stellate to cobblestone shape and the formation of junctions. In *Foxc1*$^{-/-}$ mice, the process was initiated but a cobblestone shape not attained. The expression of adherens (N-cadherin) and tight junction (ZO-1) proteins was investigated by immunoflouresence microscopy. In the normal embryo, the expression of N-cadherin was initially in cytoplasmic vesicles and later at the cell membranes. ZO-1 was first detected at the cell peripheries at E13.5. In *Foxc1*$^{-/-}$ mice, N-cadherin peripheral bands failed to form. ZO-1 was not expressed. These results suggest that the failure to form a monolayered CE in *Foxc1* mice is due to incomplete mesenchyme-endothelial conversion. Junction formation was further investigated *in vitro*. N-cadherin was cytoplasmic in pre-confluent cells and at cell edges in confluent cells. ZO-1 was not detected. These results suggest that *in vitro*, these cells are either unable to form tight junctions or the culture medium does not contain the appropriate signalling molecules.

In *Foxc1* mutants, the corneal stroma is disorganised. To understand the basis of this disorganisation, the expression of *keratocan*, a corneal proteoglycan, was compared between normal and mutant corneas using *in situ* hybridisation (ISH). Transcripts were detected in both, suggesting that *Foxc1* is not upstream of a molecular cascade involving *keratocan*. In order to begin to identify signalling molecules regulating mesenchyme-endothelium conversion, the expression of transforming growth factor-beta-2 (*tgfβ2*) and transforming growth factor receptor–II were investigated by ISH. Transcripts appeared later than the time of CE differentiation. These results suggest that *tgfβ2* is likely not part of a signalling mechanism mediating mesenchyme-endothelium conversion.

Chapter One : INTRODUCTION

The anterior segment of the eye is a highly organised structure made up of the cornea, the anterior part of the lens, the iris and the trabecular meshwork. Aqueous humor is produced by the ciliary body in the posterior chamber and flows between the iris and the lens into the anterior chamber. It flows out of the eye through the trabecular meshwork, into the Schlemm's canal and via drainage channels into the venous system. Disruption in the rate of aqueous humor outflow as a consequence of abnormalities in structure or function of the trabecular meshwork often leads to an increase in intra-ocular pressure, causing degeneration of the optic nerve and ultimately glaucoma.

Severe defects in vision are also associated with abnormalities of the cornea. In humans several inherited disorders of the cornea occur. Glaucoma is one of the conditions, symptoms of which often overlap with others, such as congenital hereditary endothelial dystrophy (CHED). Glaucoma is one of the major causes of blindness worldwide. It is a progressive disease characterized by an increase in intra-ocular pressure that results in retinal ganglion cell death and optic nerve degeneration and leads to partial vision loss and eventually irreversible blindness. It is also often associated with corneal opacity and other anterior segment abnormalities. Classification of glaucoma is based on its aetiology (primary or secondary), anatomy of the anterior segment (open angle, closed angle or narrow angle) and time of onset (juvenile or adult) (Sarfarazi, 1997). Glaucomas and malformations of the anterior segment have been associated with defects or mutations in a number of genes including *Lmx1b*, CYP1B1, FOXC1, Pax6, Pitx3, Pitx2 and GLC1A (Lines et al., 2002), to mention a few. Despite the advances in identifying genes responsible for glaucoma, the cellular and molecular bases of various forms of glaucoma remain poorly understood. Investigations into the pathophysiology of glaucoma could lead to earlier and more precise diagnosis and ultimately specific and effective therapy. The availability of mouse models for ocular abnormalities and glaucoma provides an ideal opportunity to gain insights into the multifactorial nature of glaucoma.

1.1. The cornea

The cornea is made up of three layers, the outer epithelium, the intermediate stroma and the inner endothelium. It serves to protect the intra-ocular components and to refract light. In order to accomplish these functions, the cornea must be strong and able to maintain its transparency. Most of the cornea's mechanical strength is provided by the intermediate stroma

and the avascular nature of the central cornea enables it to transmit light. The following description of the structure of the vertebrate cornea is largely based on human, mouse and avian studies.

1.1.1. The corneal epithelium

The outer layer of the cornea is a non-keratinised, stratified squamous epithelium made up of four to six layers of cells. By morphological criteria, the corneal epithelium is divided into three layers, the two-layered superficial cell layer, the intermediate wing cell layer and the deep or basal cell layer. Superficial cells are polygonal in shape and connected to each other by extensive junctional complexes. Well-developed junctional complexes regulate the movement of substances from the tear film into the intercellular spaces of the epithelium and are thus responsible for maintaining the integrity of the epithelial paracellular barrier. Prominent microvillae extend from the outer surface of the superficial cells. The presence of these surface specialisations aids in maintaining the tear film and the barrier that separates the extracellular space of the cornea from the tears. Wing cells in the middle layer of the epithelium are joined together by desmosomes and gap junctions. On the inner surface of the epithelium are the columnar basal cells that are joined together by tight and gap junctions. Hemidesmosomes connect the basal cells to the underlying basal lamina, a structure that serves to prevent the ingrowth of epithelial cells into the Bowman's layer, an acellular matrix of the cornea which lies between the epithelial basal lamina and the corneal stroma (Kaufman and Alm, 2003; Leibowitz and Waring III, 1998).

1.1.2. The corneal stroma

The stroma constitutes about 90% of the cornea. It is made up of fibroblast-like keratocytes in a lamellated collagenous extracellular matrix. The stromal keratocytes arranged between the collagen lamellae secrete collagens and other extracellular matrix components of the stroma. In humans, the stroma contains at least three different types of fibrillar collagens, type I, V and VI. Type I collagen fibrils are of uniform diameter and form stacked lamellae. The exact roles of type V are not clear. Several lines of evidence suggest that type V collagen regulates fibril diameter: Firstly, in naturally occurring type V collagen mutations in humans and in mice with a genetically constructed mutation in the α2 (V) chain of collagen type V, there are alterations in fibril diameter. Homozygous α2 (V) mutant mice have severe spinal deformities, skin fragility and disorganised corneal stroma (Andrikopoulos et al., 1995). Secondly, *in vitro* fibrillogenesis studies in which different proportions of type V and type I collagen were mixed

showed that high proportions of collagen type V favour the formation of small-diameter fibrils (Linsenmayer et al., 1998). Thirdly, the expression of dominant negative forms of type V collagen in corneal fibroblasts resulted in an increase in collagen fibril diameter to a larger size. This diameter is reminiscent of ones with a low concentration of type V collagen (Marchant et al., 1996).

Corneal clarity is dependent on the correct spacing and layering of the collagen fibres in the stromal layer. This orderly arrangement is achieved by the interaction of the collagen fibres with proteoglycans which are the major constituents of the extensive stromal matrix of the cornea. The proteoglycan core proteins are always associated with identifying side chains, the glycosaminoglycans (GAGs). The major proteoglycans of the corneal stroma are decorin, lumican, mimecan, and keratocan. Decorin contains chondroitin-dermatan sulfate side chains (CS/DS) and is thus termed dermatan sulfate proteoglycan. Lumican and keratocan contain keratan sulfate (KS) side chains, the most abundant GAGS in the corneal stroma. Lumican is a major component of not only the cornea, but also of dermal and muscle connective tissues, whereas keratocan is a stromal specific proteoglycan of the mature cornea (Dunlevy et al., 2000; Liu et al., 1998). In order for proteoglycans to maintain corneal transparency, the associated GAGs must remain relatively dehydrated. This is a function of the corneal endothelium.

1.1.3.The corneal endothelium

In humans, the endothelial cells form a monolayer of polygonal (of five to seven sides) but predominantly hexagonal cells on the inner surface of the cornea. These cells are connected to each other at their lateral surfaces by means of desmosomes and junctional complexes that are made up of gap junctions, adherens and tight junctions. Extensive interdigitations on the lateral cell membranes result in lengthy junctional barriers that often exceed the actual thickness of the individual cells. Mature corneal endothelial cells rest on a basement membrane, the Descemet's membrane. In humans, the endothelial cells begin to lay down their basement membrane at about four months of gestation. At birth, the human corneal endothelium has a density of about 7,500 cell/mm^2. This density declines with aging because the endothelial cells are unable to divide and replace aging, diseased or injured cells (see (Tuft and Coster, 1990)). Should the endothelial layer be injured or damaged, the only means of repair is through cell enlargement or spreading which restores the endothelial monolayer. This results in alteration of cell shape of the surviving cells and thus an increase in cell size. Excessive loss of cells may result in ineffective barrier function, which may lead to corneal

oedema, decreased corneal clarity and loss of visual acuity. In such conditions, normal vision can only be restored by corneal transplantation.

The major roles of the corneal endothelium are to maintain corneal transparency by regulating corneal hydration and to allow the passage of nutrients from the aqueous humour into the cornea. The mechanism by which the corneal endothelium maintains corneal hydration is termed the pump-leak mechanism. This has been so named because of the action of the Na^+/K^+-ATPase and bicarbonate-dependent Mg^{2+} ATPase pumps, located on the lateral plasma membranes of endothelial cells (the "pump") and the leaky endothelial barrier created by the discontinuous tight junctions at the periphery of the cells (the "leak"). Corneal thickness is thus maintained by the balance between the rate of passive fluid flow into the cornea and the rate of pumping of excess fluid out of the cornea. The pumps remove Na^+ from the stroma to the aqueous humor creating an osmotic gradient so that the movement of water across the endothelium is passive. The barrier allows the leakage of water from the aqueous humor into the stroma (Joyce, 2003).

1.2. Corneal development and differentiation

The eye structures are derived from four embryonic tissues, the ectoderm, mesoderm, neural tube and neural crest (Figure 1-1). Eye development begins with the formation of the optic placode in the anterior neural plate region. This placode evaginates at the level of the forebrain during neural folding and becomes the optic vesicle (Figure 1-2A-B). The optic vesicle contacts the overlying ectoderm and induces it to become the lens tissue. The induced lens tissue thickens to form the lens placode. The lens placode invaginates and at the same time, the medial part of the optic vesicles forms the optic stalk while the lateral region pushes in to form the bi-layered optic cup (Figure 2D – E). The invaginating lens placode detaches from the ectoderm to form the lens vesicle (Figure 2E – F). Soon after lens detachment, the cornea begins to form, resulting in three distinctive layers, the epithelium, stroma and endothelium. Most of the studies on corneal development have been done on chicks (Hay and Revel, 1969; Nelson and Revel, 1975) and there is some descriptive work on mouse (Kidson et al., 1999; Pei and Rhodin, 1970) and human (Murphy et al., 1984; Wulle and Lerche, 1969).

In the chick, the primary corneal stroma is laid down by the corneal epithelium. This primary corneal stroma is acellular and is made up of collagen fibrils and glycoaminoglycans. The next stage is the invasion of the space between the corneal epithelium and the lens by mesenchyme cells, which occurs in two waves. The first wave of mesenchyme ingression appears to be

initially associated with the vascular mesenchyme at the lip of the optic cup. These cells change shape and become flattened before migrating along the lens/stromal interface. This first wave of cells constitutes the endothelium of the cornea. The mesenchymal cells of the second wave invade the primary stroma and become the keratocytes, which will form the secondary stroma of the adult eye.

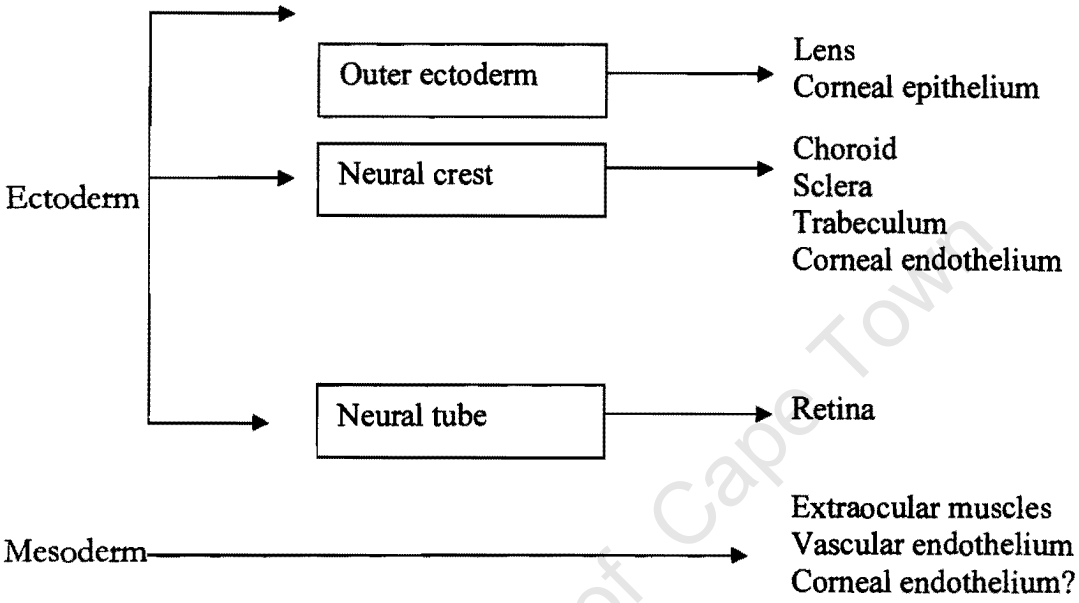

Figure 1-1. A diagrammatic representation of the derivation of eye structures from embryonic tissues.

In contrast to the two waves of mesenchymal invasion in the chick cornea, it has recently been shown that in the mouse, only a single influx of mesenchymal cells invades the space between corneal epithelium and the lens to form the corneal stroma and endothelium (Kidson et al., 1999). These cells begin to occupy the space between the lens and the corneal epithelium at E11.5. Only the innermost layer of cells of corneal mesenchyme transforms into an endothelium, but the mechanisms of this transformation are not known. This question forms the basis of the first part of the present study.

In both chick and mouse, the differentiation of mesenchyme into corneal endothelium appears to be dependent on signalling from the nearby anterior lens epithelium. Experiments conducted in the 60's provided evidence that the lens is required for normal development of the cornea. For example, when an ectopic lens was transplanted into the wall of the optic cup at the level of the posterior chamber, structures resembling a cornea and an anterior chamber formed adjacent to the implant (Genis-Galvez, 1966). When the lens was removed, rotated

180°C or re-inserted into the eye, the lenses formed a new epithelial layer over the posterior surface. Cells adjacent to the newly formed epithelial layer transformed into an endothelium, strongly suggesting that the lens is producing signals to which the cranial mesenchyme cells respond (Genis-Galvez, 1966).

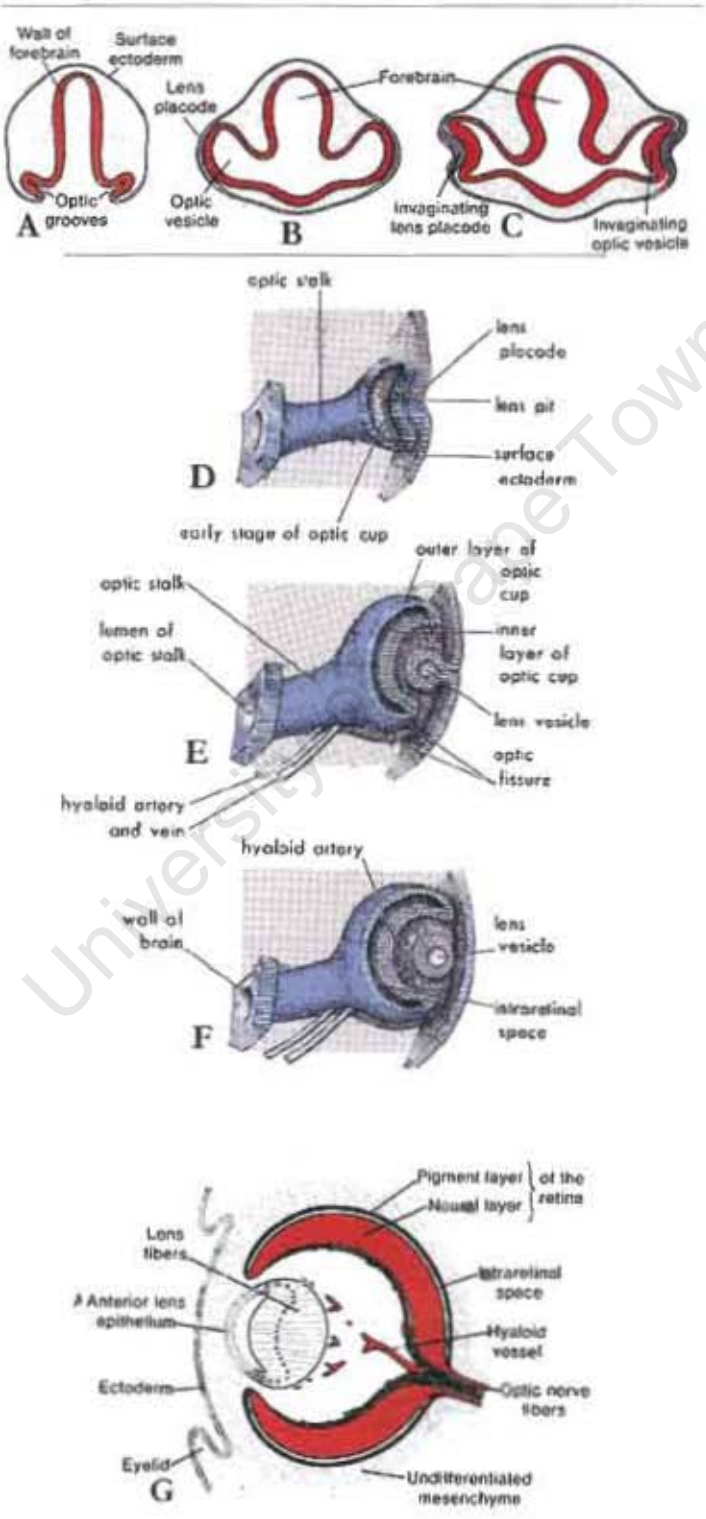

Figure 1-2. Representation of eye development (modified from www.vision.ac.za).

The conclusions from these results were based solely on histological analysis, but recent studies by Beebe and Coats (2000) provide support for these theories. They showed that implantation of a 90°C rotated lens results in the formation of the anterior chamber and the corneal endothelium adjacent to the lens epithelium. The formation of the corneal endothelium was confirmed by expression of N-cadherin, a corneal endothelial marker. N-cadherin was not detected in mesenchyme cells after the lens was removed (Beebe and Coats, 2000). Taken together, these studies suggest that a factor (s) produced by the lens epithelium induces the differentiation of adjacent competent mesenchyme cells into corneal endothelium, although the identity of the signalling molecule (s) from the anterior lens surface remains to be determined.

1.2.1. Signalling molecules implicated in the differentiation of the corneal endothelium

Amongst the candidate molecules strongly implicated in corneal endothelial differentiation are transforming growth factor beta-2 (TGFβ2), platelet derived growth factor receptor-α (pdgfrα) and transforming growth factor alpha (TGFα) or epidermal growth factor (EGF). TGFβ2 is a member of the highly conserved TGFβ family consisting of more than 30 ligands. Members of the family are known to regulate several aspects of cell behaviour including migration, differentiation and cell growth. They exert their biological activity by binding and activating type-I and type-II receptors (TGFβRI and TGFβRII), which are transmembrane serine-threonine kinases. Activity begins with binding of the ligand to TGFβRII, which induces dimerization of the receptor with TGFβRI, resulting in phosphorylation and activation of TGFβRI and subsequent activation of downstream pathways (de Iongh et al., 2001; Dunker and Krieglstein, 2000; Padgett, 1999). There are several lines of evidence implicating TGFβ2 in corneal endothelial development and in maintenance of the adult corneal endothelium. Its role in development has been shown by failure of corneal endothelium development in mice in which the gene has been knocked out (Sanford et al., 1997). In addition to the absence of a corneal endothelium, homozygous TGFβ2-null mutant mice have thin corneal stromas with fewer keratocytes due to diminished accumulation of the extracellular matrix components such as collagen type I, lumican and keratocan (Saika et al., 2001).

The expression of TGFβ receptor types I, II and III in the adult human corneal endothelial cells (Joyce and Zieske, 1997; Srinivasan et al., 1998) and in neonatal and adult rat corneal endothelial cells (Joyce et al., 2002) suggests a physiological role of TGFβ2 in either maintenance of the adult corneal endothelial phenotype or function. TGFβ2 mRNA is found in the ciliary and iris epithelia as well as in the equatorial lens in postnatal rat eyes (Gordon-

Thomson et al., 1998). However, the expression of TGFβ2 mRNA in the iris and ciliary epithelium and of the receptors in the corneal endothelium during early corneal differentiation has not been shown. In addition, the expression of TGFβ2 mRNA in the anterior lens surface at the time of corneal endothelial differentiation has not been reported.

Mouse mutants in which the platelet derived growth factor receptor-α (*Pdgfra*) gene has been knocked out (the *Patch* mutants) display abnormalities in the anterior segment of the eye. In mutant embryos, defects in neural crest-derived tissues involving the frontonasal processes and the aortic arch are observed. Using *in situ* hybridisation, it has been shown that in the mouse embryo, the *Pdgfra* is expressed in the neural crest and mesoderm-derived mesenchyme of the head at E11.5 (Schatteman et al., 1992). In fact, beginning from E9.5 – E11.5, the *Pdgfra* mRNA is found in the cranial region, the branchial arches, mesenchyme surrounding the tooth epithelium and the developing cornea - regions of neural crest derivation (Morrison-Graham et al., 1992). The developmental abnormalities in neural crest derived tissues observed in the absence of a functional *Pdgfra* strongly suggest a direct role of this gene in regulating development of crest-derived tissues. Such tissues involve the cornea of the eye. Early in development at E13.0, homozygous mutant embryos show a reduction in the amount of peri-ocular mesenchyme contributing to the cornea, and as a result, by E16.0, the thickness of the cornea becomes half that of normal corneas (Morrison-Graham et al., 1992). The presence of a functional corneal endothelium however, has not been investigated. In another set of experiments, misexpression of the *Pdgfra* in the lens of transgenic mice caused a thicker cornea (Reneker and Overbeek, 1996). Taken together, these abnormalities in the absence of a fully functional *Pdgfra* suggest a role of this gene in corneal regulation.

Corneal abnormalities in transgenic mice that express transforming growth factor alpha (TGFα) or epidermal growth factor under the lens αA-crystallin promoter suggests a role of this gene in corneal endothelium regulation (Reneker et al., 2000). In these mice, the anterior segment structures developed abnormally and the cornea was opaque. The iris had adhered to the posterior surface of the cornea and the ciliary body was reduced into a rudimentary structure. In addition, the differentiation of the corneal mesenchyme into an endothelium was impaired. Histological analysis showed that the corneal endothelium was partially formed and appeared intact only at localised regions. In addition, the corneal epithelium was reduced to a bilayer of cells with no basement membrane. Ectopic expression of the TGFα in the lens also resulted in accumulation of mesenchymal cells in the anterior lens region, resulting in a thicker corneal stroma. This phenotype and the expression of the EGF-receptor in migrating peri-ocular mesenchyme cells, as shown by *in situ* hybridisation, supports the possibility that the

TGF ligand acts as a chemoattractant for peri-ocular mesenchyme cells. The defects in the corneal epithelium and stroma correlated with the absence of the corneal endothelium because these abnormalities were only associated with regions where the corneal endothelium was absent. It was in such regions that the lens and the iris adhered to the cornea. Results from these studies suggest that the development of the corneal endothelium influences, either directly or indirectly the differentiation of the corneal epithelium and the stroma. Furthermore, they suggest that the formation of the corneal endothelium is a necessary prerequisite for the separation of the lens from the cornea. This question has not been rigorously investigated in the mouse embryo and is not part of the aims and questions addressed in the present study.

The differentiation of the corneal endothelium appears to be also regulated by a host of transcription factors that are expressed in the periocular mesenchyme and the presumptive corneal endothelial cells. These include the bicoid-related homeodomain transcription factor *Pitx2*, the LIM domain transcription factor *Lmx1b*, and the forkhead transcription factor, *Foxc1*. *Pitx2* is expressed in the periocular mesenchyme at E10.5 (Semina et al., 1996), in the extraocular muscles at E12.5 (Kitamura et al., 1999) and in the developing corneal stroma and endothelium at E14.5 and in the presumptive iris, trabecular meshwork and extraocular muscles at E15.5 (Kidson et al., 1999; Kitamura et al., 1999). In *Pitx2*$^{-/-}$ embryos, the stroma is five to ten fold thicker than normal, the anterior chamber fails to form and the lens remains attached to the cornea (Kitamura et al., 1999). Although the presence or absence of corneal endothelium in these mice has not been investigated, the failure of the lens to separate from the cornea suggests that a corneal endothelium does not develop.

The expression pattern of *Pitx2* is not affected in *Lmx1b* mutants except for the absence of mRNA in the presumptive iris stroma as these cell are missing (Pressman et al., 2000). In the wildtype embryo, *Lmx1b* is expressed in the peri-ocular mesenchyme in the eye beginning at E10.5. The expression domain expands at E11.5 to the optic cup and the presumptive corneal stroma and endothelium. By P0, the expression of *Lmx1b* is detected in the developing iris stroma and ciliary body, the corneal endothelium, corneal stroma and the trabecular meshwork. The expression pattern of *Lmx1b* suggests that it may be required for early corneal specification and also during postnatal development. *Lmx1b*$^{-/-}$ mice are characterised by absence of ciliary body folds and iris and ciliary body hypoplasia. Beginning from E15.5, the corneal stroma becomes less compact, contains blood vessels, and compared to wildtype littermates, the anterior chamber is reduced in depth (Pressman et al., 2000).
In the present study, *Foxc1* mutant mice were utilised to investigate the development of the corneal endothelium and to map the precise timing of morphological events associated with

conversion of mesenchyme to endothelium. *Foxc1* belongs to a group of forkhead/winged helix proteins, a large family of transcription factors that share an evolutionary conserved DNA-binding domain. Members of this family play significant roles in regulating tissue-specific gene expression and embryonic patterning from far diverse as *Drosophila*, *Xenopus*, zebrafish and mouse. The *Drosophila* forkhead genes, *sloppy paired* -1 and –2 are involved in the process of segmentation along the anterior-posterior axis. The *Pintallavis* forkhead gene in *Xenopus* is also involved in the anterior-posterior and dosonventral patterning of the neural tube (Hiemisch et al., 1998; Sasaki and Hogan, 1993). The zebrafish forkhead genes *Foxc1a* and *Foxc1b* play important roles in somite formation by regulating the expression of genes such as *paraxis* and the anterior-posterior patterning of early somite primordia (Topczewska et al., 2001). In the mouse, the winged helix family members *Foxc1* and *Foxc2* are expressed in embryonic mesoderm and in neural-crest derived head mesenchyme. These genes have been associated with somite patterning and differentiation and also appear to regulate kidney, heart and eye development (Hiemisch et al., 1998; Kidson et al., 1999; Kume et al., 2000; Sasaki and Hogan, 1993).

Mice with congentical hydrocephalus were first reported by Gruneberg in 1943. Homozygous embryos died at birth and on examination, revealed hemorrhagic cerebral hemispheres and open eyelids. Histological examinations revealed the absence of the cranial vault and multiple skeletal abnormalities. Later, defects in other mesodermal tissues including the kidneys and uterus were described (Green, 1970). Studies by Kume et al., (1998) in which the *Foxc1* gene (formerly known as Mf1), was replaced with a LacZ gene resulted in mice with a phenotype similar to *ch* mice. Kume (1998) also showed that the *ch* phenotype resulted from a point mutation in *Foxc1* leading to a truncated protein lacking the DNA-binding domain.

The replacement of the *Foxc1* gene with a LacZ reporter provided a convenient method of mapping expression of the gene during development. As previously recorded by Kidson et al., (1999), in the cornea, LacZ expression is observed as early as E11.5 in the periocular mesenchyme and in mesenchyme cells that occupy the lens/corneal space. LacZ expression is downregulated as development progresses and switched off completely in the cornea at E13.5 (Figure 1-3). The structural abnormalities of the cornea in *Foxc1* mutant embryos have been described in detail elsewhere (Kidson et al., 1999). In homozygous embryos, the expression of LacZ is attenuated beyond the normal period of expression. Corneal mesenchyme cells fail to establish a typical corneal endothelial monolayer suggesting a critical role of *Foxc1* in corneal endothelial differentiation.

Haploinsufficiency of the *Foxc1* gene results in several abnormalities of the eye, including eccentric irregularly shaped pupils and displaced Schwalbe's line. The nature and penetrance of these abnormalities depends on genetic background (Smith et al., 2000). Heterozygous *Foxc1* mice of the C57BL/6/6J (B6) background display irregular and misplaced pupils, but this phenotype does not exist in the 129S6/SvEvTac background. In humans, mutations in the FOXC1 gene have been associated with autosomal dominant iridogoniodysgenesis type1 (IRD1), characterised by iris hypoplasia, anterior segment dysgenesis and juvenile-onset glaucoma (Walter et al., 1996).

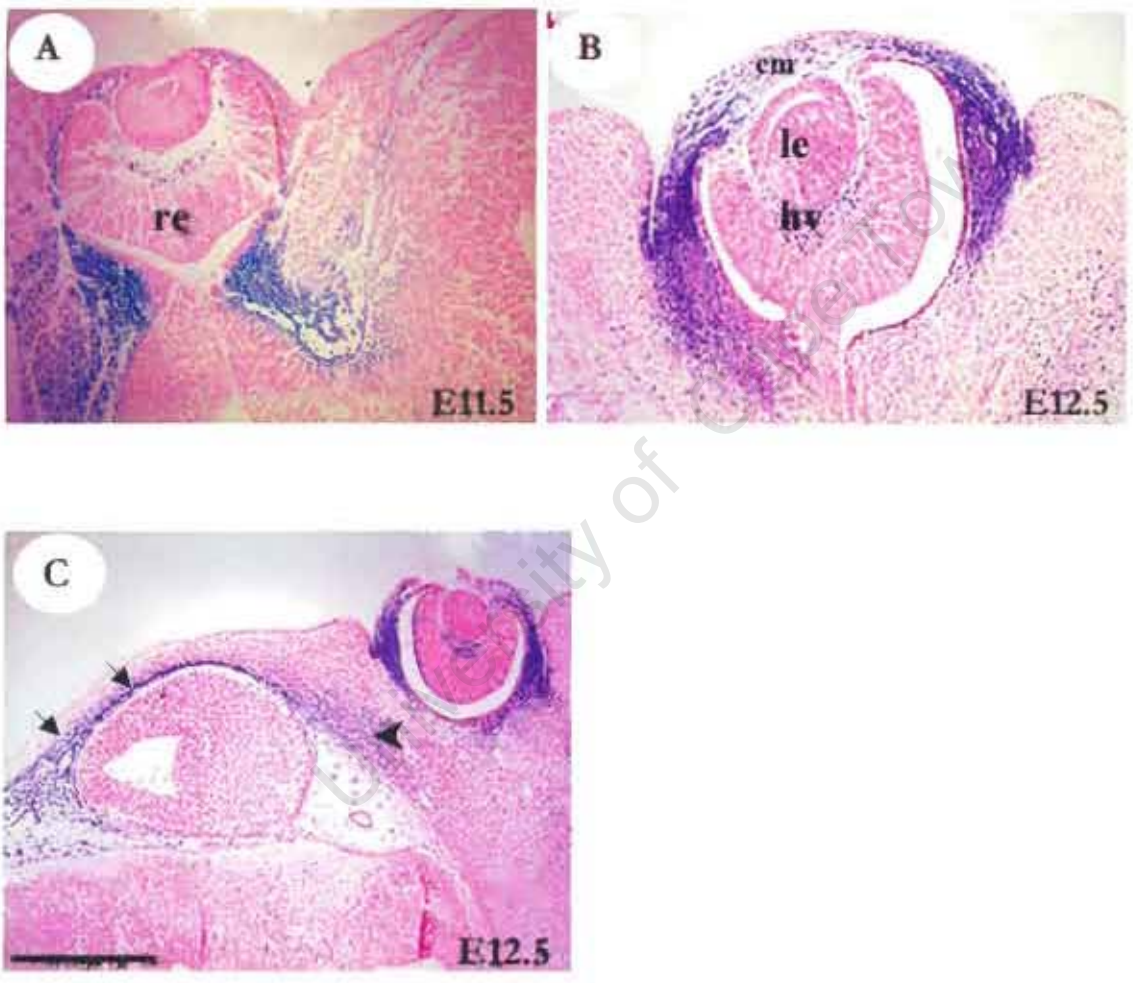

Figure 1-3. Expression of $Foxc1^{LacZ}$ in the developing eye at E11.5(A) and E12.5 (B) and in prechondrogenic mesenchyme of the skull (adapted from Kidson et al.,1999, unpublished work). (C) $Foxc1^{LacZ}$ is expressed in the prechondrogenic mesenchyme (arrowhead) and the primitive meningial layers (arrows). Le = lens, hv = hyaloid vasculature, re = retina, cm= corneal mesenchyme. Scalebar = 75μm.

Moreover, the association of FOXC1 mutations in humans, with development of Axenfeld-Rieger (AR) anomalies is consistent with the role of this gene in differentiation of neural crest-derived corneal mesenchyme. AR malformation refers to a group of dominantly inherited

ocular disorders that include IRDI, iris hypoplasia, eccentric pupils, polycoria and adhesion of the iris to the cornea. It has been suggested that AR results from disruption of migration and differentiation of neural crest cells (Lines et al., 2002).

In the absence of *Foxc1*, the differentiation of mesenchyme is impaired in tissues where *Foxc1* is normally expressed. In addition to expression in the developing eye (Kidson et al., 1999; Kume et al., 1998) *Foxc1* is expressed in the developing kidney (Kume et al., 2000), heart (Winnier et al., 1999) and endochondral skeleton (Kume et al., 1998). In the kidney, the expression of *Foxc1* is detected in the nephrogenic cord and the Wolffian duct at E9.5. Later, transcripts are detected in the metanephric mesenchyme and the condensing mesenchyme of the kidney (Kume et al., 1998). In the kidney, *Foxc1* appears to act upstream of a cascade of genes regulating the induction of the uteric bud from the Wolffian duct. Such a cascade involves *Eya1* and *Gdnf1*. *Foxc1*-null mutant mice have duplex kidneys and double ureters. This is thought to result from the misregulation of *Gdnf1* in the mesenchyme surrounding the Wolffian duct. Apart from the association of this gene with mesenchyme differentiation in the kidney, in the skull also, *Foxc1* has been implicated in proliferation and differentiation of osteogenic mesenchyme in the skull. In the absence of a functional *Foxc1* gene, the calvarial mesenchyme population exhibits reduced proliferation and the condensation and differentiation of osteoblasts is impaired (Rice et al., 2003). These findings further support the role of *Foxc1* in regulation of differentiation. However, in the skull this role is indirect through BMP-induced expression of *Msx2* and *Alx4* in the calvarial mesenchyme. *Foxc1* is required in the calvarial mesenchyme for the induction of *Msx2* and *Alx4* by BMP. Such location-specific requirement of *Foxc1* parallels the lack of corneal endothelium differentiation in *Foxc1* mutants whereas in other structures where *Foxc1* is not normally expressed, gene expression is not altered. All of these studies suggest a role of *Foxc1* in transformation of mesenchyme into epithelium.

1.3. Cell adhesion during mesenchyme–epithelium transformation

One of the many focuses of research on embryogenesis is the elucidation of the mechanisms involved in the formation of epithelial sheets. Epithelial cells *in vivo* are characterised by strong cell-cell adhesion which is necessary for the epithelial sheets to resist mechanical stress and maintain a diffusion barrier for transport of solutes across epithelial layers. In the developing embryo, epithelial cells are sometimes formed from loose mesenchyme precursor cells. The process is marked by dramatic changes in cellular shapes and sizes. The mechanisms governing such changes in cell shape and size have been investigated *in vitro*. These studies have revealed

that the establishment of an intact monolayer from a population of mesenchymal cells is a multistep process, mediated by calcium-dependent cell adhesion molecules, the cadherins. Cadherin-mediated adhesion triggers the assembly of intercellular junctional complexes, comprising of gap junctions, desmosomes and tight junctions..

1.3.1. Cadherins and associated proteins

The cadherins are a family of glycoproteins that have been identified in a variety of organisms including mammals, *Xenopus*, *Drosophila* and *Caenorhabditis elegans*. The best-described are the classical cadherins E-, N- and P-cadherin, so named because of their original identification from epithelia, neural crest and placenta respectively. E-cadherin has been shown to be essential for the formation and maintenance of epithelia. Homozygous E-cadherin mutant mice are embryonic lethal (Riethmacher et al., 1995) and loss of function of E-cadherin is associated with increased invasiveness and metastasis of tumours. N-cadherin is an adhesion molecule in pre-migratory and migrating neural crest cells (Akitaya and Bronner-Fraser, 1992) and is also required for adhesion of cardiac myocytes during heart development. Embryos homozygous for an N-cadherin mutation die at E10 (Radice et al., 1997b). *In vitro*, N-cadherin promotes neurite outgrowth and differentiation of lens epithelial cells (Ferreira-Cornwell et al., 2000). Although no developmental abnormalities are associated with P-cadherin deficient mice, female mice develop abnormalities in the mammary gland with age (Radice et al., 1997a).

Cadherin molecules occur as parallel dimers. On the extracellular side, the cadherin molecule contains five repeats, named extracellular domain 1 – 5 (EC1-5). Anchoring of the cadherin molecules to the cytoskeleton is achieved by their attachment to the catenins, which in turn mediate the association of the complex with the actin cytoskeleton. This association is achieved by binding of the distal region of the cadherin cytoplasmic tail to β- and γ-catenins. These catenins interact with α-catenin, which associates with the actin filaments (Braga, 2000) Near the transmembrane domain, the cadherin molecule binds to a fourth catenin, the phosphoprotein p120 (Yap et al., 1998).

The steps involved in establishment of cell-cell adhesion mediated by cadherins have been previously described (for recent reviews see (Braga, 2000). In brief, in contacting cells, binding of cadherin molecules between neighbouring cells requires the addition of calcium ions. A molecule of one class of cadherins binds to similar dimers on neighbouring cells, the basis of homophilic binding capacity of cadherins. Upon binding of similar molecules, cadherin molecules cluster at sites of cell-cell contact, anchored to the cytoskeleton by the catenins.

This results in remodelling of the cytoskeleton and cells subsequently attain a polarised epithelial phenotype (Figure 1-3, Braga 2000). The exact molecular mechanisms employed in each of these steps are not clearly defined.

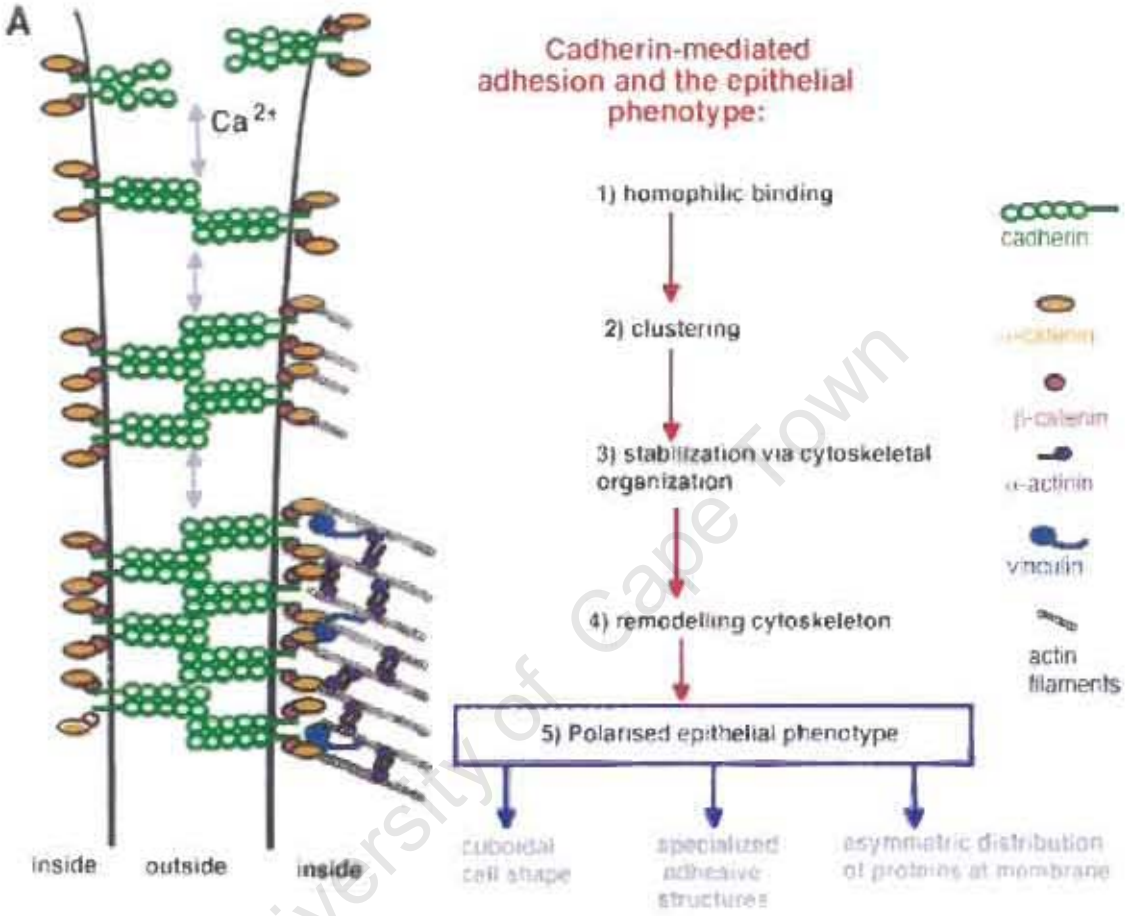

Figure 1-4. A schematic representation of cadherin-mediated adhesiveness in epithelia. Cadherin molecules bind to similar dimmers at the cell surface. Maintenance of the clustered molecules at the surface is achieved by attachment to the cytoskeleton, which occurs through binding of cadherins to catenins (see text for details). Anchoring to the cytoskeleton warrants changes in organisation of the cytoskeletal machinery and changes in cell shape (from Braga, 2000).

1.3.2. Biogenesis and turnover of cadherins

Studies in neural crest cells have shown that the N-cadherin expression pattern and localisation changes from cytoplasmic pools to cellular borders, reflecting the migrating status of the cells (Monier-Gavelle and Duband, 1995). During migration N-cadherin occurred in vesicles in the cytoplasm and at the end of migration, N-cadherin was re-expressed at the cell surface. It has been proposed that changes in cadherin localisation could be a consequence of the turnover of cadherins at the cell surface brought about through either secretory or

endocytotic pathways. Experimental evidence to support this comes from studies in which recycling of cadherin molecules were investigated in MDCK cells (Le et al., 1999). In this study, cells were surface biotinylated at 0°C and subjected to temperature shift assays. Cells grown under conditions that promote accumulation of internalised proteins and prevent them from progressing further into endocytic or recycling pathways (at 18°C), showed increased intracellular E-cadherin compared to cells seeded under normal conditions (37°C). The formation of adherens junctions correlated with the increase in plasma membrane localisation and decreased vesicular pattern of cadherin protein. In preconfluent cells, large pools of intracellular E-cadherin were found and these redistributed to sites of cell-cell contact as cells grew to confluence and more stable junctions formed. Some pools of E-cadherin at the cell surface were shown to be endocytosed and recycled back to the surface.

A number of studies have been conducted *in vitro* using MDCK cells to learn about the mechanisms employed during the formation of adherens junctions. Because cadherin adhesiveness is dependent on extracellular calcium, such mechanisms have been studied using the calcium-switch assay. In such assays, the cells are initially maintained under prolonged calcium starvation where the monolayers lose their cell-cell contacts and intercellular junctions and the transepithelial electrical resistance (TER), a measure of monolayer integrity, drops. Upon restoration of normal calcium levels in the medium, cells acquire intercellular junctions, restore polarity and obtain normal levels of TER, for reviews, see - (Matter and Balda, 2003).

It has been shown that the formation of adherens junctions begins with the establishment of initially unstable contacts. Stable adherens junctions are initiated by overlapping of cellular protrusions from adjacent cells. As more contacts are made, intercellular gaps are sealed off, correlating with the translocation of cadherin proteins to the plasma membrane (Angres et al., 1996; Yap et al., 1997). Thus it appears that the formation of cadherin junction is dependent on cell-cell contact. The exact molecular mechanisms by which cell contact regulates this process are not known. Using high-resolution differential interference electron microscopy, it has been shown that in MDCK cells, cell-cell contact is made up of distinct stages (McNeill et al., 1993). The first stage, an "exploratory" stage, is characterised by formation of multiple, independent and unstable contacts. At these early stages of junction formation, E-cadherin staining pattern is punctate, representing interdigitations at the contacting membranes of adjacent cells and in intracellular vesicles.

In order to study the dynamics of cell-cell contact formation and to further characterize the biogenesis of cell-cell junctions, Mary et al. (2002), transfected rat embryo fibroblasts and C2 myoblasts with a fusion protein of N-cadherin (N-cad) and GFP. In isolated cells, N-cadherin

expression was found in the cytoplasm and perinuclear region. Accumulation of N-cadherins at the plasma membrane coincided with the establishment of cell-cell contacts. Tracking of the fused protein by immunofluorescence revealed that N-cad/GFP occurs in vesicular structures that associate with and move along microtubules in a kinesin-dependent manner. These studies provided further evidence that cell-cell contact is one of the regulatory mechanisms controlling the assembly of N-cad junctions. In addition, they demonstrated that the maintenance of N-cadherin junctions requires an intact F-actin cytoskeleton. Disruption of the cytoskeleton by treatment with cytochalasin led to loss of N-cadherin at the plasma membrane.

1.3.3. Establishment of cellular polarity: the formation of tight junctions

The tight junctions are the most apical of the junctional complex and are also called the zonula occludens because they occlude the extracellular space forming a tight seal between cells. The quality of the seal varies depending on cell type and activity. Extremely tight barriers occur where epithelial cells must maintain high ionic gradients, for example, in the glomerulus of the kidney. Leaky junctions on the other hand, are associated with low ionic gradients but where a regulated barrier is nonetheless required (Pollard & Earnshaw, 2003) such as in the corneal endothelial cells, human ciliary epithelium of the eye (Noske et al., 1994) gall bladder and renal proximal tubule (Kottra and Fromter, 1983). In addition to the sealing properties, tight junctions create selective permeability barriers between individual cells and the extracellular environment. The selective permeability is a result of regulated transport of ions through the cytoplasm (transcellular pathway) and the regulated permeability of the spaces between the cells (paracellular pathway).

1.3.4. Structure and molecular composition of the tight junction

The structural organization of the tight junction of polarized epithelia was first revealed by electron microscopy in the early 1960's (Farquhar and Palade, 1963). They showed that the tight junction appears as a series of discrete contacts between the plasma membranes of adjacent cells. Freeze-fracture analysis of the tight junction revealed that these contacts correspond to continuous strands of intramembranous particles that form a branching network at the plasma membrane. It has now been shown that the number and continuity of these strands determine the tightness of the seal and the barrier to the diffusion of ions in the extracellular space. It has also been shown that the strands are actually made up of integral membrane proteins (Pollard and Earnshaw, 2002).

Numerous studies have subsequently shown that some tight junction proteins are located on the cytoplasmic side of the membrane. Others are transmembrane proteins, unique to the tight junction (Figure 1-5, adapted from (Matter and Balda, 2003). The first transmembrane protein to be identified was occludin which is concentrated in the tight junction strands at regions of apposition in adjoining cells. It was later shown by immunoflourescence that a pool of occludin exists along the lateral membranes (Cordenonsi et al., 1997; Fujimoto, 1995; Sakakibara et al., 1997). This pool is thought to represent a reservoir of subunits available for expansion of the junctional complex. Occludin is not the only integral transmembrane protein in the tight junction. Evidence for this comes from studies in which the expression of a dominant negative form of occludin (in which the occludin C-terminal was truncated) in MDCK cells resulted in normal distribution of the tight junction protein, zonula occludens-1 (ZO-1) although occludin was discontinuous at the sites of cell-cell contact (Balda et al., 1996). The most direct evidence of the existence of another transmembrane protein came with the observation that occludin-deficient embryonic stem cells could still assemble tight junctions (Saitou et al., 1998).

The search for other tight junction proteins led to the identification of two other classes of proteins with transmembrane domains, claudin-1 and claudin-2 (from Latin "claudere" meaning "to close") (Furuse et al., 1998). Subsequent to these findings, six more claudin gene products were identified based on homology to sequences in the EST database (Morita et al., 1999). The junctional adhesion molecule (JAM) is a recently identified transmembrane protein at the tight junction (Martin-Padura et al., 1998). It is a member of the IGg superfamily and is found at the tight junction of both epithelia and endothelia (for reviews, see - (Balda and Matter, 2000). The exact function of these proteins however, remains unclear.

For a tight junction to be functional, the transmembrane proteins must be linked to the cytoskeleton. On the cytoplasmic side of the tight junction, different groups of proteins have been identified. These include adaptor proteins, regulatory proteins, translational and post-translation regulatory proteins (Figure 1-5). The best characterized of the cytoplasmic adaptor proteins associated with the tight junction are ZO-1 and ZO-2. ZO-1 was identified as a peripheral membrane protein specifically enriched at the points of tight junction membrane contact (Stevenson et al., 1986). It is also associated with the cytoplasmic undercoat of adherens junctions in non-epithelial cells (Howarth et al., 1992; Itoh et al., 1991; Jesaitis and Goodenough, 1994). In 1996, Rajasekaran et al. (1996) showed that during junction maturation, ZO-1 associates with adherens junctions prior to final localization at the tight

junction. It has also been reported that ZO-1 accumulates in the nucleus when there is rearrangement or disruption of cell-cell contacts (Gottardi et al., 1996). Furthermore, ZO-1 has been implicated in the control of gene expression and in the regulation of epithelial differentiation (Balda et al., 2003).

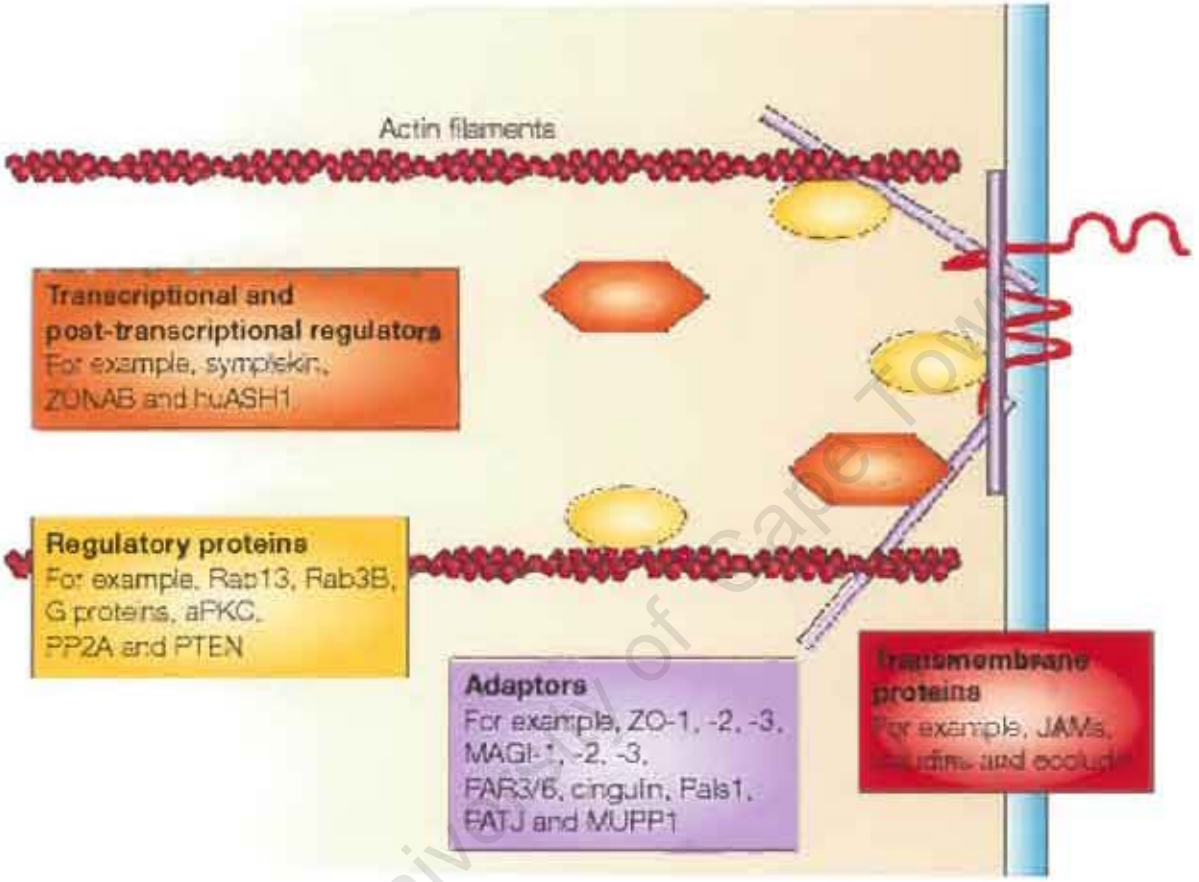

Figure 1-5. A model of protein interactions at the tight junction (Matter and Balda, 2003). Four groups of proteins (transmembrane, adaptor, regulatory and transcriptional and posttranscriptional regulators) define the components of the tight junction in epithelia. The barrier properties of the paracellular space are defined by transmembrane proteins (red box) occludins, claudins and junctional adhesion molecules (JAMs). The adaptor proteins are connected to the transmembrane proteins. ZO-1, ZO-2 and ZO-3 all bind the cytoplasmic tail of occludin. ZO-1 binds actin, ZO-associated kinases, alpha catenin and other proteins. The PAR proteins (3 and 6) are PDZ-domain containing proteins at the tight junction. PAR3 has been shown to bind to the JAM. MAGI-1, membrane-associated guanylate kinase inverted; MUPP1, multi-PDZ domain protein1; Pals1, protein associated with Lin-7. PAR, partitioning defective; PATJ, pals-associated tight junction protein ; PP2A, protein phosphatase 2A; PTEN, phosphatase and tensin homologue, ZO, zonula occludens; ZONAB, ZO-1 associated nucleic acid binding.

Evidence for the role of ZO-1 in cellular differentiation comes from studies in which the activity of ZO-1 was disrupted. Corneal epithelial cells were transfected with dominant negative forms of ZO-1 and assayed for changes in tight junction sealing properties. The disruption of ZO-1 activity (by N-terminal mutants of ZO-1) induced a cellular change from

epithelium to mesenchyme morphology. The epithelium-mesenchyme transformation (EMT) was accompanied by changes in expression pattern of other tight junction proteins, ZO-2, ZO-3 and occludin. The three proteins were found throughout the cytoplasm and were downregulated in their expression (Ryeom et al., 2000).

1.3.5. Mechanisms of tight junction assembly

Different experimental systems have been employed to analyse the assembly and regulation of tight junctions. In fact, the same model systems utilised for analysis of cadherin junction assembly have been used. These include the calcium switch protocol and the ATP-depletion method in which ATP is depleted in cells that have already formed monolayers resulting in dissociation of cell-cell junctions (Fleming et al., 2001). Alternatively, *in vitro* wound healing assays are utilised, in which confluent epithelial monolayers are wounded by scratching them with a needle or pipette tip and the reformation of junctions then studied. In addition, *de novo* assembly of tight junctions can be studied during early embryonic development (Canfield et al., 1991).

In vitro experimentation suggests that the source of intracellular calcium is critical for tight junction biogenesis. This finding comes from studies in which intracellular calcium was chelated in cells prior to the formation of cell-cell contacts (Stuart et al., 1996). This was achieved by treating cells with thapsigargin (TG), an endoplasmic reticulum (ER) Ca^{2+} - adenosinetriphosphatase (Ca^{2+} -ATPase) inhibitor. TG acts by depleting intracellular ER stores thus rendering the cells insensitive to further stimulation of ER Ca^{2+} release. In cells treated with TG prior to initiation of cell-cell contact, the biogenesis of tight junctions and desmosomes and the sorting of junctional proteins were disrupted. These defects were evidenced by lack of normal levels of TER (trans-electrical resistance) and by failure of ZO-1 to translocate from cytoplasm to the membrane. Inhibition and depletion of intracellular ER stores of calcium prior to the formation of intercellular contact, did not affect cadherin-mediated contacts, suggesting an independent mechanism for tight junction assembly. Light and electron microscopic examination revealed that cells were able to develop extensive cell-cell contacts thus showing that the effects of TG on tight junction assembly was not a result of the primary defect on initiation of adhesive contacts. Since the translocation and stabilisation of junctional proteins occur after cell-cell contacts are made, it appears that calcium stores are important in initiating calcium-dependent signalling events that lead to tight junction assembly soon after the establishment of cell –cell contacts. The exact mechanisms of how signalling mechanisms activated upon cell-cell contacts lead to junction assembly are the major focus of

research for cell biologists. Other investigators have associated such dependence of tight junction assembly on intracellular calcium levels with signalling pathways that utilise heterotrimeric G proteins and protein kinase C (PKC), (Balda et al., 2003).

1.4. General and specific aims of this study

The major questions addressed in this study culminated from pioneering research on the role of *Foxc1* on the development of the eye. The major focus was to elucidate the exact molecular pathways associated with the differentiation and conversion of corneal mesenchyme into corneal endothelium.

Eye abnormalities in *Foxc1* mutant mice were first described by Kidson *et. al.* in 1999. The eye defects mainly involved the anterior segment structures. In the normal embryo, some segment structures develop postnatally and thus in the mutant embryo, the development of such structures could not be closely monitored because homozygous mutant embryos were embryonic lethal. One of the most striking developmental abnormalities in the eye of the mutants was failure of the lens to separate from the cornea. Careful histological and electron microscopic examination revealed the absence of the corneal endothelium. This abnormality obviously triggered questions on implications for corneal endothelial dystrophies and associated glaucoma. It became apparent that detailed descriptions of the normal development of the mammalian corneal endothelium were lacking and thus this study was initiated. The major goal of this study was therefore to carefully detail the normal development of the mouse corneal endothelium and to further investigate the defects associated with failure of corneal endothelium formation in mutant embryos.

The specific aims of this study were:

1. To use scanning electron microscopy to provide an accurate description of cellular shape changes involved in the formation of the corneal endothelium and to establish with precision, the timing of this process during normal embryogenesis in mice.
2. To determine the temporal and spatial expression of and adherens junction protein, N-cadherin, associated with cell shape changes during normal corneal endothelial development.
3. To determine the spatial and temporal expression of the tight junction protein, ZO-1 during normal corneal endothelial development.
4. To develop an *in vitro* model using undifferentiated mesenchymal cells to determine the process of mesenchyme-epithelial transformation that occurs during normal corneal endothelial development.

5. To determine the expression pattern of the corneal specific proteoglycan, *keratocan* in normal embryos.
6. To examine all of the above (1-5), in *Foxc1*$^{-/-}$ mice which fail to form a corneal endothelium.
7. To determine the expression pattern of transforming growth factor beta-2, (*tgfβ2*) and transforming growth factor beta receptor-2, (*tgfβRII*), both of which are implicated in early corneal endothelial differentiation.

Chapter Two : MATERIALS AND METHODS

2.1. Mice and genotyping

Embryos from ICR mice were used for all studies. *Foxc1* null mice provided by Brigid Hogan (ex Vanderbilt University Medical Centre, presently at Duke University, USA) had been generated by homologous recombination in embryonic stem cells by replacing almost the entire winged helix domain of *Foxc1* with a lacZ/PGKneo^r cassette as shown in Figure 2-1 (Kume et al., 1998). All mice were housed in the animal facility at the University of Cape Town in accordance with the rules and regulations of the University. *Foxc1* null mice were maintained in an ICR background by brother-sister matings. The day of vaginal plug was 0.5 days post coitum (dpc) or embryonic day 0.5 (E0.5). Embryos were obtained by caesarean section at E12.5, E13.0, E13.5, E14.0, E14.5 and E17.5 for wildtype embryos and only at selected developmental stages (E12.5, E13.5 and E17.5) for *Foxc1* mutant embryos. Tail clips were obtained from embryos for LacZ staining. To further confirm the genotype of the embryos and to distinguish between homozygous and heterozygous mice, DNA was extracted from whole embryos or from tail clips of adult mice for genotyping by polymerase chain reaction (PCR).

2.1.1. LacZ staining

Mouse embryo torsos, tail clips or whole eyes were fixed in 4% parafomaldehyde in phosphate buffered saline (PBS), pH 7.3, at room temperature for one hour. After three 30 minute washes in PBS, tissues were incubated in X-gal reaction mix (containing 5mM potassium ferrocyanide, 5mM potassium ferricyanide, 1x PBS (pH 7.3), 2mM $MgCl_2$, 0.01% sodium deoxycholate, 0.02% Nonident P40, 1mg/ml X-gal (5-bromo-4-chloro-3-indolyl β-D-galactoside in 70% dimethylformamide, Roche), 20mM Tris-HCl, pH 7.3) at 37°C in the dark overnight. After this time, the stained tissues were rinsed in PBS and stored at 4°C in 70% ethanol.

2.1.2. DNA extraction and PCR genotyping analysis

PCR genotyping analysis was carried out with genomic DNA obtained from mouse tails or embryonic torsos. For DNA extraction, tissues were first digested in lysis buffer containing 100mM Tris-HCl, pH 8.0; 5mM EDTA, 0.2% SDS, 200mM NaCl and 15μg/ml proteinase K solution (Roche) at 37°C overnight. DNA was extracted by phenol-chloroform purification

and isopropanol precipitation of DNA as follows. The supernatant from the overnight digest was mixed with an equal volume of phenol and spun at 5000x g for three minutes at room temperature. The resulting supernatant was then mixed with phenol/chloroform (1:1) and spun at 4000x g at room temperature, after which the DNA was precipitated and pelleted by mixing the supernatant with an equal volume of isopropanol and incubated at 4°C for 30 minutes. The DNA pellet was obtained by spinning at 4°C for 10 minutes. The pellet was then air-dried and resuspended in distilled water. DNA was dissolved at 65°C for 8 minutes and thereafter used for PCR analysis or stored at -20°C until further use. Three primers were used for a PCR reaction in order to amplify the wildtype, heterozygote and homozygote mutant alleles. Primers used for genotyping were: *Foxc1* Forward 1 (F1): 5'-GCC CTA CAG CTA CAT CGC TCT TATC–3'

Foxc1 Reverse 1 (R1): 5'-CCC TGC TTA TTG TCC CGA TAG AAA-3'

Foxc1 Reverse mutant (Rm): 5'-ACC GTG CAT CTG CTG CCA GTT TGA G-3' (see Figure 2-1, red arrows). The PCR conditions were 94°C for 30 seconds, 35 cycles at 94°C for 30 seconds, 64°C for 30 seconds and 72°C for one minute 30 seconds, followed by 72°C for 10 minutes. PCR products were separated on a polyacrylamide gel, 250 volts at 4°C and detected by ethidium bromide staining and UV transilluminaton.

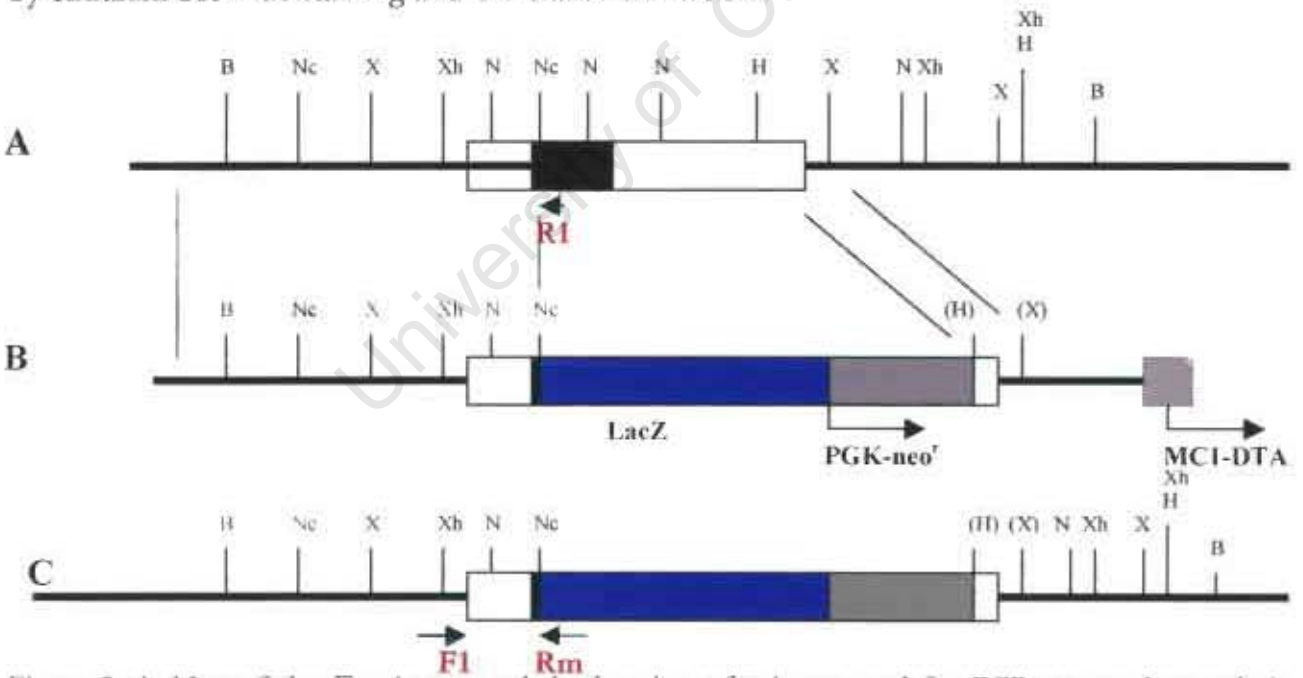

Figure 2 -1. Map of the *Foxc1* gene and the location of primers used for PCR genotyping analysis (modified from Kume et al., 1998). *Foxc1* is a single exon gene indicated with a black box. Open boxes represent 5' and 3' untranslated regions. The targeting vector consists of two fragments, a 7kb 5' homology region (SalI(S) – NcoI(Nco) fragment) and a 1.2kb 3' homology region (HindII(H) – XbaI(X) fragment). The coding region was replaced with a lacZ/PGKneo' cassette. A diptheria toxin A (MCD1-DTA) cassette was placed at the end of the 3' homology region for purposes of negative selection (Kume et al., 1998). For genotyping purposes, forward (F1), reverse (R1) and reverse mutant (Rm) primers were designed as indicated in the diagram (A, C). A = wildtype allele; B- targeting vector; C- Targeted alelle.

2.2. Microdissections and tissue preparation

Pregnant female mice were sacrificed and the embryos obtained at different stages of development beginning from E12.5. Using fine iris scissors, whole eyes were removed from embryos under the dissecting microscope and placed into ice-cold PBS, pH 7.4. Torsos or tail clips were stored at -20°C for DNA extraction and or LacZ staining. Eyes were fixed either for histological analysis, electron microscopy, immunocytochemistry or *in situ* hybridisation. For histology processing, whole eyes were fixed in 4% paraformaldehyde overnight, followed by three 30 minute washes in PBS (pH 7.4) before dehydrating in ethanol series (50% for 30 minutes, 70%, for 30 minutes and two changes of 100% ethanol for 20minutes each) at room temperature. Samples were then cleared by briefly rinsing in two changes of xylol before being embedded in paraffin.

2.3. Scanning electron microscopy (SEM)

For scanning electron microscopy, whole eyes were fixed in Karnovsky's (1.5% paraformaldehyde, 0.5% glutaraldehyde in 0.1M Sorenson's phosphate buffer, pH 7.4) overnight and thereafter rinsed in 0.1 M Sorensen's phosphate buffer. Corneas were separated from whole eyes after fixation under the dissection microscope using fine tungsten needles. Corneas and lens/retina were post-fixed in 2% osmium tetroxide at room temperature for two hours. After three 15 minute rinses in 0.1M Sorenson's phosphate buffer, samples were rinsed in distilled water before dehydration in alcohol series (50%, 70%, 90% and two changes of 100% ethanol) for 10 minutes each. Samples were then critical point dried using a CPD 020 machine (Balzers). Corneas obtained from early embryos were very small (<0.5mm) and brittle after critical point drying and thus difficult to manipulate further. To overcome this problem, another means of critical point drying was used. Individual corneas and their respective lenses were critical point dried by addition of hexamethyl-di-silazane (Sigma). The liquid was left under the hood to evaporate overnight. Individual samples were picked-up using hairs or fine tungsten needles and mounted under the dissection microscope on stubs prepared by coating with a mix of 50% glue and 50% coal. They were then sputter coated with gold palladium on a sputter coater (Balzers) for 20 minutes. Samples were viewed using a S440 scanning electron microscope (Leo, Leica). The number of corneas and genotype of embryos processed for SEM are shown in Table 2.1.

Table 2.1. Number of mouse corneas examined by SEM

	E12.0	E12.5	E13.0	E13.5	E14.0	E14.5	E17.5	Adult
+/+ & -/+	24	43	8	31	12	9	8	8
-/-	-	2	-	3	-	-	2	-

This table lists the number of corneas examined by SEM. Corneas from wildtype (+/+), heterozygotes (-/+), and mutant (-/-) embryos were processed for SEM. There were no morphological differences observed between wildtype and heterozygous corneas and thus, information from these two groups were pooled together.

2.3. Transmission electron microscopy (TEM)

For TEM, whole eyes obtained from embryos or corneas dissected from adult eyes were fixed in Karnovsky's for 14 – 18 hours at 4°C. Samples were then washed in three 15 minutes changes of 0.1M Sorenson's phosphate buffer at room temperature. They were post-fixed in 1% osmium tetroxide at room temperature for two hours after which they were rinsed in three 15 minutes changes of 0.1M Sorenson's phosphate buffer. Samples were then dehydrated in alcohol series (50%, 70%, 90% and two changes of 100% ethanol) for 10 minutes each. After dehydration, samples were incubated in three changes of propylene oxide at room temperature for 10 minutes each, thereafter in increasing concentrations (30%, 50%) of epon araldyte resin for two hours each. After this time, sections were incubated in epon araldyte resin overnight at 40°C. Following this, corneas were incubated in resin/accelerator (1:1) for an hour before polymerising at 60°C for two days. Ultra thin (0.1nm) sections were picked up on grids and stained as follows: Grids were rinsed by dipping in five 30-second changes of distilled water after which they were incubated in 2% uranyl acetate (in methylcellulose) for five minutes, followed by incubation in lead citrate droplets for ten minutes. To avoid precipitation of lead citrate, droplets were kept in an enclosed chamber with sodium hydroxide pellets. Sections were washed in three 30-second changes of distilled water, blotted on filter paper, air-dried and viewed using an EM109 transmission electron microscope (Zeiss).

2.4. Immunocytochemistry

2.4.1. Antibodies and fluorescent markers

The antibodies used in this study were: N-cadherin, zonula occludens-1 (ZO-1), Golgi-marker, phalloidin, DAPI and tubulin. The N-cadherin antibody is a rabbit polyclonal that recognises

the extracellular domain of N-cadherin (Santa Cruz Biotechnologies). The zonula ocludens-1 antibody (ZO-1) is a purified mouse monoclonal and was a gift from Brigid Hogan (Duke University). ZO-1 recognises the tight junction protein, zonula occludens on epithelia and endothelia. The Golgi marker (Sigma) is a 58kD antibody that recognises trans & cis Golgi proteins, a gift from Dirk Lang (UCT). FITC flour-tagged phalloidin (Molecular probes, Oregon, USA) recognises F-actin in cells and was a gift from Anthony Graham (King's College, London). Alexa 568 flour-tagged phalloidin was purchased from Molecular Probes (Oregon, USA). Anti -rabbit cy3 was purchased from Jackson Immuno-Research Laboratories Inc. and the anti-mouse Alexa-488 from Molecular Probes.

Whole-mount tissues. Whole eyes obtained from different embryos at different developmental stages were fixed in 4% paraformaldehyde at 4°C for 10 minutes at room temperature, washed in PBS (pH7.4), or in 100% methanol at –20°C for 10 minutes. Samples were then rinsed in PBS at room temperature and blocked in a solution of 1% BSA and 1% DMSO in PBS pH 7.4 at 4°C overnight with shaking. They were then incubated in primary antibodies (N-cadherin, ZO-1) at 1:250 dilution with blocking solution at 4°C for 24 hours, rinsed extensively in PBS, pH 7.4 and incubated in anti-rabbit cy3 and or anti-rat Alexa 488 antibody (at 1:1000 dilution in blocking solution) for two hours at room temperature. For F-actin staining, after fixation in 4% paraformaldehyde, samples were rinsed extensively in PBS (pH 7.4), incubated in blocking solution followed by phalloidin-FITC at 1:1000 dilution in blocking solution for 14 – 18 hours. After this time samples were rinsed in five 15 minutes changes of PBS at room temperature. Before viewing, samples were rinsed extensively in PBS (pH7.4) and mounted in Mowiol. The Mowiol mounting medium was made up as follows: For every 2.4 g Mowiol (polyvinyl alcohol, Hoechst), 6ml glycerol was added. While stirring, 6ml of distilled water was added and left for several hours at room temperature. Twelve millilitres of 0.2M Tris (ph 8.5) was added and the solution incubated at 50°C for one hour with occasional stirring. To reduce immunoflourescence fading, small amounts of n-propyl gallate (Sigma) was added and dissolved at 37°C. The medium was stored as 2ml aliquots at –20°C, and centrifuged at 12 000 x g for five minutes just before use to remove insolubles. Viewing was carried out using a Zeiss confocal microscope or Zeiss Axiovert 200M fluorescence microscope (Zeiss, Germany).

Cells. Culture medium was rinsed off the cells with PBS, pH 7.4 and cells were fixed either in MEMFA (1% 10X MEM, 1% formalin (37% stock) in distilled water) at room temperature for 10 minutes or in 100% methanol at –20°C for 10 minutes. The 10X MEM stock (1M MOPS, 20mM EGTA, 10mM magnesium sulphate) was pre-made up and stored at 4°C. Cells were

then rinsed in five minute changes of PBS, pH 7.4, permeabilised in 0.1% Triton-X (SAARCHEM Pty. Ltd, South Africa) for 5 minutes at room temperature and rinsed in PBS. Cells were then blocked in 1% bovine serum albumin, BSA (Roche) in PBS for one hour at room temperature. They were then incubated at 4^{0}C for 18 hours in primary antibodies diluted in blocking solution at the following concentrations. N-cadherin (1:500); ZO-1 (1:250); tubulin (1:500), phalloidin (1:1000) DAPI (1:1000) and Golgi marker (1:250). The primary antibodies were rinsed off in five 5 minute changes of PBS and the cells were incubated with the appropriate secondary antibodies at 1:2000 dilution in blocking solution as follows. For N-cadherin, anti rabbit cy3 or anti-rabbit alexa-548 were used, while anti-mouse cy3 or anti mouse alexa 488 were used for ZO-1 detection. The anti-mouse alexa-488 was used for the detection of the Golgi marker.

2.5. *In situ* hybridisation

All solutions were made up in DEPC-treated water, which was prepared as follows. 200µl of diethyl pyrocarbonate (DEPC; Sigma) was added to a litre of water. This was left stirring at room temperature for at least two hours after which water was autoclaved to inactivate the DEPC. Glassware was rinsed in DEPC-treated water and baked at 180^{0}C for two hours to destroy RNases.

In *situ* hybridisation was performed to determine the expression pattern of *keratocan*, tgfβ2, and tgfβrII in developing normal and mutant mouse eyes. The protocol followed for ISH was a modification of Stern & Holland (1993) and Hogan et al. (1998). Six micron-thick sections from paraffin-embedded embryonic eyes (E12.5, E13.5, E14.5 and E17.5) were prepared. Slides were treated for ISH as follows.

2.6.1. Synthesis of riboprobes

The *keratocan* plasmid was a gift from Carolyn Pressman (MD Anderson Cancer Center, Houston, Texas). The *keratocan* cDNA (2.9kb) had been cloned into the *EcoRI-XhoI* site of the pBluescript. To generate the sense riboprobe using the T7 RNA polymerase, the vector was linearised with *Xho I.* Antisense riboprobe was generated by T3 RNA polymerase using an *EcoRI*-linearized template. All probes were prepared in a 20µl mix containing 1X transcription buffer, 10mM dithiotreitol, 10mM each of rATP, rCTP, rGTP, UTP mix (1:2 dig-labelled UTP: rUTP), 40 units RNase inhibitor (Roche) (1µl), 20 units of RNA polymerase (T3, T7 or sp6) and 1µg of DNA template at 37^{0}C for two hours. Probes were checked and analysed on a

1% agarose gel as shown in Figure 3-17. To facilitate probe penetration into the tissue, the *keratocan* probes were hydrolysed to a size of 0.75kb using the following protocol, modified from Roche (1998). After riboprobe synthesis, the mix was made up to a volume of 100µl of TE buffer. Alkaline hydrolysis was performed by addition of half the volume (50µl) of each of 80mM $NaHCO_3$ and 120mM Na_2CO_3. The reaction mix was incubated at 60°C for x number of minutes using the following formula (Stern and Holland, 1993).

$$x = \frac{(L-0.75)}{0.08L}$$ in which x = time in minutes,

L = original length of probe, 0.08 = constant and 0.75 = the desired length of probe. Thus, the *keratocan* riboprobe was hydrolysed at 60°C for 8, 24 minutes, after which the probe was precipitated. This was performed by addition of 5µl of a 10% acetic acid solution, 11µl 3M sodium acetate, 1µl 10mg/ml tRNA, 1.2µl 1M $MgCl_2$ and precipitated with 300µl ethanol at –20°C for 12 – 18 hours. The probe was pelleted by centrifugation at 12000 x g at 4°C, air-died, reconstituted in DEPC-treated water to a final concentration of 0.2µg/µl, aliqouted and stored at -20°C until use.

The tgfβ2 and the tgfβRII plasmids were a gift from H.L. Moses (Vanderbilt University Medical Centre). A tgfβ2 cDNA (0.442kb) had been ligated into the sp72 vector. The sense and antisense riboprobes were generated from *EcoRI*- and *XhoI*-linearized DNA by T3 and sp6 RNA polymerases. The tgfβRII (0.343kb) cDNA had been ligated into the pcDNA vector. Sense and antisense riboprobes were generated from *PstI*- and *EcoRI*-linearised templates using T3 and T7 RNA polymerases. The probes were recovered by addition of 80µl of 10mM Tris-Cl, pH 8.0/1mM EDTA (TE) buffer, 10µl lithium chloride and 300µl of ethanol and precipitated at -20°C for one hour before centrifuging at 12000 x g at 4°C. The pellet was rinsed in 70% ethanol, air-dried and reconstituted in DEPC-treated distilled water.

2.6.2. Slide treatment, prehybridization and hybridization

For in *situ* hybridisation, tissues were fixed in 4% paraformaldehyde (made up in DEPC-treated PBS, pH 7.4) at 4°C for 18 hours and prepared for sectioning as described (section 2.2). Five micron sections were deparrafinized, rehydrated and washed twice in PBS for 5 minutes prior to treatment with 10µg/ml proteinase K (Roche) for 7 minutes at 37°C. For *tgfb2* in situ hybridisation, the sections were refixed in 4% paraformaldehyde and again washed in PBS for 5 minutes prior to acetylation of the tissues. The acytelation was performed by incubating the sections in a solution of 0.25% v/v acetic acetic anhydride, 1.5%v/v triethanolamine and 0.42% v/v concentrated HCl for 10 minutes at room temperature. The

sections were washed twice for 5 minutes and dehydrated in a series of alcohols (1 minute wash in 50%, 70% and twice in 100% ethanol). Afterwards, slides were either used immediately or stored in a closed chamber with desiccant granules (acetate salt, Sigma) at – 80°C until further use. For immediate use, tissues were prehybridised in hybridisation buffer containing 50% deionised formamide, 5X SSC (made up from a stock of 20 X SSC containing 3M NaCl, 0.3M sodium citrate; pH 4.5 with citric acid), 5X Denhardt's, 250μg/ml of yeast RNA and 500μg/ml of herring sperm DNA at room temperature for two hours and hybridised in the hybridisation buffer with 200 – 400ng/ml of dig-labelled probe at 60°C overnight (18 – 24 hours). For *keratocan* and *tgfbrII* probes, a slightly different method was followed. After proteinase K treatment, sections were rinsed three times in PBS, pH 7.4 before being prehybridised in hybridisation buffer containing 50% deionised formamide, 5X SSC, pH 4.5, 50μg/ml yeast tRNA (Sigma), 1% sodium dodecyl sulphate (SDS), 50μg/ml heparin (Sigma). Hybridisation was carried out at 65°C in a hybridisation chamber moistened with 50% formamide and 5X SSC for 12-16 hours. Controls were hybridised with hybridisation mix containing 200ng of the sense riboprobe.

2.6.3. Posthybridization and colour detection procedures

Stringency washes at 65°C were performed first in a solution of 50% formamide, 5X SSC and 1% SDS; followed by 50% formamide/2X SSC for 30 minutes at 60°C and twice in 0.2X SSC at 60°C. Sections were then washed at room temperature in 1X TBST buffer (diluted from a 20X stock containing 1.4M NaCl, 27mM KCL, 0.25M Tris-HCl, pH 7.5, 1% Tween-20 with levamisole (Sigma) to a final molarity of 2mM. Blocking was performed for one hour at room temperature in a solution containing 2% normal sheep serum in TBST and thereafter sections were incubated with anti-digoxygenin antibody (Roche) diluted 1:1000 in blocking solution for 12-18 hours at 4°C. They were then washed five times for 20 minutes with PBT (PBS, pH 7.4 containing 0.1% Tween-20) at room temperature and thereafter rinsed in high pH buffer (100mM NaCl, 100mM Tris-HCl, pH 9.5; 50mM MgCl; 1%Tween-20). They were then incubated in high pH buffer containing 10% polyvinyl acetate (Sigma), 100mM NaCl, 100mM Tris-HCl, pH 9.5; 5mM MgCl, 1%Tween-20, 4,5μg/ml nitroblue tetrazolium (NBT) (Roche) and 3.5μg/ml 5-bromo-4-chloro-3-indolyl-phosphatase (BCIP, Roche) at 37°C until an appropriate blue precipitate formed. The staining reaction was stopped by rinsing the sections in Tris-HCl (pH 5.5), thereafter in distilled water and mounted in Mowiol. Sections were photographed using a Fujichrome ASA64 colour film on a Nikon Microphot-FX microscope.

2.7. Cell isolation, culture and manipulation

2.7.1. Isolation and culture of primary corneal mesenchyme cells

Tissue culture dishes and medium. Cells were cultured on 12mm glass coverslips (Marienfield, Germany) that were coated with fibronectin (Sigma) as follows. Coverslips were rinsed briefly in 70% ethanol and thereafter in three dips of PBS and sterilised under UV for 10 – 15 minutes. A 1:100 dilution of fibronectin (Gibco) in Ham's F12 (Highveld Biological Pty. Ltd.) was made up. Coverslips were coated with the fibronectin solution in 24-well tissue culture plates (Cellstar) at 37°C for one hour. Cells were cultured in Dulbecco's Modified Eagle's Medium (DMEM, Highveld Biological Pty. Ltd), 10% foetal calf serum (FCS, Highveld Biological (Pty) Ltd.) or 10% foetal bovine serum (FBS; Highveld Biological (Pty) Ltd.), 1μg/ml insulin, 100 I.U. each of penicillin and streptomycin, in a 37°C/5% CO_2 incubator.

Corneas were harvested from both wildtype and homozygous mutant embryos at E12.5, under sterile conditions as follows. Pregnant mouse embryos were sacrificed by CO_2 inhalation and the embryos removed, transferred to ice-cold PBS and kept on ice for the duration of the dissection. Eyes were isolated and the corneas carefully removed using fine tungsten needles. Under the dissecting microscope, corneas were orientated on coverslips such that the endothelial surface was facing downwards. The explants were left on a droplet of medium for one hour at 37°C/5%CO_2 to allow complete adherence of the explants to the coverslip surface. After this period, the dishes were filled with culture medium and left for 48 hours after which the explants were carefully removed under a tissue culture lamina hood using flamed tungsten needles. Medium was replaced every two days and the cells were cultured for a maximum of 8 days.

2.7.2. Isolation and culture of mouse embryonic fibroblasts

Mouse embryonic fibroblasts were isolated with minor modifications to a previously described protocol (Robertson, 1987). Pregnant ICR mice were sacrificed at either E12.5 or E13.5 and embryos with associated placentae and foetal membranes removed and transferred into PBS (pH 7.4). Embryos were dissected free of placentae and membrane and minced using a sterile razor blade and transferred to a syringe with 10 ml of 0.05% trypsin/0.02% EDTA (Sigma). Cells were dissociated by gently swirling on a rotor for 15 minutes at room temperature. An equal volume of FCS (Highveld Biological Pty. Ltd.) was added to inactivate the

trypsin/EDTA and the mixture was allowed to stand at room temperature for five minutes to allow clumps to settle. The supernatant was transferred to a sterile 50ml plastic centrifuge tube and cells were pelleted by centrifugation at 1000 x g for five minutes at room temperature. Cells were resuspended in 20ml of DMEM (Highveld Biological (Pty) Ltd.) supplemented with 10% FCS and 100 I.U. each of penicillin and streptomycin. Cells were plated in fibronectin-coated coverslips in 24-well plates at 37°C/5%CO_2 as described for culture of primary corneal mesenchyme (section 2.7.1.).

2.7.3. Culture of HeLa cells

Frozen stocks of HeLa cells were thawed at 37°C and mixed 1:1 with culture medium (DMEM, 10%FCS, penicillin and streptomycin). Cells were pelleted by centrifugation and the supernatant discarded. The pellet was resuspended in culture medium, plated in fibronectin-coated coverslips (prepared as previously described) and cultured in a 37°C/5%CO_2 incubator.

2.8. Image analysis and statistical methods

Micrographs from scanning electron microscopy were obtained as follows. For each cornea examined, a whole view was taken and at least three regions representing top, middle and bottom of the corneal surface captured. In most cases, the edge of the corneal surface was also photographed. A whole view of the lens and two or three regions of the anterior lens surface were captured. Images were saved as TIFF files and converted into JPEG format in Photoshop version 5.5. Cell length was estimated as follows. Two data points (in centimetres) were obtained from measurements of the maximum and minimum lengths of the cells, representing horizontal and vertical cell surfaces. These values were then converted to microns, based on the scale of the micrograph. Only the maximum values from each cell were plotted in a graph to estimate the changes in cell length between developmental stages examined. All statistical analyses were performed with Microsoft excel software (Microsoft office 2000).

Immunoflourescence images were captured using either a Zeiss Axiovert 200M fluorescent microscope fitted with an Axiocam High Resolution digital camera using the Zeiss Axiovision software package. *Whole-mount tissues:* The corneal surface was divided into at least four fields of view, representing the entire corneal surface. Images were then taken from each field in black and white and assigned colours in photoshop 5.5.

Cells. The area on which cells were grown on a coverslip was divided into four to six fields of view. Representative images from each field of view were captured and assigned colours in photoshop 5.5.

Chapter Three : RESULTS

Studies on vertebrate corneal development have shown that in avians and mammals, the corneal endothelium is formed as a result of the transformation of mesenchyme that occupies the space between the lens and the prospective corneal epithelium (Beebe and Coats, 2000; Hay and Revel, 1969; Kidson et al., 1999). In the mouse embryo, the ingression of mesenchyme into this space begins at E11.5. Previous studies have not fully described the dynamics involved in the actual process of transformation nor do they reveal, with sufficient accuracy, the exact timing of the process. In this project, a SEM study of the inner corneal surface at various developmental time-points was carried out so that a systematic analysis of cellular shape changes in both wildtype and mutant embryos would be carried out. This chapter can be divided into three parts, based on specific questions addressed in this study. The first part is a detailed analysis of corneal endothelial development in the normal mouse embryo and a comparative analysis of these processes during the development of the corneal endothelium in *Foxc1* mutants. The second part deals with the analysis of intercellular formation during corneal endothelial morphogenesis in both wildtype and mutant embryos. The third and last section is a report on studies performed to monitor the dynamics involved during the formation of intercellular junctions in an *in vitro* model for both wildtype and mutant corneal mesenchyme cells.

3.1. Identification of mouse genotypes

The phenotype of *Foxc1* mutant mice has been previously described (Kume et al., 1998). In brief, *Foxc1*-null embryos are characterised by congenital hydrocephalus and open eyelids at birth. In these embryos, the hydrocephalus is first visible at about E12.5 and is quite prominent by E13.5 as can be seen in Figure 3-1A. Figures 3-1A(A) and 3-1A(B) show a comparison between mutant and normal embryos at E13.5. At this stage, in both normal and mutant embryos the eyelids are still open. As development proceeds, in the normal embryo, the eyelids close at about E15.5 and the pups (Fig. 3-1A,D) are born with closed eyelids. However, *Foxc1* mutant embryos do not close their eyelids and pups are born with open eyelids as shown in Figure 3-1A(C). These characteristics allowed for easy identification of mutant embryos and DNA genotyping was used only for confirmatory purposes. However, genotyping was essential for distinguishing between wildtype and *Foxc1* heterozygotes. To do this, both DNA genotyping and LacZ staining of tail clips were carried out. A result of a typical PCR genotyping analysis is shown in Figure 3-1A(B). Two fragments of 126 and 390bp were amplified. The smaller product indicates the wildtype allele (Fig. 3-1B, lane 2) and the

390bp product indicates the mutant allele (Fig. 3-1B, lane 3). Heterozygotes were identified by the presence of both alleles (Fig.3-1B, lane 4).

A

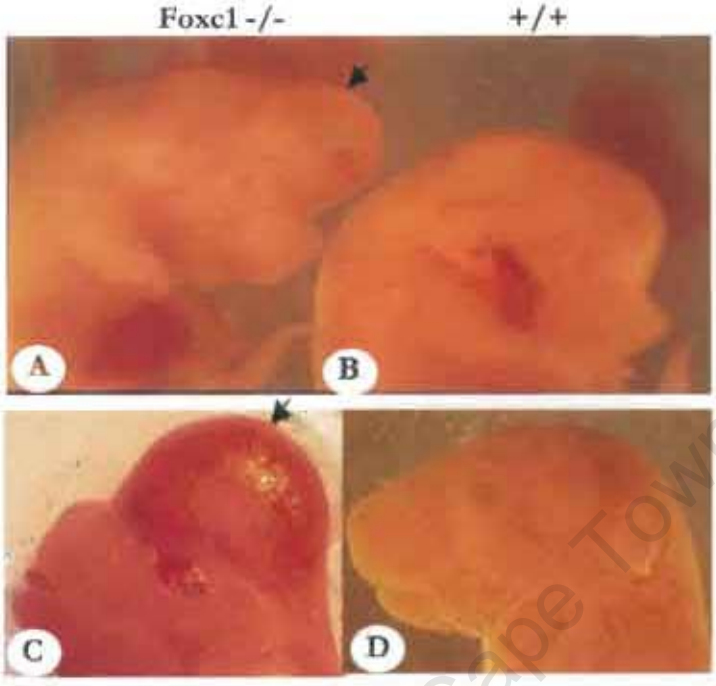

B

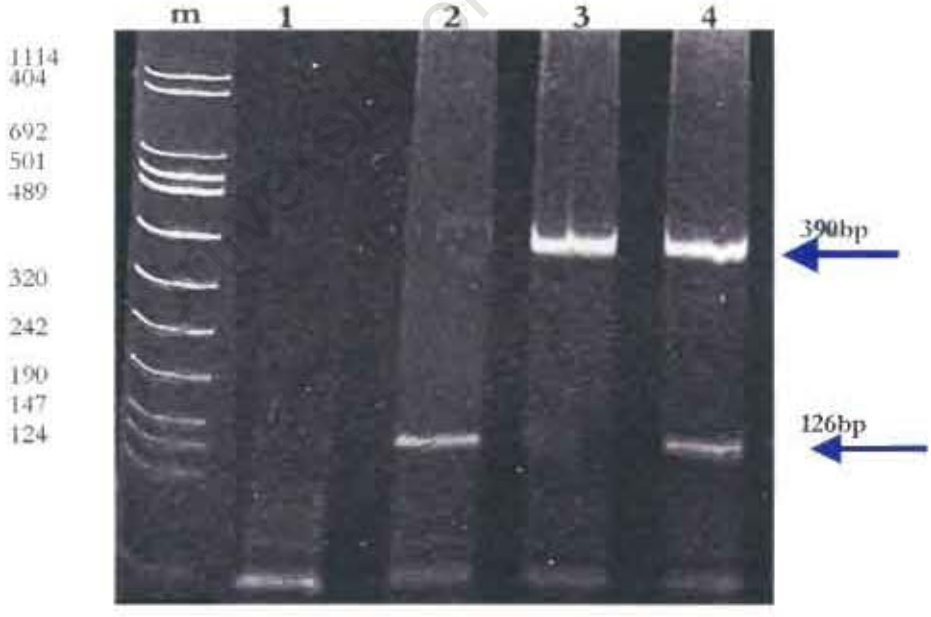

Figure 3-1A. External morphology of *Foxc1* mutant (A, C) and normal (B, D) mice at E13.5 (A, B) and E17.5 (C, D). *Foxc1* homozygous mutants were easily identifiable because of severe hydrocephalus (see A, C, arrows). *Foxc1* homozygotes are born with open eyelids (C), while normal embryos are born with closed eyelids (D). Figure 3-1B. Polyacrylamide gel showing results from a typical PCR analysis. The 126bp band represents the wildtype allele and the 390bp fragment represents the mutant allele. Heterozygotes were identified by the presence of both alleles. m – marker, 1 –negative control, 2 – wildtype; 3 = mutant and 4 = heterozygote.

3.2. Scanning electron microscopy (SEM) of the inner corneal surface during corneal endothelial development

Previous histological and transmission electron microscopy studies have indicated that a continuous corneal endothelium with cell-cell junctions has formed in the normal mouse embryo by E14.5 and that this does not seem to form in the *Foxc1* mutant (Kidson et al., 1999). Since junction formation is dependent on cells making contact with each other, the first question this study addressed was to determine whether this failure is due to a failure of the mutant cells to change shape and therefore not come into contact with each other and be able to initiate junction formation. The question could not be easily answered by examination of serial cross sections only. To get a holistic view of the cellular dynamics during corneal endothelium development, a SEM study was carried out on both wildtype and mutant embryos at E12.5, E13.0, E13.5, E14.0, E14.5, E16.5 and E17.5. Eyes were obtained from embryos at all these stages (Table 2.1), fixed and processed for SEM.

However, during early development *in vivo*, prior to the formation of the anterior chamber, the corneal mesenchyme adheres to the lens capsule via collagenous fibres. The anterior surface of the lens is also covered with perilenticular blood vessels and associated vascular mesenchyme. In order to carry out an analysis of the innermost prospective corneal endothelial cells, it was necessary to separate the prospective cornea from the lens in such a way that the corneal cells did not remain attached to the lens surface. Therefore, a series of pilot experiments was carried out 1) to establish the best way of exposing the inner corneal surface without damage to the cells and 2) to confirm whether or not the exposed cells were indeed the corneal endothelial cells.

The separation of the lens from the cornea prior to fixation proved to be unsuitable because a large number of mesenchyme cells remained attached to the lens. To solve this problem, the separation was performed after fixation, a technique that proved to be advantageous in several ways. Firstly, it minimized the adherence of corneal mesenchyme cells to the anterior lens surface, and secondly, on removal, the lens usually remained attached to the retina, thus exposing and allowing convenient identification of the anterior lens surface. Examination of such anterior lens surfaces from a representative number of lenses at various developmental time points revealed that the lens surfaces were largely free of prospective CE cells (Figs. 3-2B and 3-2D). The corneal surfaces from which the lenses were separated were identified by the morphological appearance of mesenchyme cells and the identification of the surface where the lens was attached to the cornea (Figs 3-2A, 3-2C and 3-2E, dotted lines).

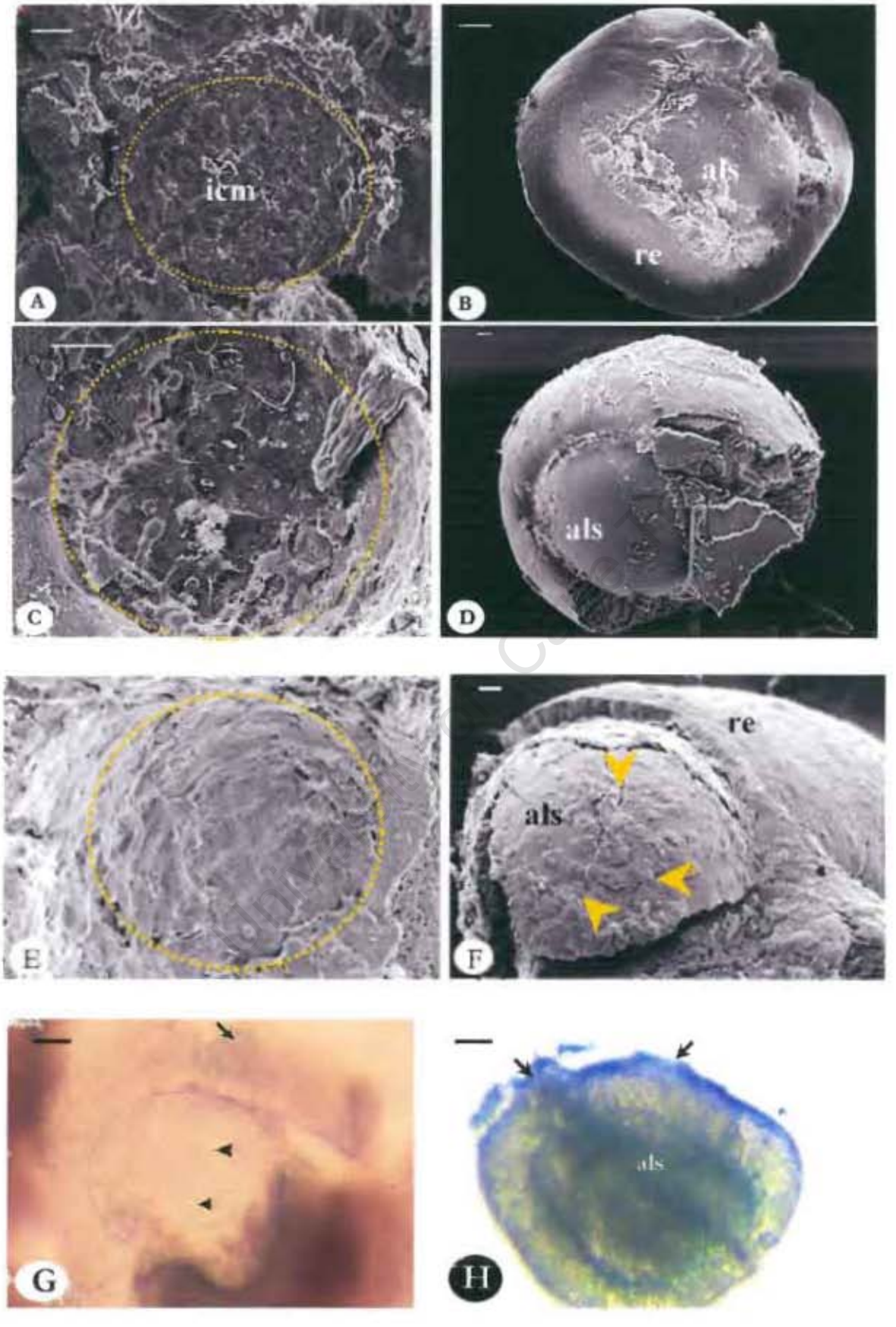
icm
A
als
re
B
C
als
D
E
re
als
F
G
als
H

Figure 3-2. Separation of the cornea (A, C) from the lens (B, D) resulted in exposure of the inner corneal surface (A, C, dotted line). Removal of the lens with the retina (re) attached (B, D) provided a convenient identification of the anterior lens surface (als). The cornea and lens in A and B were harvested from E12.5 embryos, whilst C and D were from E13.0 wildtype embryos. icm = inner corneal mesenchyme. Scale bar: A, B = 30μm; C-D = 20μm. Separation of the cornea (E, G) and the lens (F, H) from eyes obtained from LacZ positive mutant embryos at E12.5. The inner corneal surface (G, dotted line) had some slighltly blue cells on the surface (G, arrowheads). The corneal mesenchyme surrounding the cornea (G, arrows) was LacZ positive. The lens surface (H, als) was diffusely blue (H). The surrounding corneal mesenchyme from outside of the eye region was also LacZ positive (H, arrows). Scalebra: G, H = 100μm.

In the mutants, it was particularly difficult to separate the lens from the cornea because of the very reason that the lens never separates from the cornea *in vivo*. It was thus difficult to establish for certain whether or not, the prospective corneal mesenchyme cells remained attached to the anterior lens surface. In order to address this problem, three approaches were attempted: 1). SEM of the anterior lens surfaces from which the corneas (Figs 3-2A, 3-2C, 3-2E, 3-G) were separated was perfomed. 2) LacZ staining of the separated lens (Fig 3-2H) and corneas (Fig 3-2G) was performed. 3). N-cadherin staining of the corneal surface to mark corneal mesenchyme cells was carried out. Results from the SEM study showed that the lens surfaces from mutant embryos revealed that more cells remained attached to the lens surface (Fig.3-2F, arrowhead) compared to their wildtype littermates (compare with Fig 3-2B, D). LacZ staining of the separated lens and cornea showed that the lens was diffusely blue (Fig. 3-2G). This made it difficult to quantify the amount of mesenchyme cells remaining on the lens surface. However, there were few blue cells on the inner corneal surface (Fig. 3-2H, arrows), suggesting that a proportion of these cells remained on the inner corneal surface. Staining of the corneal surface with an N-cadherin antibody, a marker of corneal mesenchyme cells showed that the inner corneal surface was positive for N-cadherin (Fig. 3-3-11B,D). Examination of the inner corneal surface also showed that there were patches on the inner cornea that did not stain for N-cadherin. These were regions from which the cells had remained attached to the lens surface and exposed the underlying corneal mesenchyme. In these region, cells were not N-cadherin positive (Fig. 3-11B, D circles and Fig. 3-12B, D, circles). All of these results (SEM, LacZ, and N-cadherin staining) suggested that a proportion of corneal mesenchyme cells were on the corneal surface. These results thus paved the way for further investigations into mesenchyme-epithelial transformation on the inner corneal surface. In most cases, at all stages of development, the innermost layer of the corneal cups and their respective lenses were examined using SEM.

3.3. Changes in morphology of corneal endothelial cells during morphogenesis

In order to investigate the cellular changes involved in establishment of a monolayered corneal endothelium in the normal embryos, SEM was used. This process was compared to mutant embryos in order to gain insights into the nature of developmental defects associated with corneal endothelium differentiation in *Foxc1* mutants. For wildtypes, embryos at E12.0, E12.5, E13.0, E13.5, E14.0, E14.5, and E17.5 were studied, while for *Foxc1* mutants, embryos at E12.5, E13.5 and E17.5 were studied. In the wildtype cornea at E12.0, soon after the early migrating cells have occupied the space between the lens and the cornea, the inner corneal surface appeared as a meshwork of irregularly arranged stellate shaped cells (Fig. 3-3A-D). The

diameter of the inner corneal surface (Fig. 3-3A and 3-3B) was between 110 to 165µm (n= 6,). On average, each cell was about 15µm in length (see Fig. 3-10A) and had long extensions that overlapped at certain points. Cells appeared fibroblastic with lamellopodia (l) and filopodia (f), typical of migrating cells (Fig. 3-3D, arrows). Fine fibrils presumably, collagen (col,) were observed in the intercellular spaces between mesenchyme cells (Figs. 3-3B and 3-3D). A few dividing cells could be seen (Fig. 3-3B, arrowheads). Variations in the morphology of mesenchyme cells were observed within and between littermates. In some cases, mesenchyme cells appeared slightly more flattened than others (compare Fig. 3-3B and Fig. 3-3D which were obtained from different litters). This heterogeneity could be a result of differences in mouse mating times and slight differences in the rate of early embryonic development. Nonetheless, it was clear that at this stage mesenchyme cells appeared loosely arranged across the entire corneal surface.

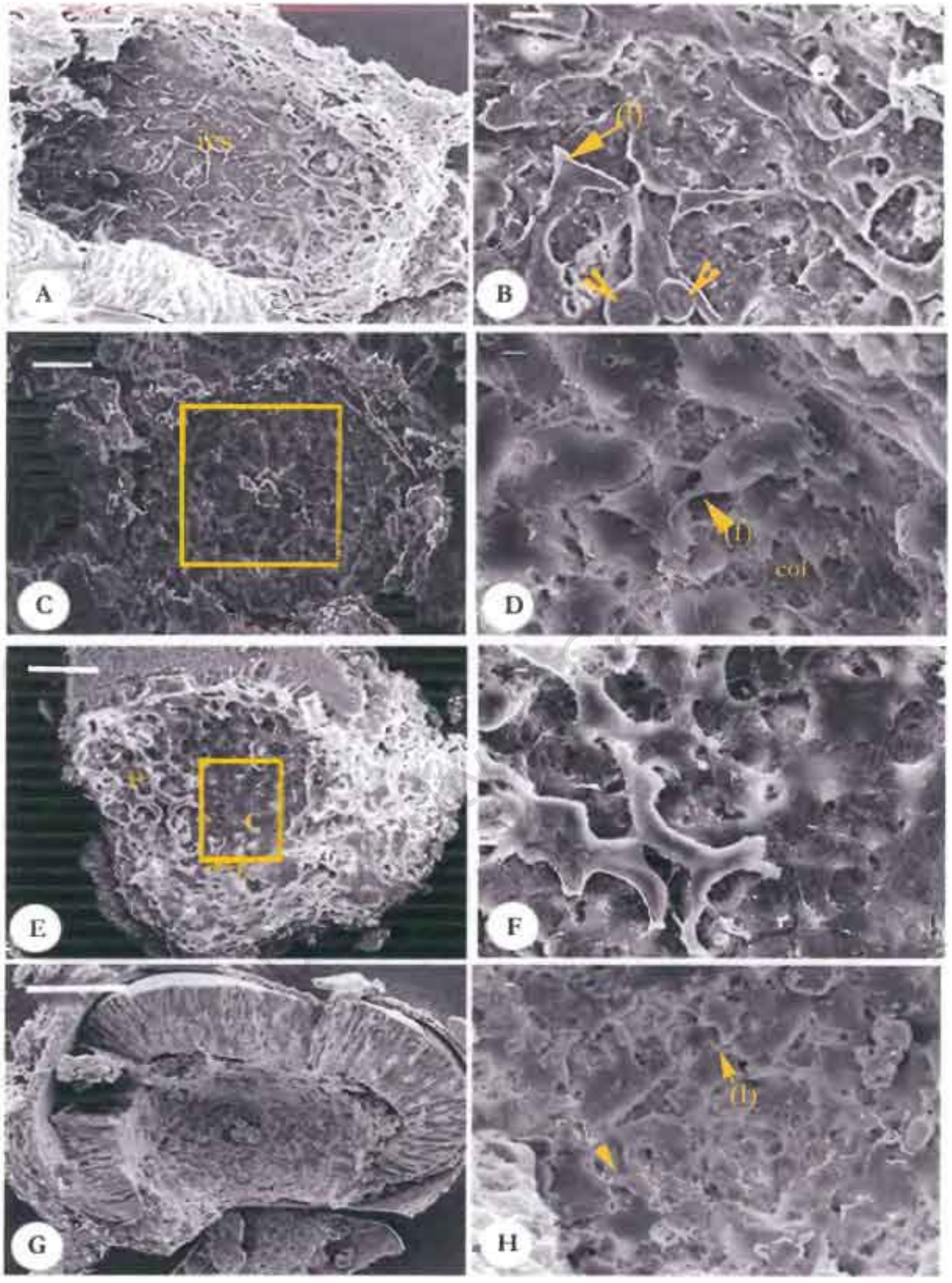
A
B
C
D
E
F
G
H
col

Figure 3-3. Surface morphology of the corneal endothelium in wildtype at E12.0 (A-D) and E12.5 (E-F) and *Foxc1* mutants at E12.5 (G-I). At E12.0 in the normal embryo, presumptive corneal endothelial cells appear as a meshwork of irregularly arranged mesenchyme cells (A, ics). The two figures (A) and (C) represent corneal meshwork from two different litters showing variations in the extent of cell flattening. Figures B and D show high magnification of the boxed areas in A and C. Fine collagen fibres (col) are intermingled with cells and a few dividing cells can be seen (B, arrowheads). A comparison of corneal mesenchyme between wildtype (E, F) and *Foxc1* mutant embryos (G, H, I, J) at E12.5 shows that in the wildtype, cells at the centre of the cornea (c) are more flattened compared to the peripheries (p). Figure F and H are higher magnification images of the boxed areas from E and G respectively. In the mutant, the extent of cell flattening is uniform throughout the entire corneal surface. Cells have numerous lamellopodia (l) (H, arrows) and very few filopodia. ics = inner corneal surface. Scale bar: A, C, E, G, I =30μm; B, D, F, H, J = 2μm.

At E12.5, the corneal endothelial surface was still made up of loose mesenchyme cells with interspersed collagen. In some corneas, the central cells were more flattened with less intercellular spaces and there was a clear difference between the central (c) and the peripheral (p) corneal cells (Fig 3-3E). The cells at the periphery were fibroblastic in shape with large intercellular spaces (Fig. 3-3F). These cells are the presumptive mesenchyme of the future angle structures of the eye, which will develop into the trabecular meshwork. The maximum length of the corneal cups increased to about 176μm (ranging from 120 to 176μm), indicating that while individual cell flattening occurred, proliferation contributed to the expansion of the corneal cup as shown in previous studies using BrdU labeling (Kidson et al., 1999). Corneas from *Foxc1* mutant mice were also examined at E12.5 (Fig. 3-3G). The cells were generally flattened and loosely arranged (Fig. 3-3H). In these mutant embryos, unlike the wildtype embryos, the central cells were not different to the peripheral cells (see Figs. 3-3G-H). The degree of cell flattening was uniform across the entire surface in both corneas examined (Figs. 3-3G-J). The diameter of the corneal surface was about 160μm (n=2) and the average maximum cell length 14μm (Fig. 3-10).

At E13.0 in the normal embryo, there was a marked difference between the center (Fig. 3-4C) and the periphery (Fig. 3-4D) of the cornea. The central cells were flattened and overlapping in a somewhat uneven manner (Fig. 3-4C). At the periphery, cells were interspersed with fine collagen fibres in between the intercellular spaces (Fig. 3-4B and 3-4D). The average corneal cup diameter was about 167μm (n= 6, ranging from 156 to 185μm). Cell length was about 10μm on average, ranging from 8μm to about 14μm (Fig. 3-10).

At E13.5 in the normal embryo, corneal mesenchyme cells appear either as "hillocks" across most of the inner corneal surface (Fig. 3-5A and 3-5B) or as a flattened layer with cell-cell borders that are more pronounced at the center of the cornea (not shown). Corneal cup diameter increased to an average of 194μm (n= 6) and the average maximum cell length was about 10μm (Fig. 3-10). At E13.5 in the *Foxc1* mutant, the separation of the cornea (Fig. 3-5C) from the lens (Fig. 3-5D) revealed an extensive vascularization of the lens surface (Fig. 3-5F, bv). Some blood cells were seen intermingled with corneal mesenchyme (Fig. 3-5E, rbc, arrows). The pattern of cell flattening was very different to that of the wildtype littermates. There were small intercellular spaces and no cell-cell borders were visible (Fig. 3-5E). The average diameter of the corneal surface was 185μm (n=2) while the average maximum cell length was about 9μm (Fig. 3-10).

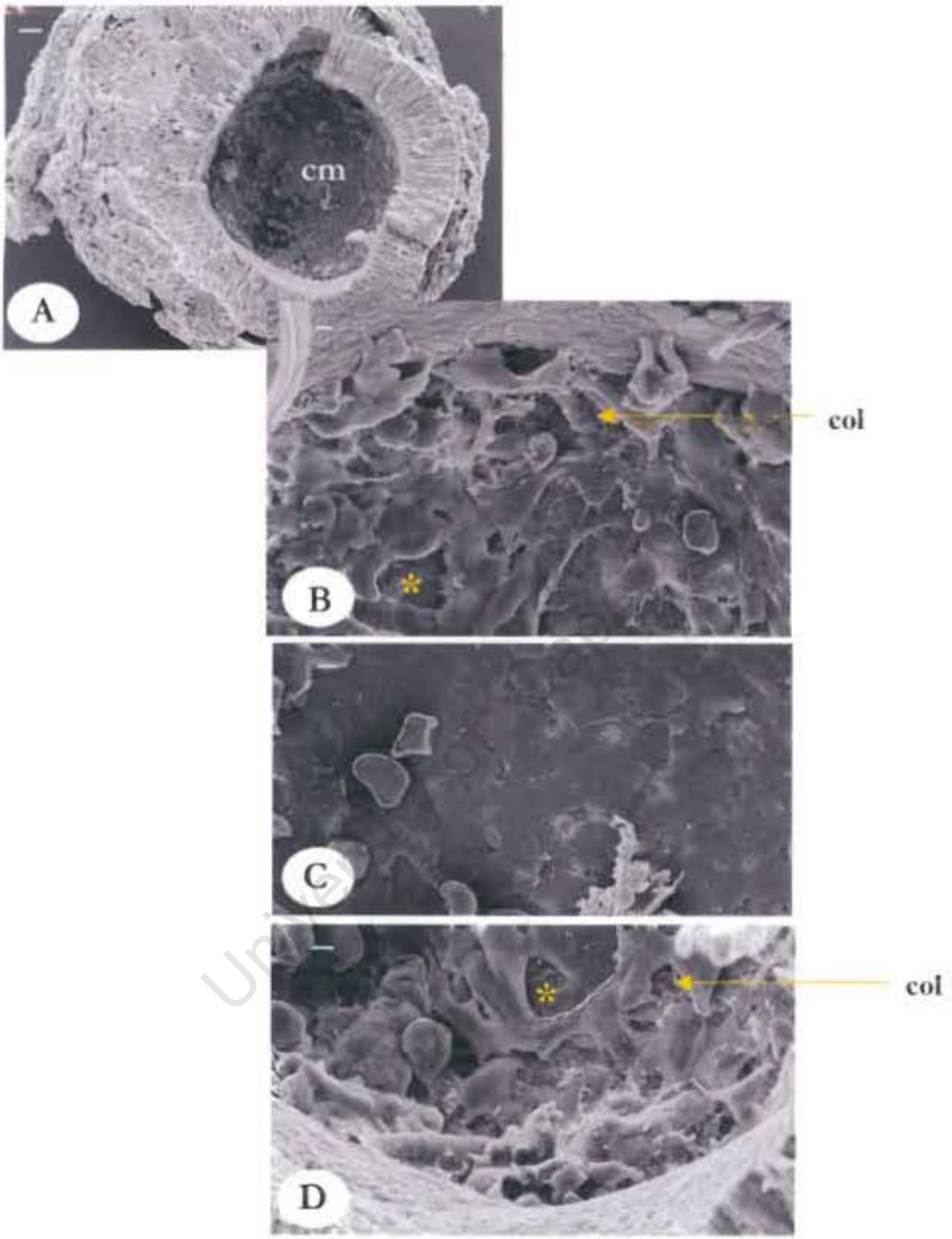

Figure 3-4. Surface view of the inner corneal surface at E13.0 in the normal embryo. Figures B-D represent three regions taken from top middle and bottom of the inner surface of the cornea A. The central region of the corneal endothelium (C) appears more flattened compared to the peripheries - B (edge), (D) bottom. Larger intercellular gaps (B, D, asterisks) and fine collagen fibres (col) can be seen along the peripheral regions. Number of corneas examined = 8. Scalebar A = 20μm; B - D = 3μm.

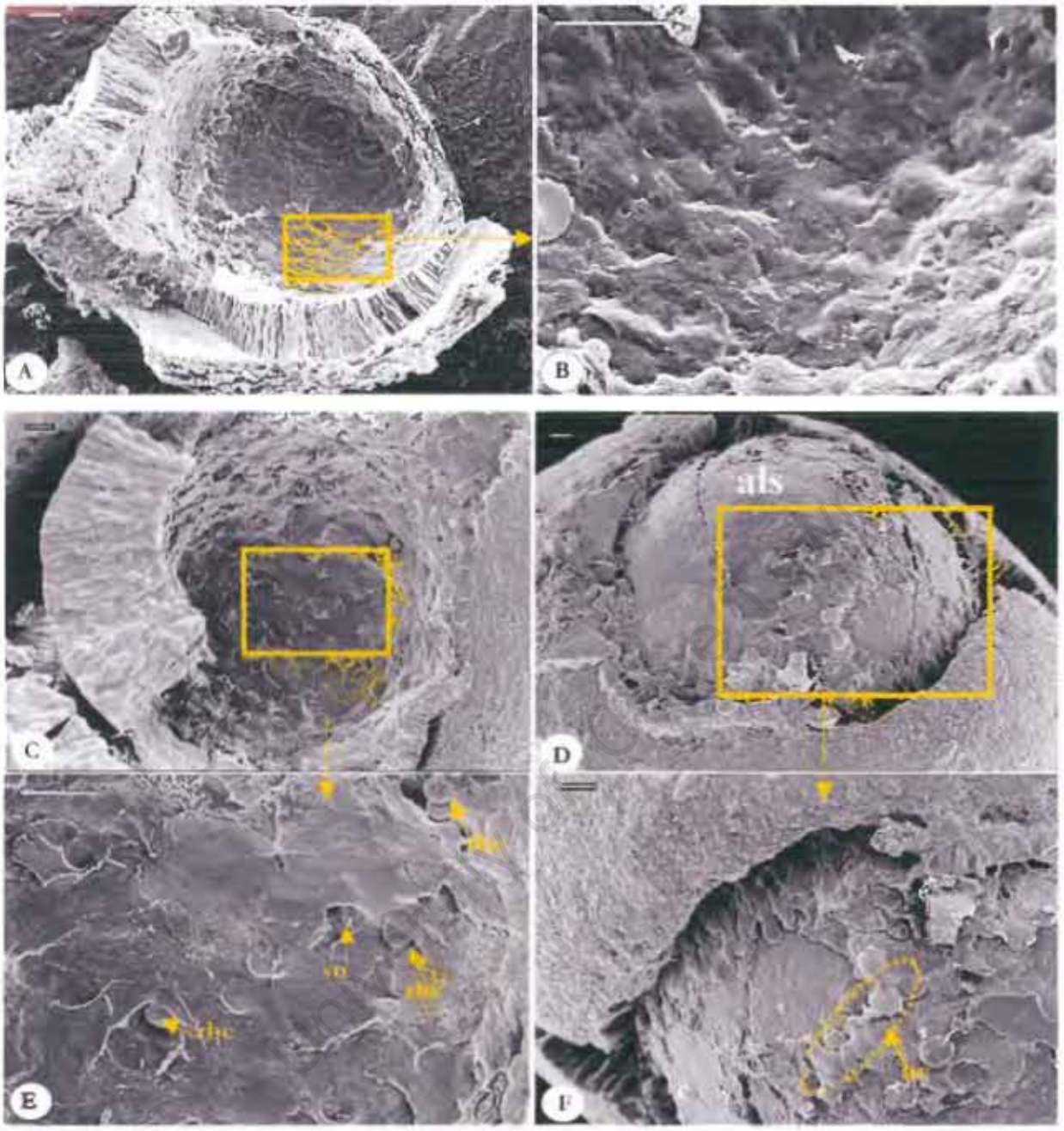

Figure 3-5. Surface morphology of the inner corneal (A, C) and the lens surface (D, F) in wildtype (A, B) and *Foxc1* mutants (C-F) at E13.5. In the wildtype (n=31), the inner corneal surface appeared flattened with no intercellular spaces visible between the cells (A). Close examination of the cells near the centre of the cornea appeared as "hillocks" (B). In the mutant (n=3), corneal mesenchyme cells have clearly flattened but intercellular spaces (E, sp) still visible. Red blood cells (rbc) can be seen between the intercellular spaces (E, arrows). Some cells are attached to the anterior lens surface (als) intermingled with blood vessels (bv) on the surface of the lens (F, arrow) scalebar = 20μm.

At E14.0 in the wildtype, the inner corneal surface (Fig. 3-6A) was uneven. At the center, intercellular borders were visible (Fig. 3-6E, arrows). Cells at the peripheral regions were more flattened than at the previous stage, but intercellular spaces still visible (Fig. 3-6C, asterisks). The average corneal endothelial diameter was about 250μm. Distinct intercellular junctions were apparent at E14.5, and there was complete loss of intercellular spaces along the entire corneal surface (Fig. 3-6B and 3-6F). At the angle of the eye, between the sclera and the cornea, the adjoining iris strands could be seen as overhanging mesenchyme (Fig. 3-6D, irm). At this stage, the average corneal cup diameter in the normal embryo increased dramatically to 320μm (n = 4) and the maximum cell length was 11.29μm ranging from 8.4μm to 14.5μm.

Examination of the corneal surface in the normal embryonic eye at E17.5 showed that the corneal endothelial cells formed a monolayer with very distinct intercellular borders. The cells were irregular in size, ranging between 10μm and 14μm. The corneal cup (Fig. 3-7A and 3-7B) increased in size compared to the previous stage and the average corneal cup diameter was 470μm (n = 3). The corneal endothelial cells showed several burst vesicles (Fig. 3-7C, arrows). This bursting of the vesicles was most likely a processing artifact, as confirmed by absence of such bursting in samples that were cryofixed and viewed by SEM (Mlumbi T, unpublished Honours project, UCT, 2000).

Due to the delicate nature of the corneal endothelium, the surface was easily torn off during dissection, thus revealed the underlying corneal stroma with bundles of collagen fibres arranged in swirls (Fig. 3-7A and 3-7E, col). Close examination of the lens (Fig. 3-7D) that was separated from the cornea in Figure 3-7B, showed that the anterior lens surface was richly supplied with perilenticular vessels. Red blood cells could be seen (Fig. 3-7F, arrowheads). In the mutants, the separation of the cornea (Fig. 3-8A) from the lens (Fig. 3-8B) resulted in a significant number of cells adhering to the anterior lens surface (Fig 3-8B, als). There was no defined endothelial border that separated the corneal endothelium from the outer scleral region, instead a porous mass of mesenchyme (Fig. 3-8A, cm) was observed on the corneal surface and also adhered to the lens surface (Fig. 3-8B, cm). Higher magnification of the corneal region from which the lens was attached in Fig. 3-8A, showed that the mutant corneal endothelial cells were extremely flattened and slightly overlapping cells with no interconnecting junctions at this stage (Fig. 3-8C). Examination of the anterior lens surface (als) also showed extremely flattened cells with no apparent intercellular borders (Fig. 3-8D). These mutant corneal mesenchyme cells were still separated by large spaces and were an average maximum length of 21μm.

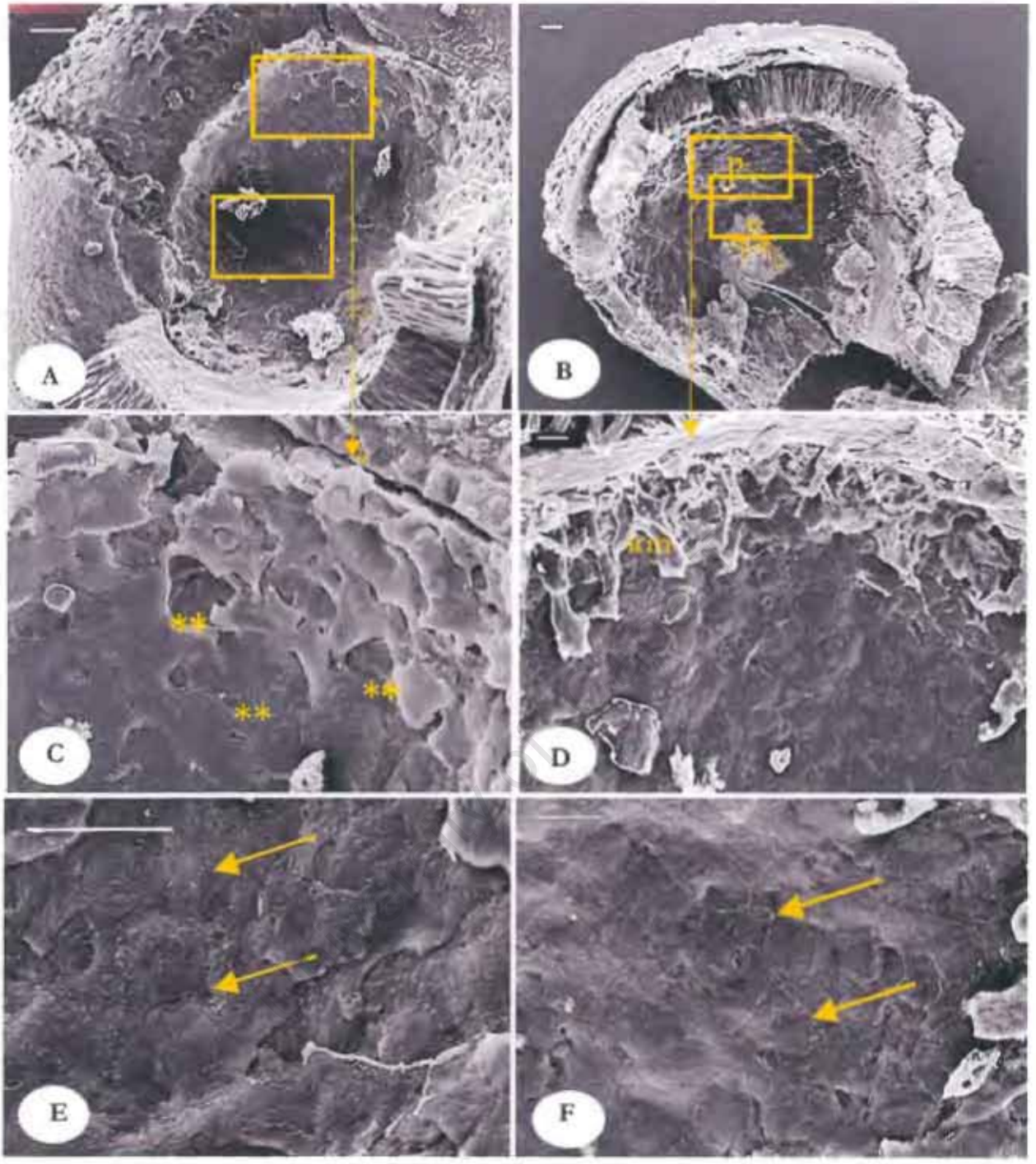

Figure 3-6. Surface view of the corneal endothelium at E14.0 (A, C, E) and E14.5 (B, D, F) in wildtype embroys. At E14.0, the corneal endothelial cells have flattened throughout the surface creating an uneven monolayer of cells (C, E). At the peripheral regions, a few intercellular spaces are still visible (C, asterisks). Number of corneas examined = 12. At E14.5, distinct intercellular junctions are visible across the entire endothelial surface from the periphery (D) to the centre (F, arrows). Along the peripheries, at the angle of the eye, iris mesenchyme (irm) cells can be seen (D) n = 9. Scalebar: A-B= 20μm; C-F = 10μm.

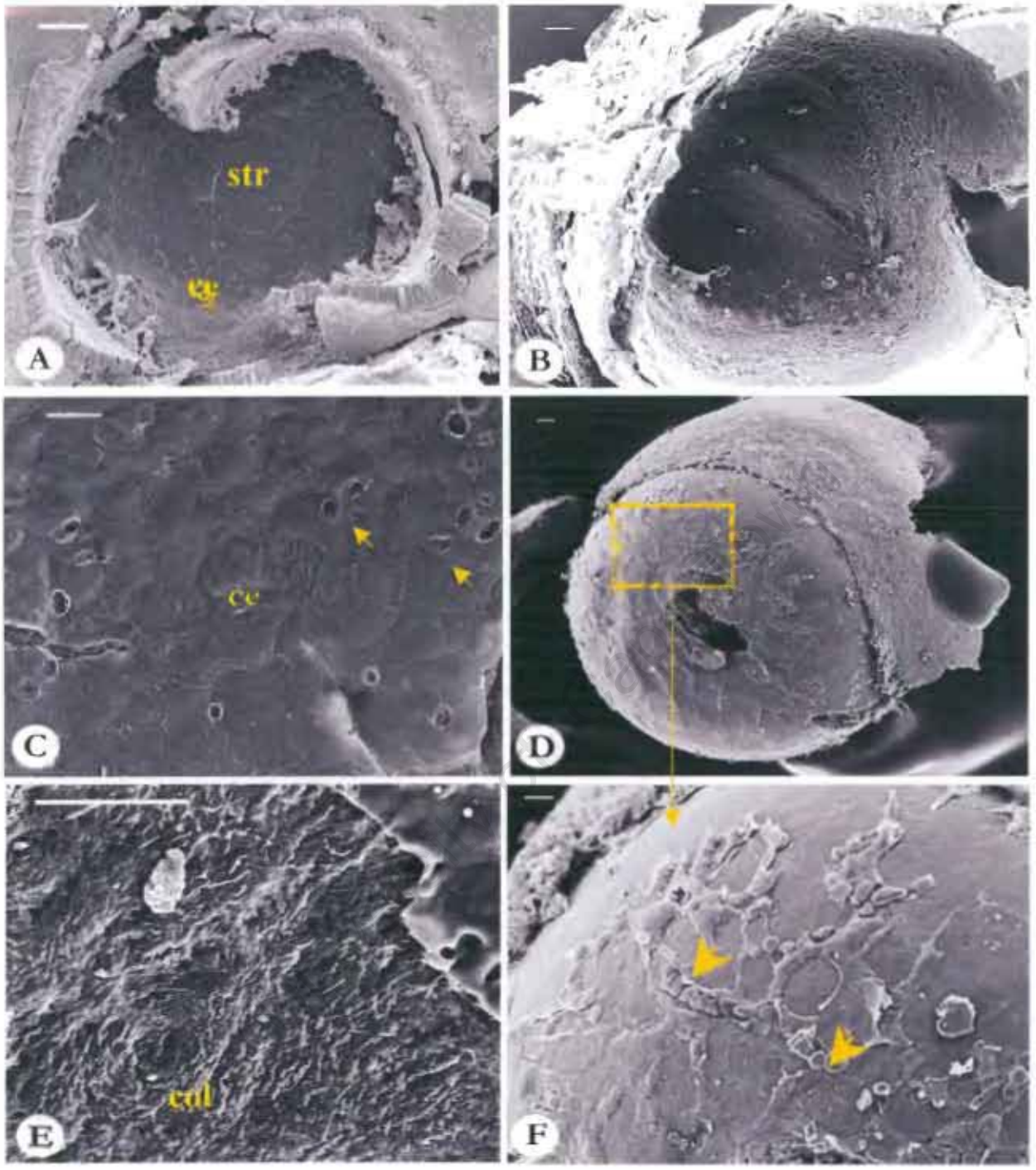

Figure 3-7. Surface view of the corneal endothelium in the wildtype embryo at E17.5. Corneal cups (A and B) were harvested from two different embryos. In A, the corneal endothelial surface was scrapped off at the centre (c) of the cornea to expose the underlying corneal stroma (str) in which collagen bundles occur as swirls (E, col). Cells of the corneal endothelium form a cobblestone pattern but appear irregular in size (C, ce). The lens in D was separated from the cornea in B. Examination of the lens surface reveals the presence of lenticular blood vessels nourishing the embryonic lens surface. A few open blood vessels show the inner red blood cells (rbc) (D, F arrowheads). Scalebar: A-B = 30µm, C-F = 10µm. Number of corneas examined = 8.

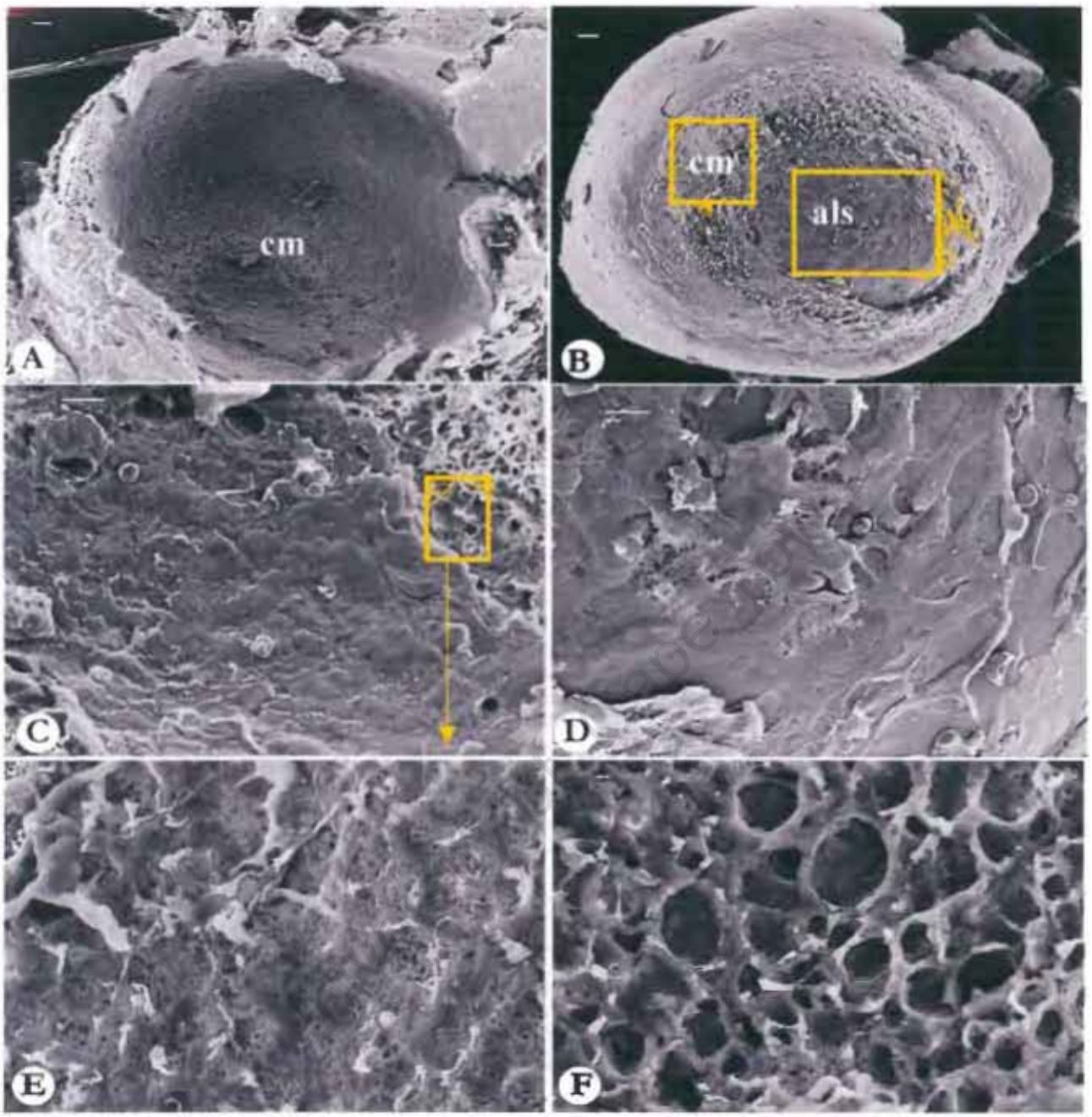

Figure 3-8. Scanning electron micrographs of lens and inner corneal surfaces from E17.5 mutant embryos. The lens (B) was separated from the cornea (A) to expose the inner corneal surface. A large region of the corneal endothelium was occupied by loose collagenous matrix and only a small region into which the lens surface was attached showed few flattened cells (C). Examination of the anterior lens surface (B, als) revealed that mesenchyme cells remained attached and displayed a fibroblastic morphology with no apparent cell-cell borders. Red blood cells (rbc) were seen intermingled with cells (D). The region surrounding the inner corneal surface appeared as a porous matrix of cells intermingled with collagen (E). Higher magnification of the loose collagenous matrix (cm) of the cornea and on the lens surface is shown in F. Scalebar: A-B = 20μm; C-D = 10μm; E-F = 1μm. Number of corneas examined = 2.

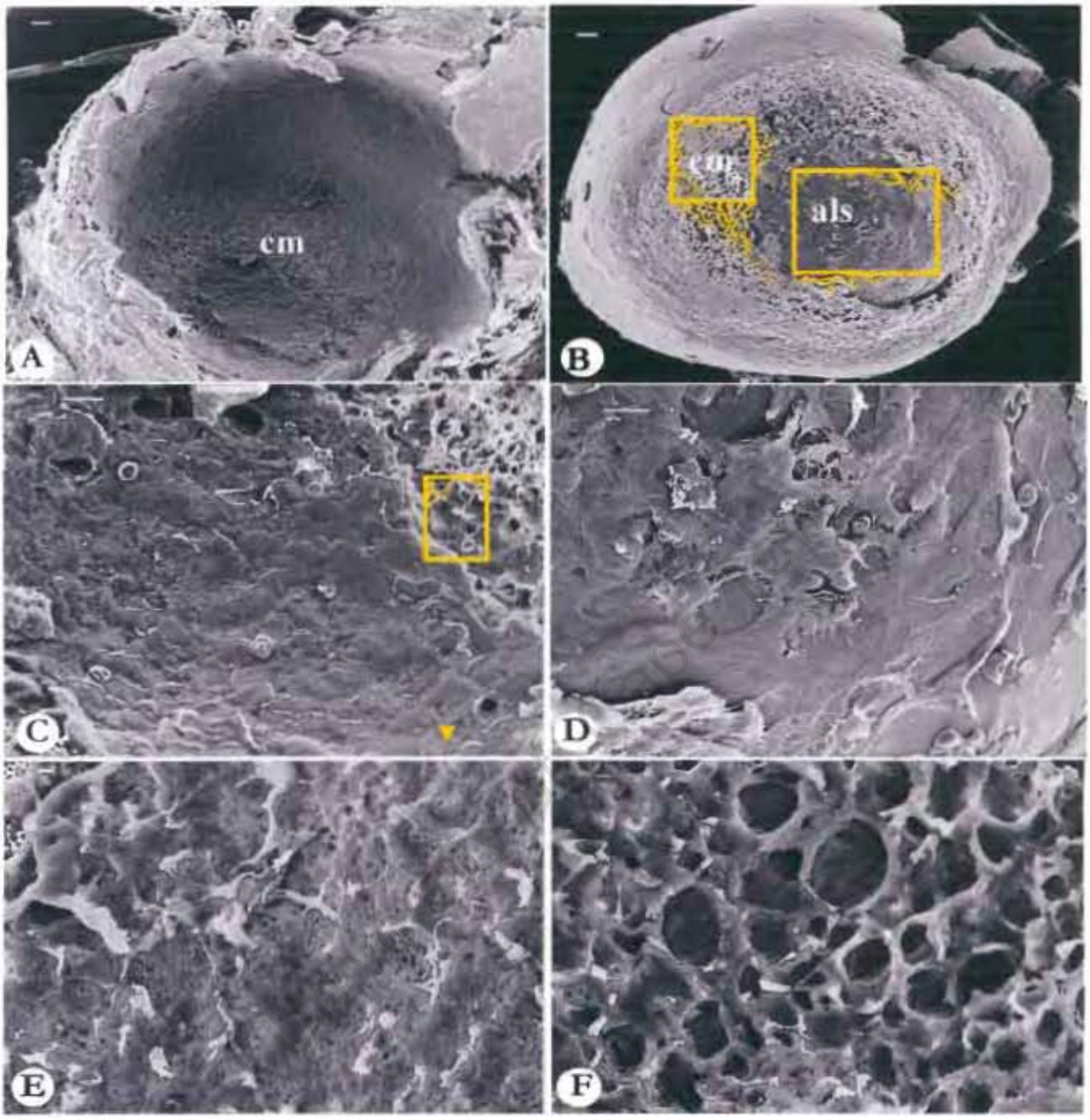

Figure 3-8. Scanning electron micrographs of lens and inner corneal surfaces from E17.5 mutant embryos. The lens (B) was separated from the cornea (A) to expose the inner corneal surface. A large region of the corneal endothelium was occupied by loose collagenous matrix and only a small region into which the lens surface was attached showed few flattened cells (C). Examination of the anterior lens surface (B, als) revealed that mesenchyme cells remained attached and displayed a fibroblastic morphology with no apparent cell-cell borders. Red blood cells (rbc) were seen intermingled with cells (D). The region surrounding the inner corneal surface appeared as a porous matrix of cells intermingled with collagen (E). Higher magnification of the loose collagenous matrix (cm) of the cornea and on the lens surface is shown in F. Scalebar: A-B = 20μm; C-D = 10μm; E-F = 1μm. Number of corneas examined = 2.

In the normal adult mouse eye (>6 weeks old), the separation of the cornea (Fig. 3-9A) from the lens was fairly easy due to the bigger size of the eye and that the anterior chamber was already formed and thus the cornea not adherent to the lens surface. The corneal endothelial cells were more regular in size with distinct intercellular borders (Fig. 3-9B). The average maximum diameter was 3mm (n = 4, ranging from 2 – 4mm).

To obtain quantitative information on the cell flattening process, changes in the maximum length of corneal mesenchyme cells were measured at various developmental stages. In the normal embryo, the average cell length declined from 16μm at E12.0 to 11μm at E12.5 and 9μm at E13.0 (Fig. 3-10). From E14.5, the length slightly increased to 11μm. At E17.5 the average cell length was 10μm and 13μm in the adults. Comparison of maximum cell length between littermates (wildtypes and homozygous mutants) at E12.5 – E17.5 showed that the mutant cells remained longer. On average, the maximum cell length (21μm) of the mutants exceeded that of wildtypes at E17.5 (about 13μm) (Fig. 3-10). The next step was to determine the relationship between cell shape changes and the expression of proteins associated with adherens and tight junction assembly, cadherins and zonula occludens-1 (ZO-1) respectively.

3.4. Junction Formation and cell shape changes during corneal endothelium development

The shape changes from stellate to interconnected squamous cells during mesenchyme-endothelial conversion suggested significant alterations in intercellular adhesion properties of the cells, as judged by the formation of intercellular borders. To characterize the molecular changes that accompany cell shape change during the transformation of mesenchyme to endothelium, the expression pattern of the adherens junction protein, N-cadherin was monitored. Corneas were harvested from wildtype embryos at E12.5, E13.5, E14.5, and E15.5 and from mutant embryos at E12.5, E13.5 and E15.5. Cadherin expression between mutant and wildtype neonates was compared at postnatal day 0 (P0). The temporal and spatial analysis of the tight junction protein, ZO-1, was also monitored in the wildtype embryos at selected developmental stages beginning from E12.5 to the adult (E12.5, E13.5, E14.5, P0 and adult). The expression of ZO-1 was also investigated in the mutants at E12.5, E13.5, E14.5 and E17.5). For these analyses, corneas were separated from whole eyes after fixation and processed for immunoflourescence as described in Materials and Methods (section 2.5.1).

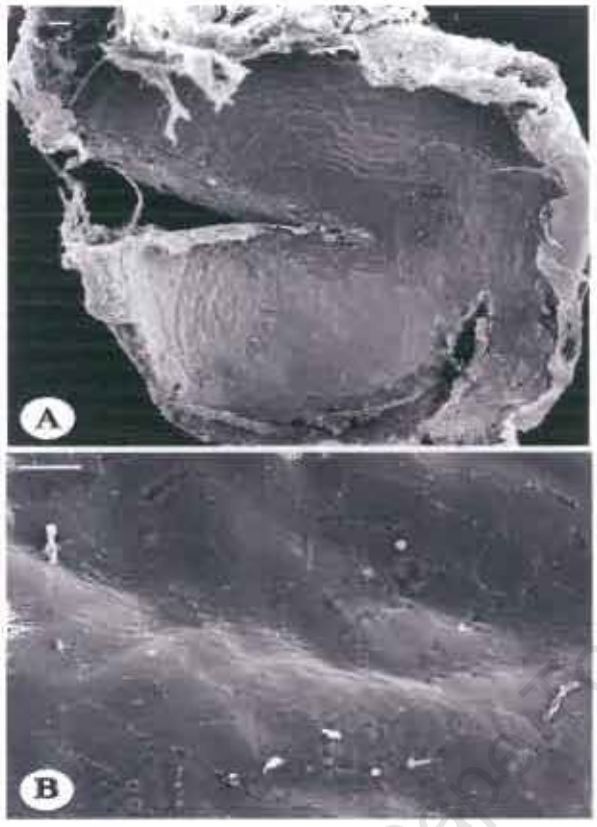

Figure 3-9. Surface morphology of the corneal endothelium in the wildtype adult mouse. Corneal cups harvested from adult mouse eyes were processed for SEM. The presence of a well-developed anterior chamber facilitated the separation of the cornea from the lens thus revealing the inner corneal surface (A). Examination of the corneal endothelial surface revealed a monolayer of hexagonal cells. All cells are interconnected and are regular in size (B). Scale bar: 10μm. Number of corneas examined = 8.

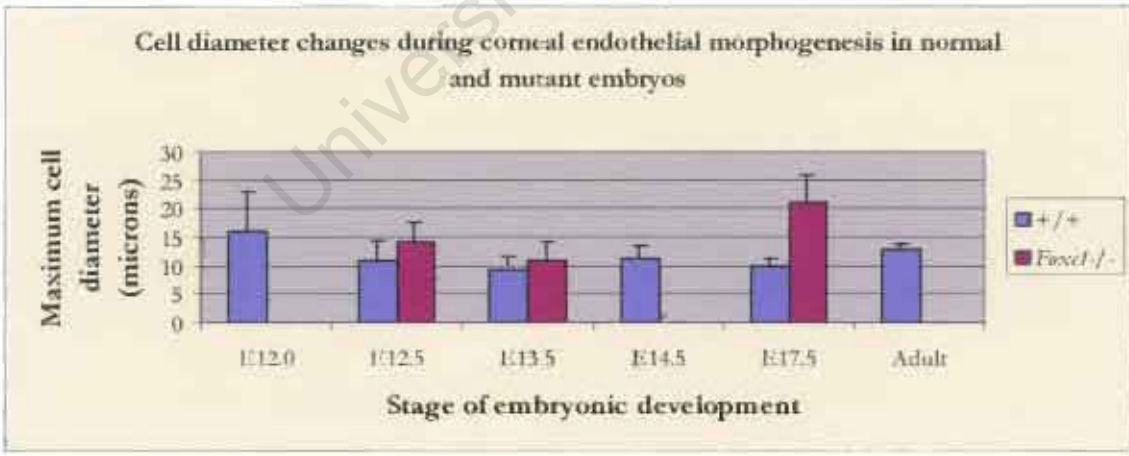

Figure 3-10. Changes in diameter of cells during corneal endothelium development. At E12.0 soon after ingression of cranial mesenchyme into the lens/corneal space, the average length (maximum) of cells is 16 microns, ranging from 9μm to 25μm. This declines at E12.5 to 11.4μm. The diameter of cells remains relatively constant between E12.5 – E17.5. No significant differences in cell diameter were observed between E14.5 – E17.5. Comparison of cell length between wildtype and mutants shows that mutant cells remain taller than wildtype cells at E13.5-E17.5. The difference in length is greatest at E17.5 in which the mutant cells are 21.1μm average length compared to 14.2μm of the wildtype.

At E12.5 in the normal embryo (n = 9), N-cadherin occurred as brightly staining spots with no clearly defined pattern (Fig. 3-11A). In addition, a more diffuse general background staining was observed (Fig. 3-11A). This punctate pattern was similar to that obtained from mutant corneas at this stage (n = 5, Fig. 3-11B). At E13.5, in both wildtype (n= 6) and mutant corneas (n = 4), the punctate pattern of N-cadherin persisted and appeared to be intracellular (Fig. 3-11C and Fig. 3-11D).

At E14.5, a faint plasma membrane localization of N-cadherin was observed (see Fig 3-11E, arrow). This was accompanied by brightly staining perinuclear N-cadherin spots (n= 8, Fig. 3-11E). In order to investigate the exact localization of these spots, dual labeling with phalloidin was performed. F-actin staining was pericellular (Fig. 3-11G and 3-114H). In the mutant, N-cadherin was seen as brightly staining cytoplasmic spots (Fig. 3-11F), suggesting that these cells failed to form adherens junctions.

The expression of N-cadherin was also examined at E15.5 and compared with that of the mutant. In the normal embryo, N-cadherin formed a continuous band along the cell membranes (n = 3, Fig 3-12A), a pattern that was also observed at postnatal day (P0) 0, (Fig. 3-12C). In the mutant, neither at E15.5 nor at P0, no plasma membrane localization of N-cadherin was observed. Brightly staining perinuclear rings were observed (n= 3, Fig. 3-12B and 3-12D). In areas where cells had remained adhered to the lens surface, the underlying stroma was exposed and showed no N-cadherin localization (Fig. 3-12B, asterisks).

In the adult, N-cadherin was observed at cell-cell borders and in the cytoplasm of the cells (Fig. 3-12E and Fig. 3-12F). In the cytoplasm, the N-cadherin was either perinuclear Fig. 3-12E, arrows) or in cytoplasmic vesicles near the membrane (Fig. 3-12F, arrows).

ZO-1 protein expression during corneal endothelial morphogenesis was also investigated in wildtype and mutant cornea. At E12.5, no ZO-1 protein was detected (n = 6, Fig. 3-13A). A discontinuous staining pattern at the plasma membranes was observed at E13.5 (n = 8, Fig. 3-13B). The staining pattern became intense and continuous at E14.5 (n = 8, Fig. 3-13C), similar to that displayed in the adult corneal endothelium (Fig. 3-13D). The expression of ZO-1 was not detected in *Foxc1* mutant corneas at any of the stages examined.

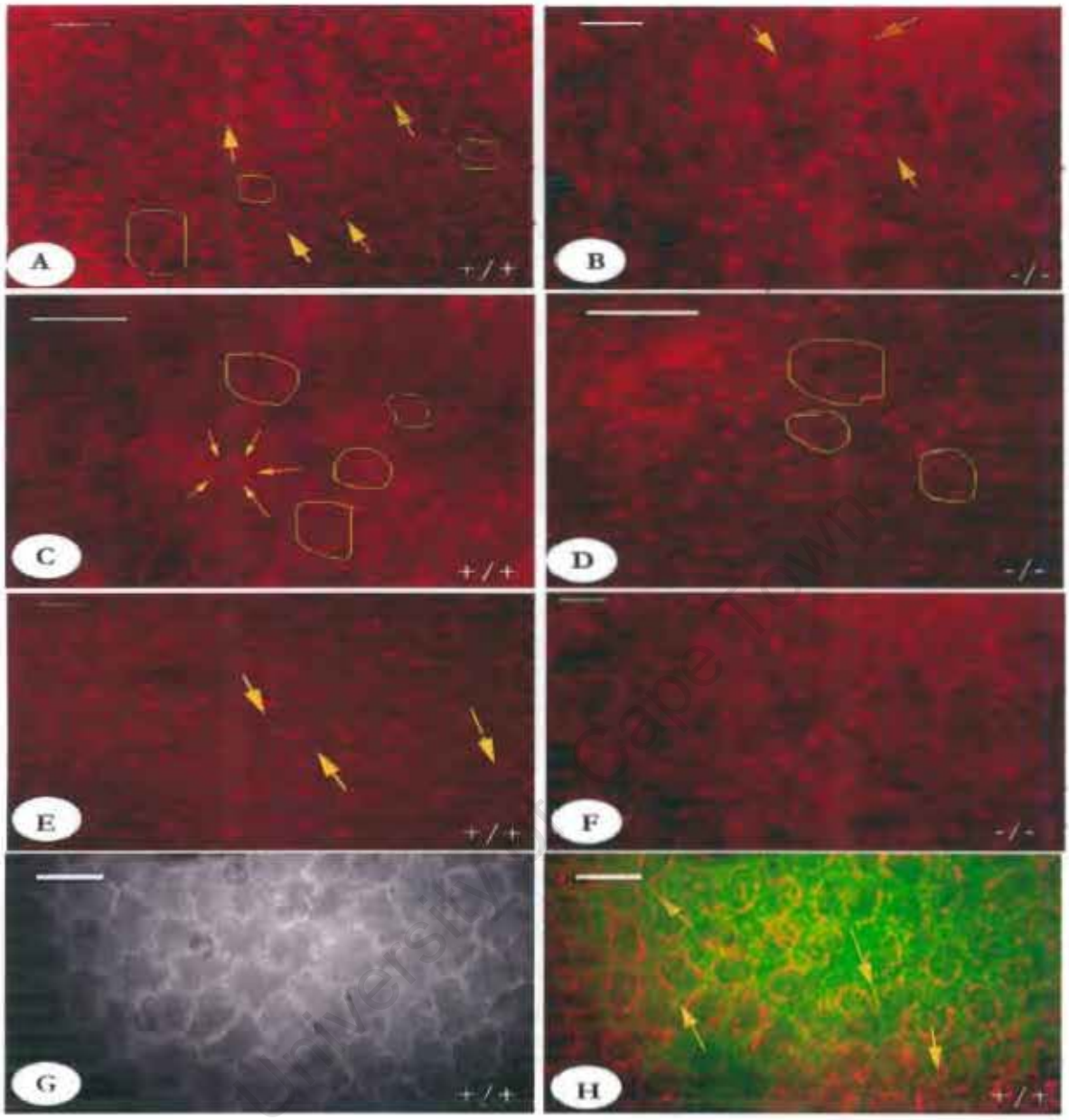

Figure 3-11. Immunofluorescence images showing the expression of N-cadherin on the developing corneal endothelium in the wildtype at E12.5 (A), E13.5 (C), E14.5 (E) and mutants at E12.5 (B), E13.5 (D) and E14.5 (F). Corneas at E14.5 in the wildtype corneas were co-immunostained for N-cadherin and F-actin (G, H). At E12.5, N-cacherin was detected in intracellular vesicles in both the wildtype and mutant cells (A and B, arrows and circles). At E13.5, the N-cadherin appeared as bright intracellular spots in the cytoplasm and at membranes of cells in both wildtype and mutant inner corneal mesenchyme (C, D, circles). At E14.5 in the normal embryo, N-cadherin pattern was perinuclear with faint plasma membrane localization (E, H, arrows). In the mutant, no plasma membrane localization of N-cadherin was observed. N-cadherin staining was still seen as bright perinuclear spots (F). In the wildtype, F-actin formed continuous pericellular bands at E14.5 (G). Co-immunostaining with N-cadherin at this stage shows an overlapping pattern at the plasma membrane where adherens junctions have been made (H, arrows). In this Figure, N-cadherin was visualised as a bright perinuclear signal (H, red) Scale bar: 20μm.

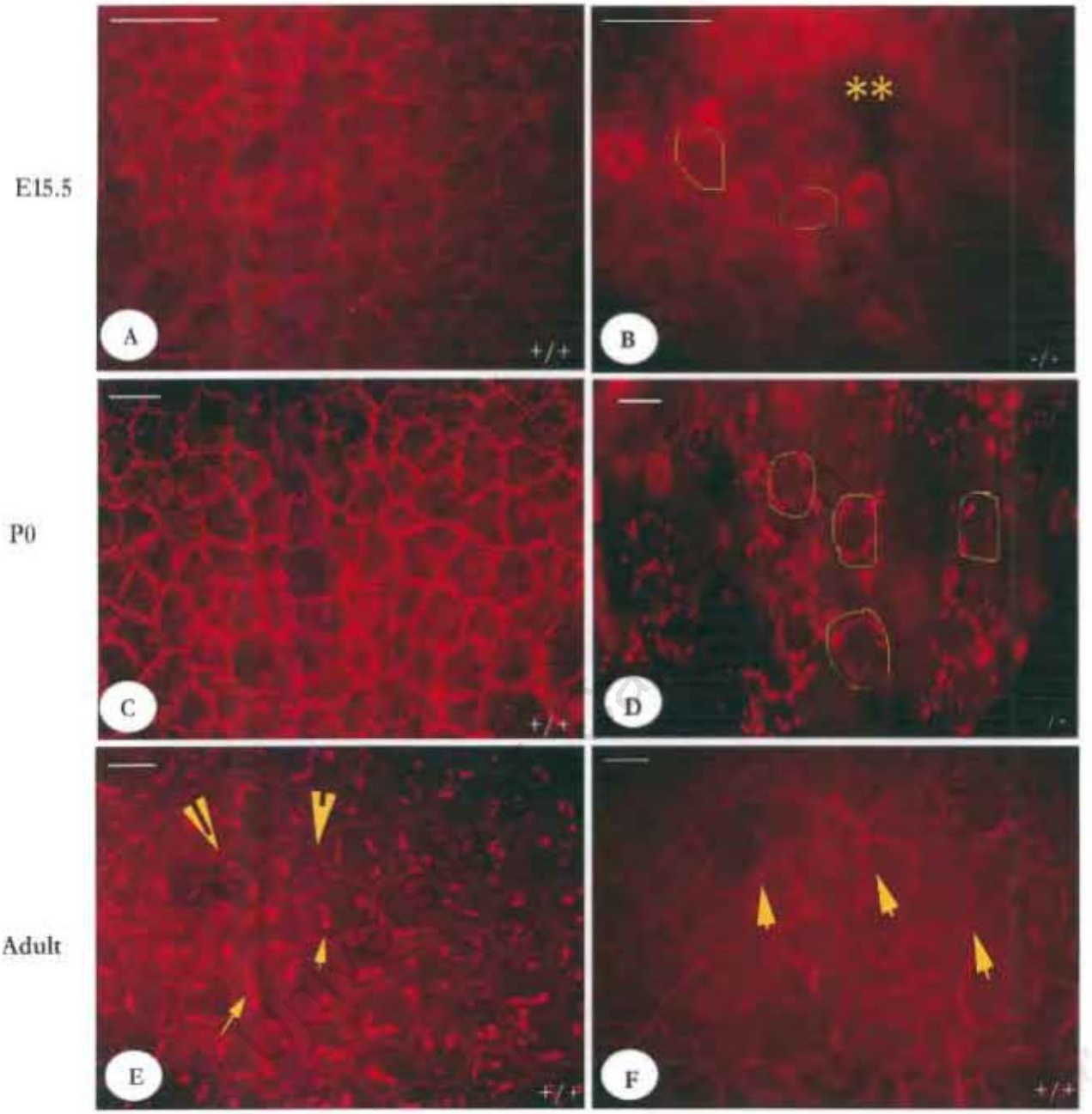

Figure 3-12 Immunofluorescence images showing the expression of N-cadherin in the corneal endothelium in the wildtype at E15.5 (A), postnatal day 0 (P0, C), adult (E-F) and mutants at E15.5 (B) and P0 (D). At E15.5, in the wildtype corneal endothelium, N-cadherin occurred as a continuous belt at the plasma membrane of adjoining cells (A). In contrast, the mutant corneal endothelial surface showed a perinuclear pattern with no plasma membrane localisation (B, circles). In order to visualise this, corneas were viewed at 100X magnification. At P0 in the wildtype neonate, the continuous belt of N-cadherin was still visible (C) whilst the mutant corneal mesenchyme cells maintained a brightly staining perinuclear ring (D, circles). In the adult, the corneal endothelium showed a pericellular pattern of N-cadherin (F, arrowheads) with either bright perinuclear staining (F, arrows) or with single dots near the membrane of each cell (F, arrows). Scalebar = 20μm.

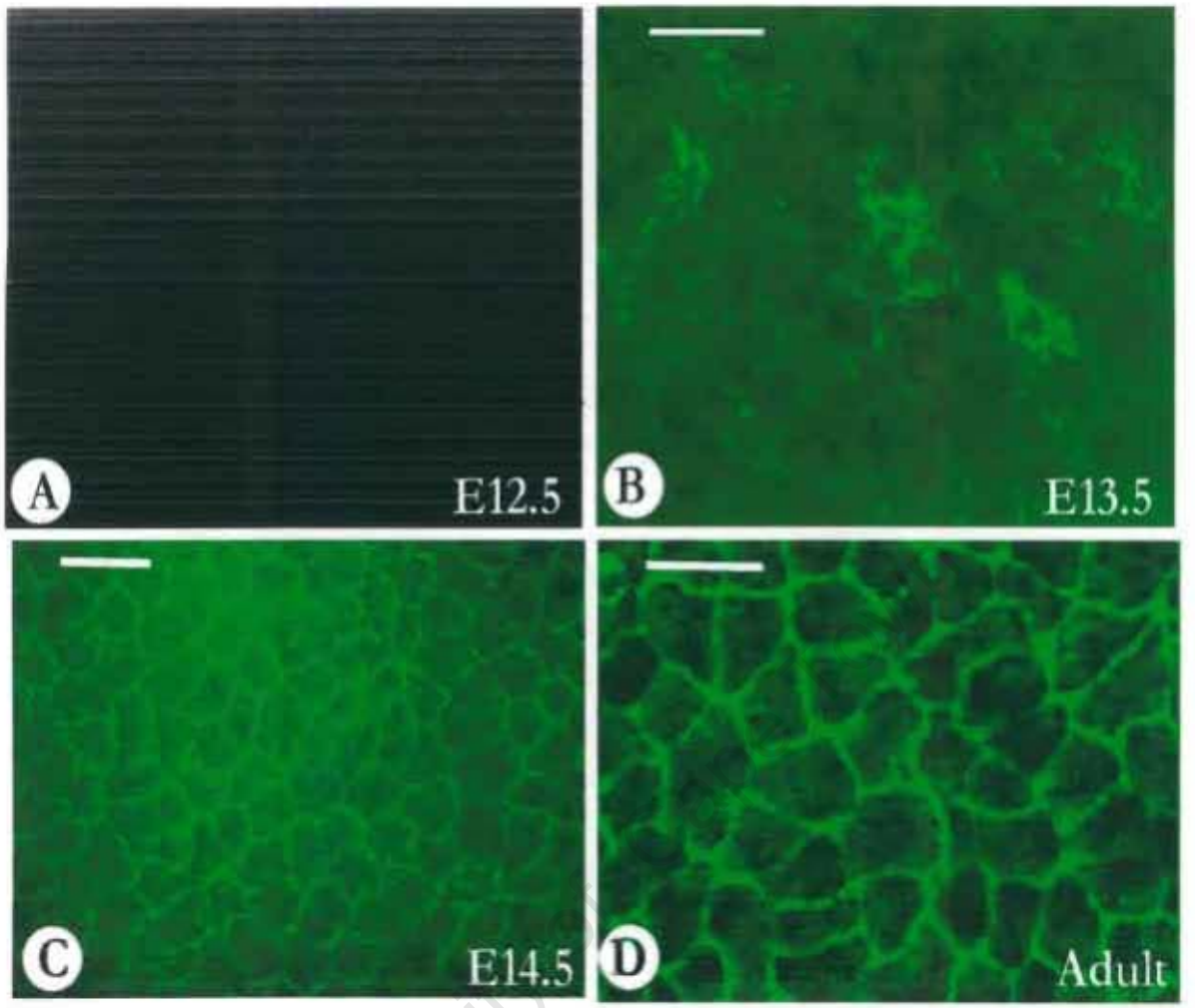

Figure 3-13. Systematic analysis of ZO-1 expression during the development of the normal corneal endothelium. At E13.5, ZO-1 signal appears as bright discontinuous spots at points of cell-cell contact. A diffuse cytoplasm signal is also observed (B). The expression of ZO-1 intensifies at the membrane at E14.5 (C) and an even more continuous localisation is obtained in the adult (D). Scalebar = 20µm.

3.4.1. Junctional complexes do not form in *Foxc1* mutants

Scanning electron microscopy results in the present study showed that although cells are able to make contact during development, a monolayer of corneal endothelial cells fails to form in the mutants. In order to compare the ultrastructure of intercellular junctions in the corneal endothelium between normal and *Foxc1* mutants, transmission electron microscopy on normal and mutant corneas at E17.5 was performed.

In the normal embryo at E17.5, corneal endothelial junctions were visible (Fig. 3-14B, boxed region, dotted line). Individual endothelial cells formed interdigitations at their lateral surfaces. The stromal keratocytes (str) were arranged in parallel layers with collagen fibres (col) arranged

in a parallel fashion in between the cells (Fig. 3-14A). In contrast, no such extensive corneal endothelial junctional complexes were visible in the mutant. Contacting cells did not make proper junctional complexes (Fig. 3-15B). The inability to form proper junctional complexes in these mice paralleled the failure to synthesize tight junction proteins and to localize adherens proteins to the membrane.

3.5. The expression of the corneal proteoglycan, *keratocan*, and candidate signaling molecules implicated in corneal endothelial differentiation

The absence of a normal endothelium in *Foxc1* mutants raised the question of whether the abnormal stromal organization in these mutants was due to failure to express stromal proteoglycan, *keratocan*, or a defect resulting from lack of an endothelial barrier. To answer this question, *in situ* hybridization was used to determine and compare the expression pattern of *keratocan* between normal and wildtype corneas at E17.5. In normal embryos, the expression of *keratocan* was also determined at E12.5. Eyes from wildtype and mutant mice were harvested and processed for *in situ* hybridization with the *keratocan* probe (Fig.3-16A) as described in Materials and Methods (section 2.6).

In the normal cornea, *keratocan* mRNA was detected at E12.5 when mesenchyme cells ingress to the space between the lens and the cornea (Fig. 3-17A). At E17.5, an intense expression of *keratocan* mRNA was observed in the corneal stroma and endothelium (Fig 3-17B-D). *Keratocan* was also detected in the cornea of the mutant at E17.5 (Fig. 3-17E) suggesting that *keratocan* is not downstream of *Foxc1* in a cascade of genes regulating corneal development.

Signaling molecules between corneal mesenchyme and the anterior lens epithelium that are involved in corneal endothelial differentiation have not been identified. Previous studies have implicated molecules transforming growth factor beta-2 (*tgfb2*) in corneal endothelial differentiation (Reneker et al., 2000). For this reason, the expression pattern of *tgfb2* in the undifferentiated corneal mesenchyme and corneal endothelium was determined at E11.5 – E12.5 prior to corneal endothelium formation and at E13.5. Eyes from wildtype embryos were harvested and processed for *in situ* hybridization with the *tgfb2* and *tgfbRII* probe (Fig. 3-16B, C). There was no expression of *tgfb2* observed at E12.5 (not shown). The expression was only localized at E13.5 (Fig. 3-18C). Interestingly, in embryos in which the lens was transplanted into the facial mesenchyme, *tgfb2* expression was maintained in the anterior lens surface (Fig. 3-18D, arrows). This suggests that the expression of *tgfb2* in the anterior lens surface does not necessarily require interaction with the adjacent corneal mesenchyme.

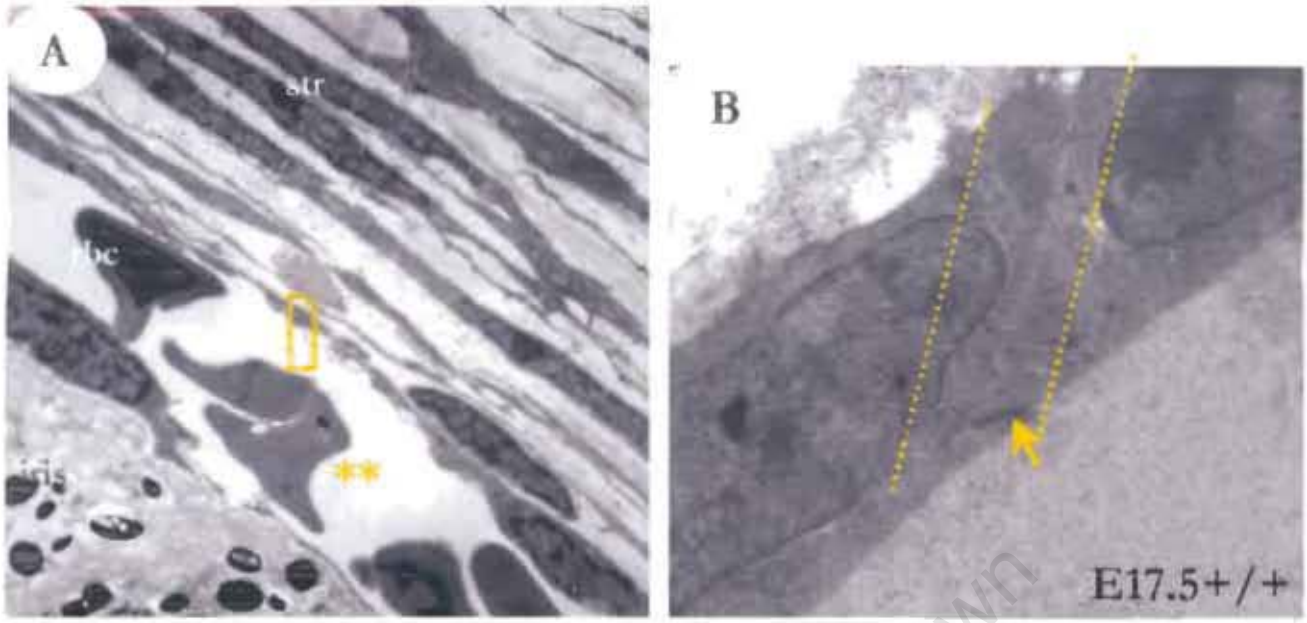

Figure 3.14. Transmission electron micrograph of wildtype mouse cornea at E17.5. The anterior chamber (asterisks) has been formed at this stage. The presence of blood cells (rbc) is noticeable in the chamber above the iris. Corneal endothelial cells are interconnected with junctional complexes (B, selected dotted area) and tight junctions on the apical side (B arrow). Magnification: A= 4400X. B= 50000X.

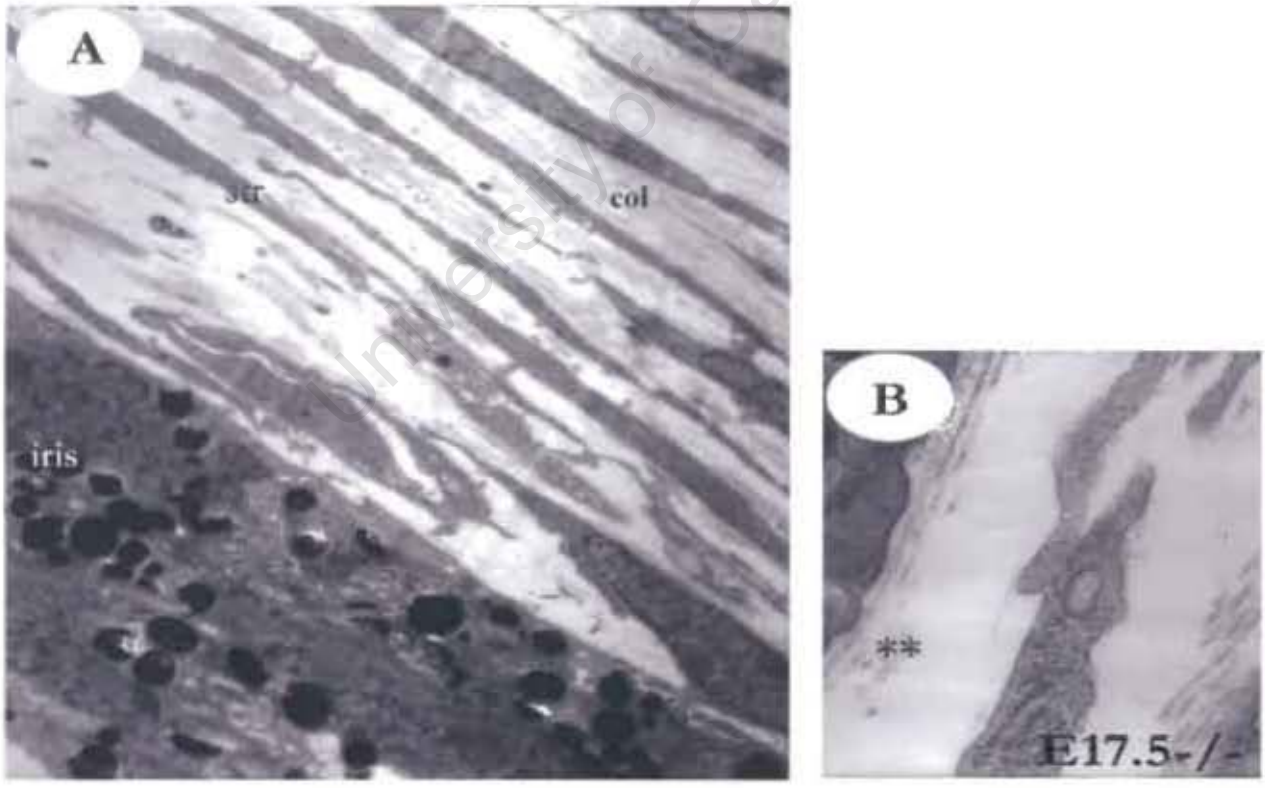

Figure 3.15. Transmission electron micrograph of *Foxc1* mutant mouse cornea at E17.5. In the mutant, the anterior chamber has not been formed and the iris and the cornea are in close apposition to each other. Higher magnification of "corneal endothelial" cells shows that these cells made contacts but with not apparent tight junctions. Collagen fibers are also visible in between the cells (B, asterisks). Str = stroma; col = collagen fibres. Magnification A = 4400X; B = 30000X.

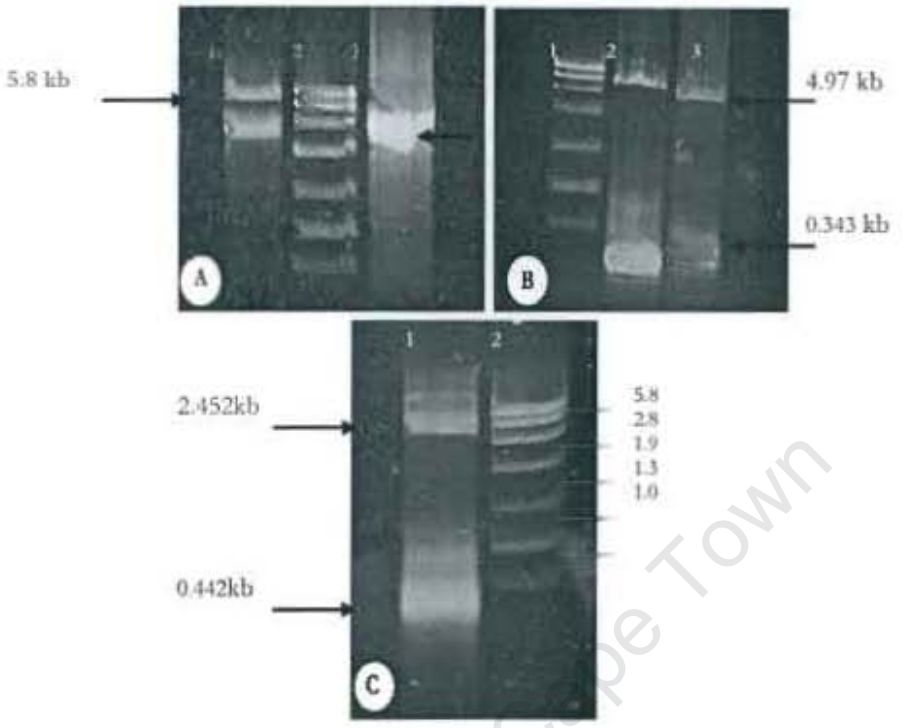

Figure 3-16. Agarose gels showing typical riboprobes obtained from linearised plasmids used in this study. The keratocan plasmid was linearised (2.9kb) and sense (A, lane 1) and antisense riboprobes (A, lane 3, arrow) synthesized. The *tgfbrII* riboprobes (0.343kb) were synthesized from *EcoRI and XhoI* (4.97kb) linearised plasmids (B). The *tgfb2* riboprobes (0.442kb) were also synthesized from EcoRI and XhoI linearised plasmids (2.452kb) in pBluescript vector (C).

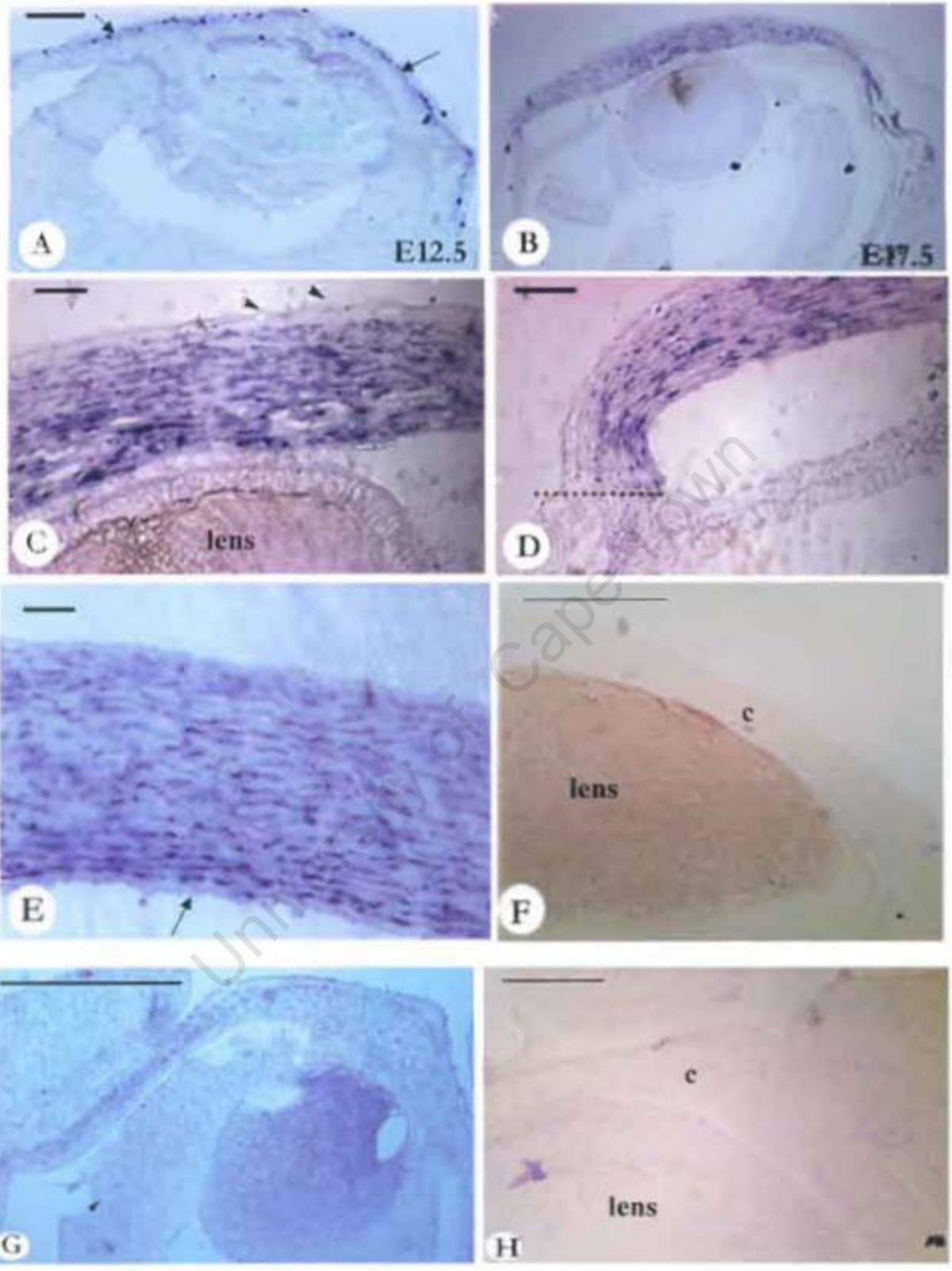

Figure 3-17. Expression of *keratocan* in wildtype eyes was detected by *in situ* hybridization using a dig-labelled riboprobe. *Keratocan* transcripts were detected as early as E12.5 as the migrating mesenchyme cells ingress into the corneal space (A, arrows). By E17.5, only the parallel-arranged stromal keratocytes (str) keratocan (C,D). The corneal epithelium (C, arrows) and the endothelium (E, arrows) do not express keratocan. The *keratocan* expression marked the border between the corneal stroma and the sclera at the limbus (D, dotted line). *Keratocan* transcripts were also detected on the corneal stroma and sclera of the mutant cornea, (G, arrows). Figures F and H show sections through the cornea and lens from wildtype (F) and mutant (H) eyes that were hybridized with the sense probe, showing no expression of *keratocan* in the cornea. C= cornea, re = retina, str = stroma. Scalebar = 50μm.

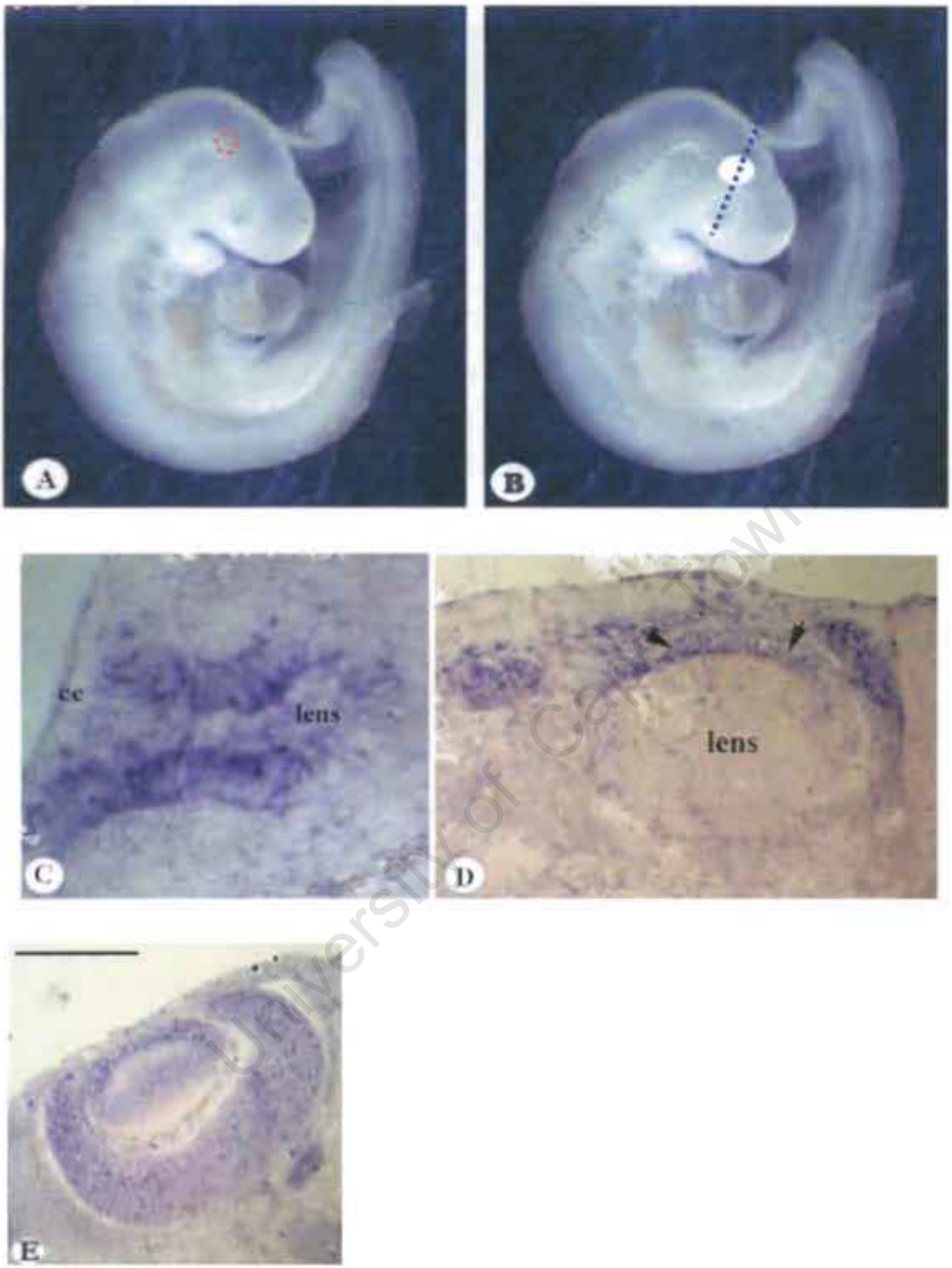

Figure 3-18. *In situ* hybridiation using *tgfβ2* probe on cultured embryonic heads with ectopic lenses. (A) Wildtype embryos were harvested and ectopic lenses transplanted into the peri-ocular mesenchyme (B, white insert). Dotted line (B) shows how the embryos were sectioned for histological and *in situ* hybridisation. Embryonic heads were either bisected or cultured as whole heads for a period of 12 or 24 hours. After this time in culture, embryos were processed for *in situ* hybridisation. C– section through the endogenous eye showing expression of tgfβ2 in the lens epithelium. D – transplanted ectopic lens showing expression of tgfβ2 in the anterior lens epithelium (D, arrows). ce = corneal epithelium. Scalebar = 25μm.

Tgfb2 is known to exert its activity through binding to type I and type II receptors (Dunker and Krieglstein, 2000). The expression of these receptors at the time of endothelial differentiation has not been reported. In the present study, the expression of *tgfbRII* was investigated at E12.5, E13.5 and E17.5 in the normal embryo. There was no expression of *tgfbRII* at E12.5 (not shown) and E13.5 (Fig. 3-19A) in the normal cornea. At E17.5, the expression of *tgfbRII* was observed in the corneal stroma and endothelium (Fig. 3-19B). *TgfbRII* was thus expressed at the time when corneal endothelium had differentiated, suggesting that it is not part of molecules involved in corneal endothelial differentiation.

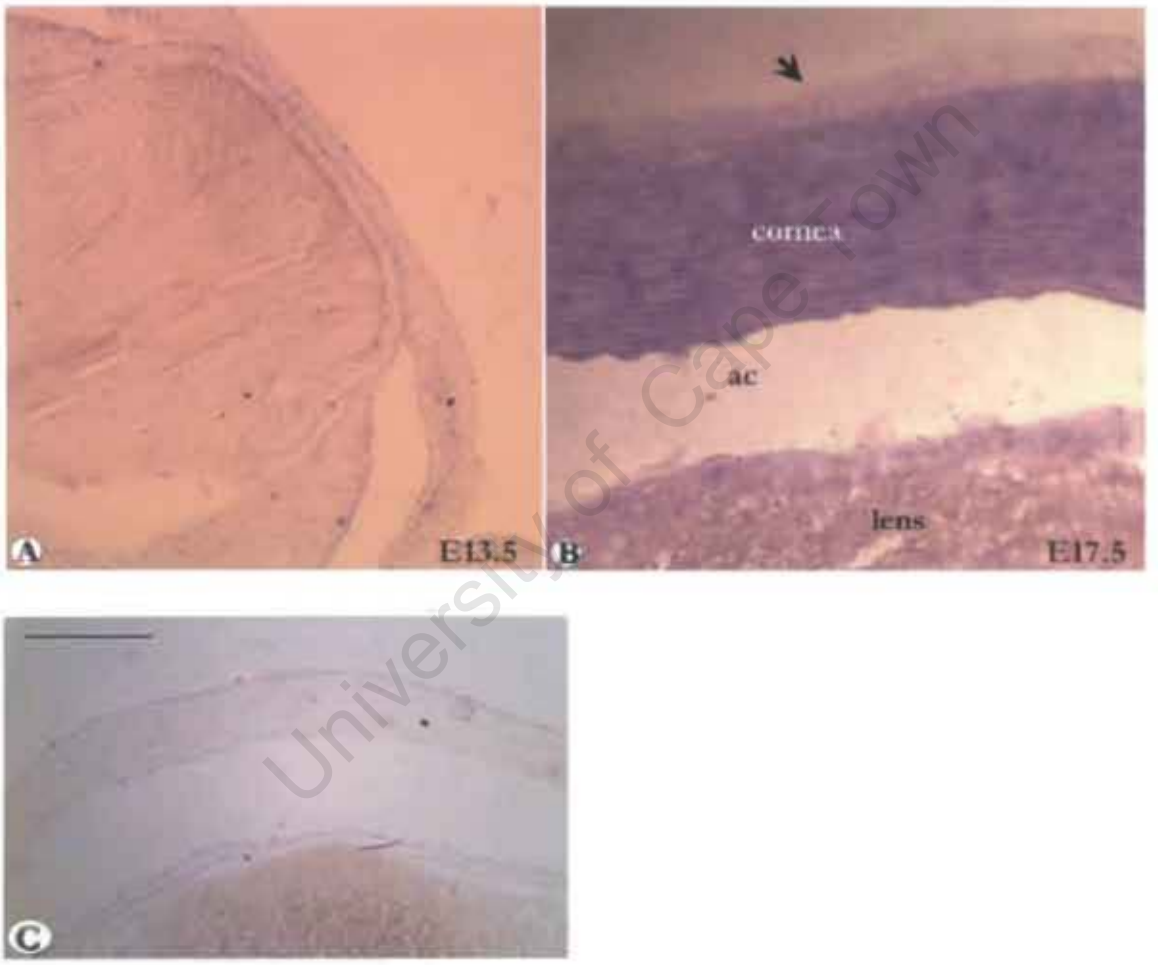

Figure 3-19. In situ hybridization on E13.5 and E17.5 wildtype eyes. No expression of the receptor was detected at E13.5 (A). At E17.5, the corneal stroma and endothelium plus the lens epithelium show positive expression (B). The epithelium is negative for *tgfbrII* (see B, arrowhead). No expression of the receptor was shown when the section was hybridized with a sense probe (D). Scalebar = 50μm.

3.6. Establishing an *in vitro* model of corneal endothelium development

In this study, SEM analyses of corneal endothelium development in *Foxc1* mutants suggest that the failure to form endothelium in these mice is in part due to incomplete mesenchyme endothelium conversion. However, these results do not provide information about the causative factors for failure to translocate N-cadherin to the cell membrane nor do they give a clue to the failure to synthesize tight junction protein ZO-1. In order to investigate the ability of corneal mesenchyme cells to assemble junctions *in vitro,* and to further explore the dynamics involved in junction formation, an *in vitro* model was developed.

3.6.1. Growth of corneal mesenchyme *in vitro*

Although conditions for the isolation of adult mouse corneal endothelium cells have been described (Joo *et al.*, 1994), culture of presumptive corneal endothelial cells has not been described. In the present study, cultures of corneal endothelial precursors from explants of corneas from E12.5 were carried out. This *in vitro* system was developed in order to assess the ability of corneal mesenchyme cells to assemble adherens and tight junctions *in vitro*. The main goal was to make use of growth factors, growth media supplements and embryonic lens conditioned medium to induce corneal endothelial differentiation in mutant cells.

Corneas were separated form lenses at E12.5, prior to normal corneal differentiation. The separation was carried out before fixation and thus some cells adhered to the anterior lens surface. Cells migrated from the explants and after 48 hours explants were removed. In instances where epithelial cells migrated from the explants, they were identified on the basis of their morphology. They formed small aggregates (Fig. 3-20A), and expressed ZO-1 (Fig. 3-20C). In contrast, mesenchyme cells were identified by their typical fibroblastic morphology (Fig. 3-20B) and failure to express ZO-1 after 2 days in culture (Fig. 3-20D).

3.6.2. Formation of adherens and tight junctions in culture

In the present study, immunoflourescence results on whole-mount corneal endothelia showed that N-cadherin expression began at E12.5 in the normal embryo and became visible at the cell-cell junctions at E14.5. It was not possible to explore the changes in cytoskeletal reorganization using whole-mount tissues. The use of exogenous growth factors to induce corneal endothelial differentiation was also not possible (see appendix). Corneal endothelial

cell precursors were thus cultured to further investigate the dynamics of junction formation *in vitro*.

Corneal explants obtained from normal and wildtype embryos were cultured in fibronectin-coated glass coverslips over a period of four to eight days. The explants were cultured by attaching the innermost layer of the cornea to the substratum and mesenchyme cells migrated out. The formation of cell-cell junctions was determined by examining the distribution of cadherins and ZO-1. In pre-confluent cells that did not make contacts, N-cadherin signal was perinuclear (Fig 3-21A). Dual labeling with a Golgi marker (Fig. 3-21B) showed that the N-cadherin protein in isolated cells was associated with the Golgi (Fig. 3-21C). This pattern is similar to that described for MDCK cells in which E-cadherin was associated with Golgi in cells that did not form contacts, suggesting that the protein was newly synthesized and still packed in Golgi vesicles (Le et. al., 1999).

At the cell surface cadherins are known to associate with beta-catenins that link them to the actin cytoskeleton. The establishment of stable cell-cell junctions is thus linked with rearrangement of actin fibres from a radiating arrangement to a circumferential pattern at the cell surface (see – Vasioukhin and Fuch, 2001). In the present study, the association of cadherins with the F-actin cytoskeleton was investigated in cells obtained from both wildtype (Fig. 3-22) and mutant embryos (Fig 3-23). Cells were stained with phalloidin and N-cadherin to localize the expression of F-actin and adherens junctions respectively. As shown in Figure 3-22, F-actin appeared as stress fibres in both wildtype (Fig. 3-22B) and mutant (Fig. 3-23B) cells. N-cadherin was expressed in a vesicular pattern at points of cell-cell contact (Fig. 3-22A and Fig. 3-23A). Co-staining of phalloidin with N-cadherin showed that at points of cell-cell contact, N-cadherin spots co-localized with F-actin (Fig. 3-22D and Fig. 3-23D). In HeLa cells, which express N-cadherin, a continuous cobblestone pattern of N-cadherin was observed at confluency (Fig 3-24A).

The next step was to determine whether N-cadherin expressing cells were able to form tight junctions. The distribution pattern of the tight junction associated protein, ZO-1, was investigated. There was no ZO-1 at points of contact, regardless of confluence and number of days in culture (not shown). Both wildtype and mutant cells were not able to survive for longer than eight days in culture before they started to senesce.

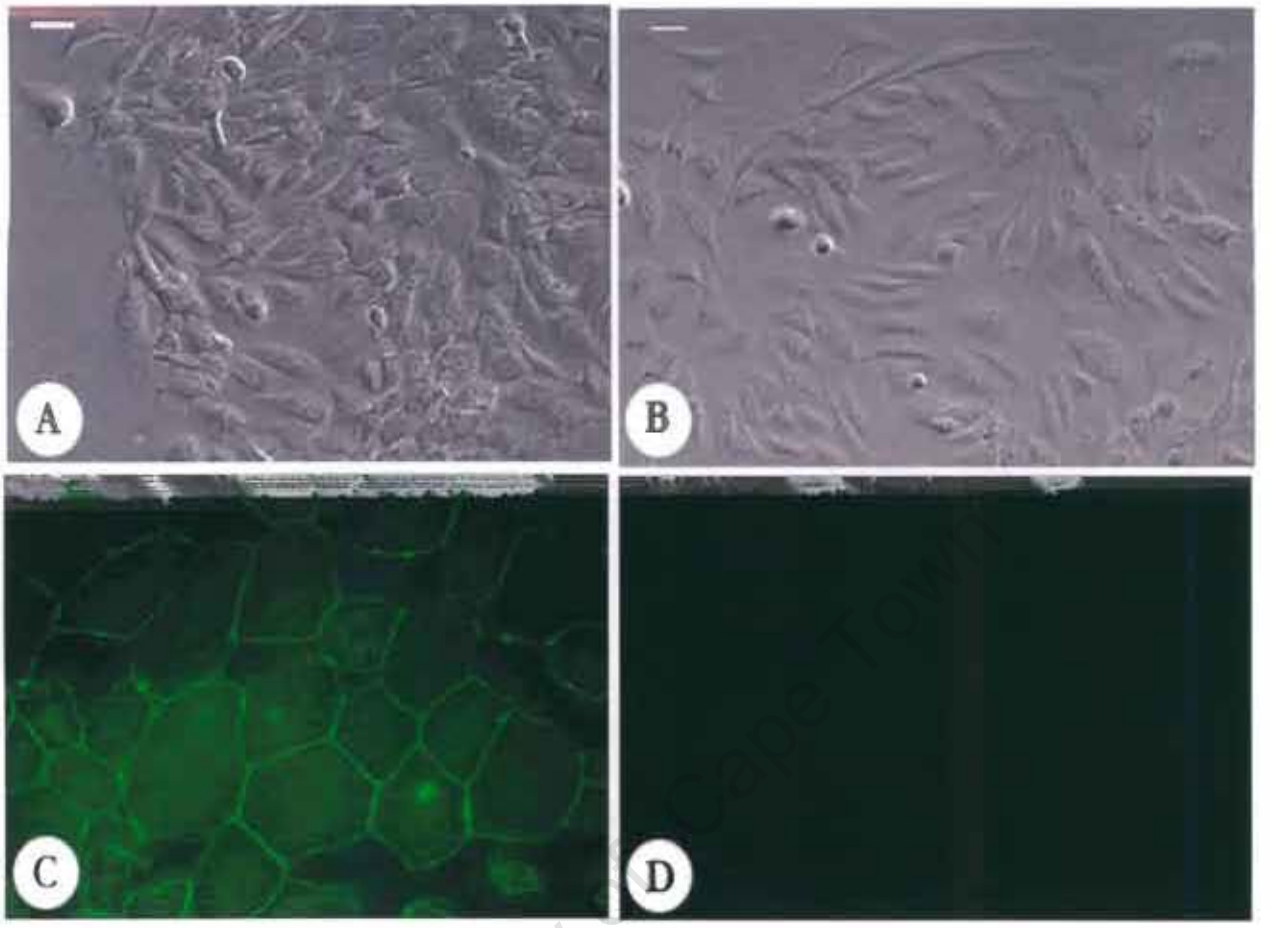

Figure 3-20. Corneal mesenchyme cells after two days in culture. Phase-contrast images (A-B) and immunoflourescent analysis of ZO-1 (C-D) in cells that migrated from the explant after two days in culture. Corneal epithelial cells (A) were identified by the expression of ZO-1 (C) at points of cell-cell contact soon after migration. In contrast, ZO-1 expression was not detected in corneal mesenchyme cells (D). Scalebar = 20μm.

Figure 3-21. Immunoflourescence localisation of N-cadherin in single cells cultured for a period of 6 or 4 days. The distribution of N-cadherin was compared between single isolated cells and confluent (contacting) cells. (A) N-cadherin signal is detected in the perinuclear region. (B) Staining with a Golgi marker is consistent with the presence of N-cadherin in Golgi. (C) Dual labelling shows the colocalisation of both proteins in the golgi area. These results are consistent with reports that cell-cell contact regulates cadherin trafficking from cytoplasm to the membrane. Scalebar = 20μm.

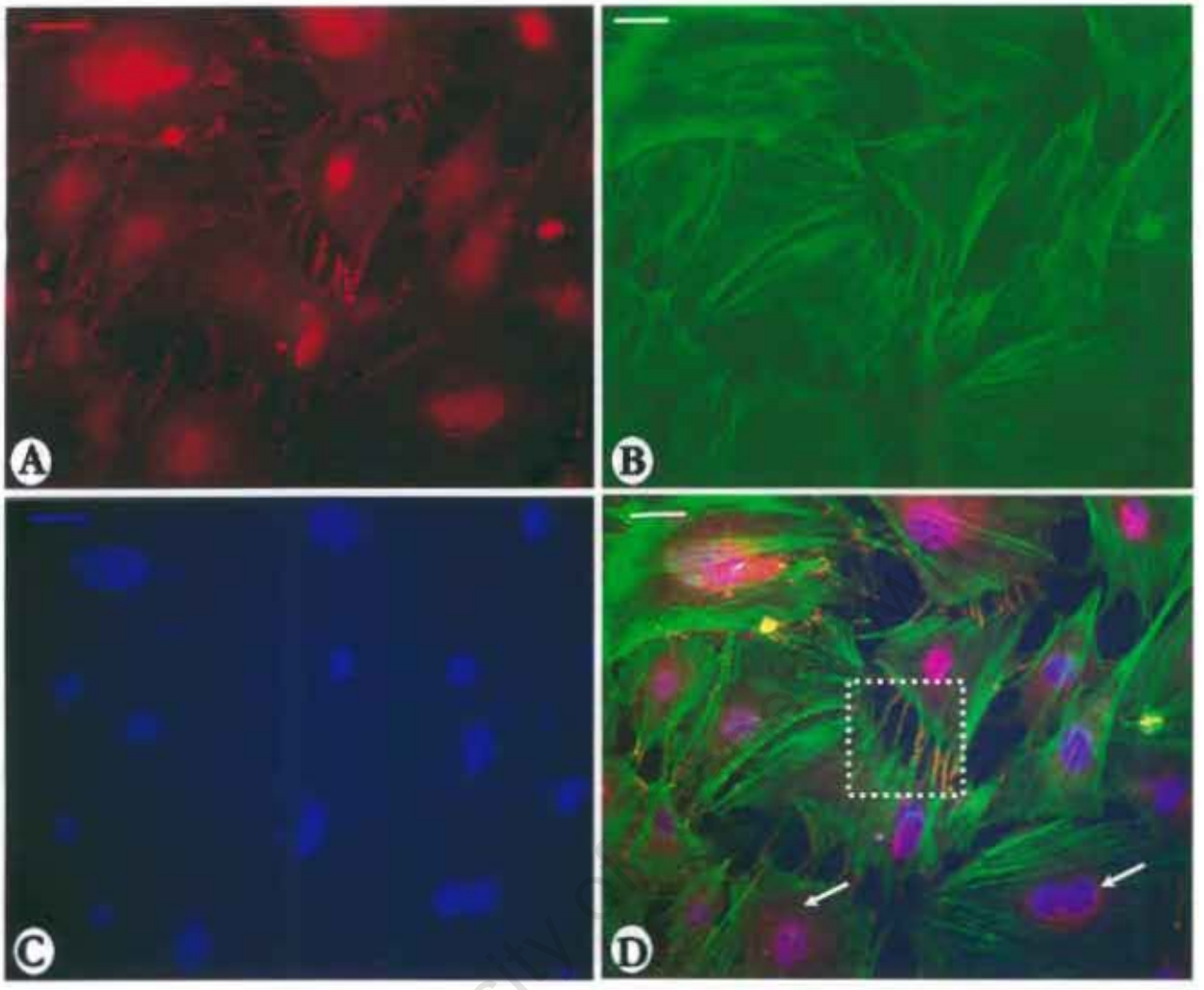

Figure 3-22. Distribution of N-cadherin in cultured corneal mesenchyme cells. (A) Immunoflouresence staining of N-cadherin in cells cultured for a period of 4 days. In these cells, N-cadherin was in vesicles along the edges of cells at points of intercellular contacts (A). The signal was also seen strongly along the perinuclear region (D, arrows). Nuclear staining was used to localise the nuclei of cells (C) F-actin fibres were strongly staining as radiating fibres (B) and colocalised with N-cadherin at focal adhesion points where cells made contact with each other (D, boxed area). Scalebar = 20μm.

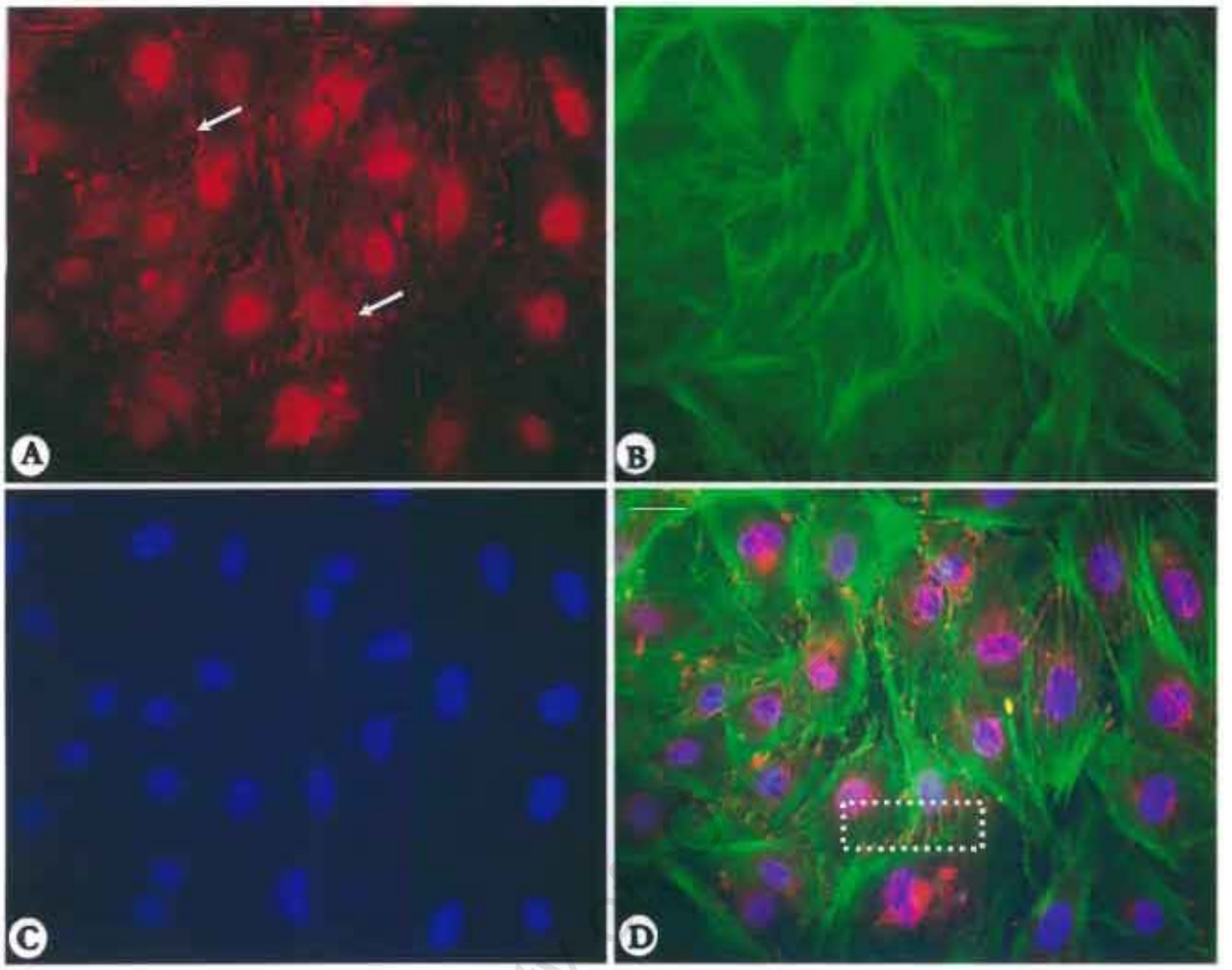

Figure 3-23. Distribution of N-cadherin in cultured mutant corneal mesenchyme cells. (A) Immunoflouresence staining of N-cadherin in cells cultured for a period of 6 days. N-cadherin was in vesicles along the edges of cells at points of intercellular contacts (A, arrows).. Nuclear staining was used to localise the nuclei of cells (C) F-actin fibres were strongly staining as radiating fibres (B) and colocalised with N-cadherin at focal adhesion points where cells made contact with each other (boxed area, D) Scalebar = 20μm.

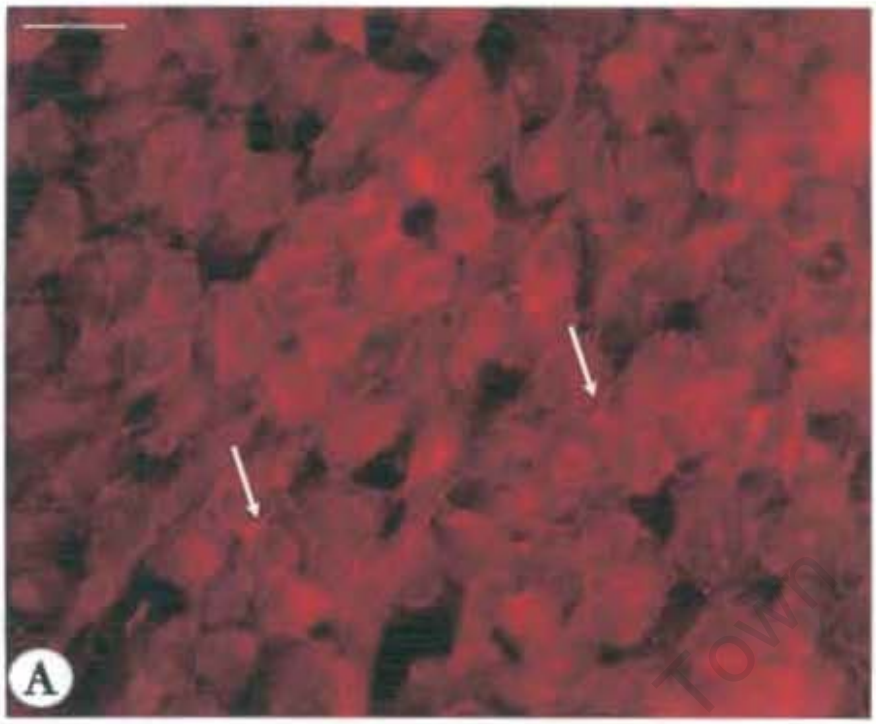

Figure 3-24. The distribution of N-cadherin in confluent HeLa cells. N-cadherin was strongly localised along the edges of cells at points of intercellular contacts (A, arrows). Scalebar = 20μm.

Chapter Four : DISCUSSION

The formation of a corneal endothelial monolayer from a population of stellate shaped cells provides an ideal system for the study of intercellular junctions and cellular shape changes during embryonic development. There is very little information on the mechanisms underlying the development of the mammalian corneal endothelium. Such information is essential to understand the aetiology of corneal endothelial dystrophies and their effects on vision. Most studies on the corneal endothelium have concentrated on age-related cell density changes (Bourne et al., 1997; Joyce et al., 1998; Joyce et al., 1996; Murphy et al., 1984). These and other studies have demonstrated that in humans, the corneal endothelial cells do not proliferate to keep pace with the rate of cell loss that occurs during aging. As a result of insufficient proliferative capacity, damage to the corneal endothelium from accidents, trauma or diseases that cause corneal oedema or loss of corneal clarity can only be rectified by corneal transplantation. Loss of corneal clarity can also result from corneal endothelial dystrophies, many of which are associated with glaucoma, one of the leading causes of blindness worldwide. The availability of mouse models with defects in corneal endothelial morphogenesis provides an ideal opportunity to study these processes. In the present study, *Foxc1* mutant mice in which corneal endothelial development is defective were used to study the cellular mechanisms underlying corneal endothelial development. In order to begin to address questions related to these processes, an understanding of the precise details of corneal endothelial development is crucial. The aim of the first part of this thesis was to describe in detail the normal development of the corneal endothelium in mice.

Studies on both chick (Hay and Revel, 1969; Johnston et al., 1979; Noden, 1975) and mouse (Osumi-Yamashita et al., 1994; Trainor and Tam, 1995) have definitively shown that the corneal endothelium is derived from cranial mesenchyme. The differentiation of a monolayered corneal endothelium from this mesenchyme occurs by a process of mesenchymal-epithelial transformation (MET). The process of MET also occurs in other developing tissues in the embryo, for example during kidney development and during the formation of somites from paraxial mesoderm (Gilbert, 2000). In the kidney, the process of MET occurs when the uteric bud (an epithelium-lined tube-like structure) protrudes into undifferentiated mesecnhyme, which responds to inductive signals by MET transformation (for recent reviews, see (Kanwar et al., 2004). The epithelia thus produced differentiate into typical transporting cells with tight junctions. Most of the studies on kidney have focused on eludicating the complex signalling pathways involved in MET process. In contrast, there is very little information on the cellular changes during this process. This is mainly because

although it is possible to track cell migration and fate changes using molecular markers and dyes, it is not very easy to monitor the precise details of the shape changes *in vivo*. Most of the information on cellular morphological changes during MET has been obtaind from *in vitro* studies.

Morphological events during mesenchyme-endothelial conversion

For reasons similar to that described above, not much is known about the morphological transformations that accompany the conversion of mesenchyme to corneal endothelium. In particular, the precise timing and mechanisms of shape changes have not been reported and the exact molecules responsible for the induction to an endothelial phenotype have not been identified. Histological and electron microscopic examination of mouse embryonic corneas (Kidson et al., 1999; Pei and Rhodin, 1970) have provided limited information on the mechanisms of cell shape changes. This study provides a much more detailed analysis of changes and focuses in particular, on the stages (E12.0 – E14.5) when the most dramatic shape changes occur.

In order to carry out this study, careful exposure of the inner corneal surface was necessary. At these early developmental stages, the cornea and the lens are still attached to each other and the anterior chamber has not been formed. Thus, after removal of the lens it was crucial to ascertain that the exposed cells were indeed corneal mesenchyme. This was achieved in two ways: firstly, for heterozygous and mutant embryos, cells were stained for LacZ and the corneas and lenses separated after fixation. Histological sections of lacZ positive corneas have previously shown that the presumptive mesenchyme cells and the vasculature surrounding the lens at the early embryonic stages is positive for LacZ (Kidson et al., 1999). In the present study, it was also shown that the lens surfaces were positive for LacZ, suggesting that these were either mesenchyme cells remaining at the lens or the vascular mesenchyme associated with lenticular blood vessels. Secondly, many lenses were removed and viewed by SEM. It was shown that very few and often none of the corneal mesenchyme cells remained attached to the lens surface.

A systematic analysis of cell shape changes during normal development of the corneal endothelium showed that soon after mesenchyme cells occupy the corneal space, they appear as an irregularly arranged meshwork. The cells have long extensions with collagen fibres interspersed. Although the appearance of the corneal meshwork is similar at the early stages, there are variations in cell shapes and sizes between different litters. This could be a result of

the differences in timing of mouse matings leading to slight differences in developmental age. Transformation of cell shape and size was found to begin by flattening, a process that occurred from the centre of the cornea and proceeded outwards. Thus as the cells began the process of flattening, the central cells started forming intercellular boundaries whilst the cells at the edges still maintained the stellate morphology. As development proceeded, the intercellular borders became more distinct and the gaps at the corneal periphery closed up. Eventually, a honeycomb pattern was attained.

The pattern of cell flattening reported here differs from the reports of chick where it has been stated that cells flatten prior to migration into the corneal region and the corneal endothelium formed in a periphery towards centre direction (Hay and Revel, 1969). However, analyses of cell shape changes from these chick studies were made from histological examination only. (not surface viewing using scanning electron microscopy.) A further limitation of the above studies was that there are little molecular markers available, which can be used to mark the intermediate differentiation status of these cells before and after migration.

The initiation of intercellular junctions during MET in the corneal endothelium

The results of the present study have shown that the establishment of a monolayer is accompanied by formation of tight intercellular contacts. To-date, there are no early markers for undifferentiated and migrating corneal endothelial cells. Previous studies performed on histological sections of already differentiated embryonic mouse corneal endothelium have shown that these cells express N-cadherin at points of cell-cell contact (Reneker et al., 2000). These studies however, do not report on when the protein is initially expressed and therefore do not provide information on the early stages of junction formation that occurs with mesenchyme-endothelial conversion. The next question addressed in this study was whether the presumptive corneal endothelial cells express N-cadherin.

An examination of N-cadherin distribution was performed on whole corneas using immuno-flourescent microscopy. Soon after the prospective corneal mesenchyme cells have occupied the corneal space, N-cadherin appears as bright intracellular cytoplasmic spots. As soon as cells flatten and intercellular spaces occluded, N-cadherin distribution forms a continuous pericellular ring between adjacent cells. These results suggest that the induction of cell shape changes is in parallel with changes in distribution pattern of N-cadherin from a cytoplasmic to a pericellular continuous distribution on the cell surface. This change in cadherin distribution pattern is similar to that reported in cultures of MDCK cells in which E-cadherin re-

distribution from cytoplasmic vesicles to the cell surface is dependent on cells making stable contacts (Le et al., 1999). These studies have shown that in cells that did not form contacts, cadherin distribution (E-cadherin) remained intracellular in vesicles, whereas in confluent cells that form contacts, cadherin localisation became pericellular and continuous.

Studies conducted in cultured cells have also shown that the changes in cell shape during mesenchyme-epithelial transformation are accompanied by major shifts in cytoskeletal organisation. Microfilaments reorganise from stress fibres into peripheral circumferential bands (for a review of cell shape changes see Braga, 2000). All of these processes have been studied *in vitro* and it is often challenging to study them *in vivo*. The present study shows that as soon as corneal mesenchyme cells make contact and junctional proteins translocate into the cell surface, at E14.5, dense peripheral bands of actin appear at the cell surface, suggesting reorganisation of the actin cytoskeleton that accompanies cell-cell adhesion.

The formation of tight junctions during corneal endothelial morphogenesis

Previous studies in vitro have shown that the formation of tight junctions is the preceded by the formation of adherens junctions (McNeill et al., 1993; Rajasekaran et al., 1996). Tight junctions are marked by the expression of zonula occludens-1 (ZO-1) protein at the cell membrane. In order to investigate whether a similar process of cell junction formation occurs during corneal endothelium development, in this study the formation and distribution of ZO-1 during endothelial morphogenesis was investigated. Results showed that the protein was first detectable as a diffuse signal at the cell surface soon after cells began the process of flattening. The distribution became more distinct and continuous soon after this, coinciding with the flattening of cells as shown by SEM. The interesting point arising from these results is the appearance of ZO-1 at the cell surface occurred earlier than cadherin localisation. These results are in conflict with reports from other studies in which ZO-1 junctions and the detection of ZO-1 is preceeded by cadherin lcoalisation (McNeill et al., 1993; Rajasekaran et al., 1996). However, they can be explained in two ways. Firstly, the expression of cadherin at the cells surface may not be detectable earlier due to the strong signal of intracellular vesicles. Secondly, it is possible that at these early stages ZO-1 is not only associated with the tight junctions but also with adherens junctions. This thought is consistent with reports from other studies in cultured cells in which ZO-1 was found to be associated with adherens junctions prior to final localisation at the tight junction (Rajasekaran et al., 1996).

Growth of presumptive corneal endothelial cells in culture

Adult human (Baum et al., 1979; Joyce et al., 1996; Nayak and Binder, 1984; Yue et al., 1989), porcine (Engelmann et al., 1999), murine (Joo et al., 1994) and bovine (Crawford et al., 1995) corneal endothelial cells have been cultured. In these studies, the corneal endothelial cells were obtained from Descemet's membrane-endothelial explants. Due to the large size of the corneal cups from the adult corneas of these species, it was simple to remove the Descemet's membrane and therefore chances of stromal or epithelial cell contamination were minimal. In all of these studies, it was fairly easy to identify corneal endothelial cells using morphological characteristics only (polygonal cell morphology and cobblestone pattern at confluency). No molecular markers were necessarily required to identify them. Cells obtained from these adult tissues are however, not suitable for the study of mesenchyme-epithelial transformation. Firstly, even in primary corneal endothelial cells that have been successfully cultured, it is difficult to maintain cell proliferation for a sufficient period to generate large numbers of cells before they senesce (Joyce, 2003). Secondly, the cells obtained from such explants are already differentiated endothelial cells and therefore not suitable to study MET processes. Lastly, cell-cell junctions have already been formed and the proteins involved already synthesised, packaged and appropriately translocated to the apical membranes. In the case of murine tissues, in addition to the above limitations, the corneas are small in size and the number of cells may not be sufficient to study MET. These problems could potentially be overcome by culture of embryonic precursor cells. To-date, there are no reports on successful culture of murine embryonic presumptive corneal endothelial cells. Efforts to culture presumptive corneal endothelial cells from mouse embryos have in addition been hampered by lack of appropriate markers to identify the cells at this early stage. Even the population of cells derived from cranial neural crest cannot be identified with certainty due to the lack of mouse cranial neural crest markers.

In the present study, presumptive corneal endothelial mesenchyme was cultured in order to examine the formation of intercellular junctions accompanying the conversion of mesenchyme into endothelium. In order to obtain the appropriate undifferentiated mesenchyme, the correct age of the embryos was identified. Previous studies have shown that at E12.5 of development, the corneal mesenchyme cells are still undifferentiated (Kidson et al., 1999) and thus mesenchyme was cultured from this stage embryos. The lens was separated from corneas and the corneal explants cultured by attaching them endothelial side down on a culture well. Mesenchyme cells migrated from the explant and the cells displayed a typical mesenchyme morphology. Corneal mesenchyme was distinguishable from epithelial cell contamination

based on morphology. In general, epithelial cells were compact, small in size and formed aggregates. The expression of ZO-1 by epithelial cells soon after cells have migrated from the explants also provided a convenient means of identifying epithelial cells.

Thus it was possible to identify mesenchyme cells at early stages of culture as these cells were not positive for ZO-1. Although corneal endothelial cells express ZO-1, this protein is only expressed in differentiated cells when intercellular junctions have been formed and a cobblestone pattern attained. The dynamics of cadherin formation was then investigated in these undifferentiated corneal mesenchyme cells. In non-contacting pre-confluent cells, N-cadherin was found in a perinuclear pattern and at the cell membrane in cells that made contact. This pattern of cadherin localisation has also been reported in pre-confluent rat embryonic myoblasts (Mary et al., 2002) and in MDCK cells (Le et al., 1999). In these studies, the perinuclear cadherin localisation was associated with the Golgi and thought to represent newly synthesised protein. In the present study, co-staining with the Golgi antibody confirmed that the N-cadherin distribution colocalised with the Golgi in non-contacting cells. However, N-cadherin failed to make a continuous ring at the cell surface even in cells that made contact. Instead, a small puncta of N-cadherin forming a serrate pericellular pattern were obtained, suggesting the formation of unstable junctions.

Other studies have shown that in epithelial cells *in vitro*, the formation of cadherin rings and the association with the actin cytoskeleton is a sign of the establishment of strong cell-cell adhesion (Adams et al., 1998). The results obtained from the present study suggest that *in vitro*, (a) in these corneal mesenchyme cells, stable junctions are unable to form during their normal lifespan in culture and (b) interaction between different cell types that occurs *in vivo* is required to form stable junctions with tight contacts. This might be due to the fact that the cells fail to receive appropriate signals to trigger the formation of an endothelial monolayer. The most obvious signalling required *in vivo*, is from the anterior lens epithelium. The exact molecules responsible for this induction have not been identified, but candidates include transforming growth factor β2 (*tgfβ2*) (Reneker et al., 2000). Results from the persent study have shown that *tgfβ2* is likely not part of a signalling cascade of molecules involved in early corneal endothelial differentiation. The expression of *tgfβ2* mRNA was not detected by *in situ* hybridisation at the time of corneal endothelial differentiation.

A model of N-cadherin trafficking proposed by Mary et al. (2002), suggests that the transport of N-cadherin through Golgi, endocytotic and secretory vesicles to the plasma membrane occurs along microtubulues and is driven by kinesin motor proteins. The model further

suggests that the transport and localisation of the protein is regulated by cell-cell contact and as soon as the protein is at the plasma membrane, it associates with the F-actin cytoskeleton, through binding with the catenins. Other studies (Adams et al., 1998) have shown that the localisation of cadherin in contacting cells begins as punctate aggregates at points of cell contact. Each of the vesicles is in contact with a bundle of actin filaments branching off under the cell membrane. As stable contacts are made, the actin cables along the areas of cell-cell contact disappear and result in the formation of circumferential actin bands at the cell membranes of contacting cells (for reviews see - (Vasioukhin and Fuchs, 2001). The important point from these results is that the during the formation of polarised epithelia, the actin filaments reorganise from a perpendicular to a lateral orientation parallel to the adjoining cell membranes. In order to investigate whether there were changes in actin dynamics on formation of cell-cell contacts in the present study, cells were stained for F-actin. Consistent with the failure to form proper junctions, the distribution of F-actin remained scattered as stress fibres only co-localising with N-cadherin at focal adhesion points.

As described earlier, investigations into the cell biology of corneal endothelial cells have been limited by the inability of these cells to proliferate for a longer period *in vitro*. The present study is the first to successfully culture presumptive corneal endothelial cells but, these cells grew only for a limited period in culture and thus the process of differentiation and changes in protein distribution could not be explored further. The maximum period in culture was 6-8 days before they start senescing. This is a general trend for corneal endothelial cells and in other systems, has been overcome by making use of oncogenes to immortalise cells and improve the lifespan of the cells in culture (Joo et al., 1994; Wilson et al., 1993). However, the use of such techniques in cultures of presumptive corneal cells may not be ideal for the study of the dynamics of cell junction formation for the following reasons. Firstly, immortalisation may result in continued cell proliferation, a process that is not necessarily ideal for junction formation. Secondly, studies on immortalised fibroblast cell lines have shown that the induction of mesenchymal-epithelial transformation by transfection with E-cadherin failed, probably due to upregulation of genes that promote epithelial-mesenchymal transformation (EMT) or due to negative regulation of E-cadherins (Vanderburg and Hay, 1996). It has been shown that the expression of viral oncogens such as *src, ras* and *mos* on MDCK cells promote the conversion into fibroblasts, presumably due to modulation of E-cadherin binding (Behrens et al., 1993). Our laboratory is making use of the conditional temperature sensitive SV40 large T antigen to immortalise corneal mesenchyme cells. The idea is to generate large numbers of cells at a permissive temperature and then transfer them to a non-permissive temperature for normal proliferation once sufficient numbers have been generated. This will be done for

normal and mutant cells. Cells will then be transfected with full length *Foxc1* plasmid in order to investigate the exact mechanisms of junction formation during corneal endothelial morphogenesis and the exact role of *Foxc1* during the process.

The differentiation of the corneal endothelium in *Foxc1* mutants is impaired

It has been shown that in the absence of a functional *Foxc1* gene, the corneal endothelium fails to form (Kidson et al., 1999). The mechanisms leading to, as well as the consequences of the failure to form an endothelium have not been described. The understanding of these mechanisms has implications for the study of human disorders that are related to human mutations in FOXC1. It has previously been shown that mutations in *Foxc1* result in dominantly inherited developmental dysgeneses of the mouse iridocorneal angle (Smith et al., 2000) similar to those reported in human patients with Axenfeld-Rieger Anomaly (ARA) (Shields, 1983). Some patients with ARA have mutations in FOXC1 (Mears et al., 1998; Nishimura et al., 1998).

To be able to understand the basis of the abnormality in *Foxc1*$^{-/-}$ corneal development, in the present study, a systematic analysis of corneal mesenchyme changes during corneal differentiation was performed. (Only a few stages were selected due to the small number of mutant embryos that could be obtained from these mice.) Identification of embryo was based on their phenotype, genotype and LacZ staining of embryonic tails. Mutant embryos were easily identifiable by the presence of hydrocephalus, seen as bulging out of the forebrain. From these embryos, the individual corneas were separated from the lens, the inner corneal surface exposed and individual corneas and their respective lens surfaces were examined at every stage. It had previously been shown that the migration of presumptive corneal mesenchyme cells into the space between the lens and the cornea occurs in *Foxc1* mutants (Kison et al., 1999), therefore the purpose of SEM examination was to investigate what happens to these cells after migration. The problem however, was that some of the cells remained attached to the lens surface. LacZ staining of whole eyes prior to separation of the cornea from the lens failed to provide an accurate measure of cells remaining adhering to the lens surface. The problem was further confounded by the fact that perilenticular blood cells on the lens surface are also LacZ positive as previously shown (Kidson et al., 1999). Staining of the inner corneal surface with an N-cadherin antibody, a marker of corneal endothelial cells revealed that the cells on the inner corneal surface cells were positive for N-cadherin. However, it could be argued that these cells are not prospective corneal mesenchyme cells but merely cells that happen to express N-cadherin. Further studies are thus needed to clarify this problem. Such

studies would require the staining of a reasonable number of embryos for LacZ and carry out histological sections of lenses before and after separation in order to provide a measure of the proportion of cells adherent to the anterior lens surface. In order to establish with certainty that indeed the corneal mesenchyme cells are *Foxc1* positive, these cells could be stained with both N-cadherin and Foxc1 antibodies. Colocalisation of these antibodies would thus confirm that these cells are indeed prospective corneal endothelial cells.

Examination of the anterior lens surface revealed that at early stages before the formation of the anterior chamber and separation of the lens from the cornea, more cells remained attached to the surface of the lens compared to wildtype littermates. The attachment of these cells to the anterior lens surface may be related to abnormal cell-cell adhesion, interrupted differentiation of mesenchymal cells or abnormal production of the extracellular matrix material. All these cellular processes have been proposed to be defective in *Foxc1* mutants (Smith et al., 2000). It has been shown that the extracellular matrix of the iridocorneal angle of *Foxc1* mutant mice is disorganised and has very little collagen and elastic tissue. In addition, the ECM in the other parts of the *Foxc1* mutants (sternocostal cartilages, sternum and kidneys) lacks collagen fibrils and proteoglycans, suggesting that *Foxc1* is involved in regulation of the synthesis and organisation of ECM (Smith et al., 2000). Abnormalities in ECM organisation might therefore alter cellular behaviour such that cell-matrix and cell-cell interactions and ECM composition are altered. Further experiments are required to determine whether *Foxc1* is directly or indirectly involved in ECM remodelling and synthesis. Such experiments would require the identification of genetic pathways acting upstream or downstream of *Foxc1*. These studies using microarray analyses are currently underway in our laboratory.

Previous studies have shown that at E13.5, the mutant corneal mesenchyme cells are less flattened and remain associated with the lens capsule and blood vessels (Kidson et al., 1999). SEM examination of the corneal surface in this study confirmed that cells do flatten and indeed are associated with blood vessels. The process of cell transformation begins at the same time as in normal embryos and is characterised by cell flattening and retraction of cell arms. However, the central-outward pattern of cell flattening in normal corneas was not observed in mutant corneas. In these corneas, the presumptive corneal endothelial cells appeared uniform with no differences between the central and the peripheral corneal surface. Striking differences between normal and mutant corneas were observed at E17.5, in which the mutant cells failed to form intercellular borders. By this time, the cells still appeared more fibroblast-like with bundles of collagen fibres. The process of transformation from stellate to squamous was thus incomplete. The failure to form an organised cell layer is not related to cell proliferation

changes because previous studies using BrdU labelling have shown that there were no differences in rates of cell proliferation between normal and mutant corneal mesenchyme (Kidson et al., 1999). A possible explanation is the failure of a signalling cascade interacting with presumptive corneal mesenchyme.

It has been shown that the murine corneal endothelium and stroma are derived from the same population of mesenchyme (Hay and Revel, 1969; Osumi-Yamashita et al., 1994; Trainor and Tam, 1995). After differentiation, the two different cell types show different morphological characteristics. The stromal cells remain stellate but soon organise and become arranged in a parallel manner with arrays of collagen fibers arranged between the cell layers. These cells are called stromal keratocytes and are responsible for the formation of a collagenous matrix. The proper arrangement of the stromal fibrils and the correct orientation of the collagen fibres are important for corneal curvature and clarity (Kaufman and Alm, 2003). The mechanisms that govern the formation of the stromal architecture are not clearly understood, but the proteoglycans in the stroma are thought to regulate collagen matrix assembly in addition to their role in maintaining the correct corneal hydration. The stroma is characterised by the expression of a stromal specific proteoglycan, *keratocan. Keratocan* is a keratan sulfate proteoglycan that plays an important role in matrix assembly. Human mutations of the KERA gene are associated with cornea plana that manifests decreases in vision acuity due to the flattened curvature of the cornea (Pellegata et al., 2000). In mice in which the *keratocan* gene has been deleted, the collagen fibres in the stroma are less organised and the fibril diameter increased (Liu et al., 2003). Although the expression pattern of keratocan in developing mouse corneas has been reported (Liu et al., 1998), in the present study, the pattern of *keratocan* expression during corneal development was investigated in order to compare with that of *Foxc1* mutants. In the normal embryo, *keratocan* is strongly expressed in the corneal stroma and becomes specific at E17.5, coinciding with the formation of distinct intercellular borders. In the mutant, the expression of keratocan mRNA was reduced in the cornea stroma, but extended into the corneal stroma. Although these results implicate *Foxc1* in the regulation of *keratocan* in the corneal stroma, they do not suggest that Foxc1 is directly upstream of a signalling cascade involving *keratocan.*

The next question this study addressed was whether the mutant corneal mesenchyme cells are capable of synthesising the adherens junction protein, N-cadherin. The expression of N-cadherin in the presumptive corneal endothelial mesenchyme was comparable to that of wildtype cells. N-cadherin was localised in intracellular vesicles during early stages of corneal morphogenesis. In contrast to wildtype cells, the protein failed to form a pericellular ring at

the points of cell-cell contact at later stages. Even at birth, N-cadherin protein forms a clear perinuclear ring in the cytoplasm of cells. These results suggest that the mutant cells are unable to make stable cell-cell contacts. They raise the possibility that *Foxc1* acts upstream of a cascade of molecules involved in the trafficking of cadherins from the cytoplasm to the cell membrane.

Previous studies have reported that the mutant corneal mesenchyme cells do not express the tight junction marker, ZO-1 (Kidson et al., 1999). A systematic analysis of ZO-1 protein performed in this study confirmed this. In order to explore the mechanism of cell flattening and junction formation in mutant cells further, presumptive corneal mesenchyme cells were cultured and the dynamics of junction formation examined. Even in cultured corneal mesenchyme cells continuous belts of cadherins at the cell surface failed to form. Actin was seen as stress fibres in the cytoplasm of cells, forming focal adhesion points at the cell periphery, in association with N-cadherin spots. The deduction from these experiments is that some signalling mechanism is required for the acquisition of cell polarity and thus, the expression of ZO-1. Such signalling mechanism is presumed to be an inductive interaction between the corneal mesenchyme cells and the lens epithelial cells during corneal morphogenesis *in vivo*. Studies in our laboratory are underway to investigate this mechanism by making use of immortalised corneal mesenchyme cells from wildtype and mutant embryos and subjecting these cells into various lens factors.

A model of murine corneal endothelium development in the normal and *Foxc1* mutant embryos is thus proposed

From the results of the present study, the following model of murine corneal development is proposed. In the mouse embryo, the undifferentiated corneal mesenchyme is a meshwork of irregularly arranged cells overlapping with their neighbours. At this stage, the cells are typical migrating cells with lamellopodia and filopodia. They express cadherin molecules in intracellular vesicles. The process of mesenchyme epithelial transformation begins as early as E12.5, soon after the mesenchyme cells occupy the corneal space. This occurs by cell flattening, retraction of cell arms and formation of intercellular borders, a process that begins as early as E12.5. Cell flattening occurs in a central-outwards direction and leads to sealing of intercellular gaps. Cell-cell contacts established during this process are paralleled by changes in the distribution pattern of cadherin molecules from a punctate vesicular pattern in the cytoplasm to vesicular perinuclear rings at E14.5. Eventually, as tight intercellular borders are formed and a visible honeycomb pattern is made, N-cadherin becomes detectable at the cell

surface and the cytoplasmic pool diminishes. The formation of cadherin junctions coincides with the appearance of dense peripheral bands of actin at the cell surface. This pattern suggests the establishment of stable cadherin junctions anchored to the cytoplasm by actin. The initiation of a polarised monolayer begins at E13.5 as the tight junction protein is detected at the plasma membrane of adjoining cells (Figure 4-1).

In the mutants, the process of cell flattening and cell shape change is initiated at E12.5. Cell-cell contacts are established but a monolayer of interconnected cells fails to form. The expression of cadherins begins as a punctate pattern in the cytoplasm of cells at stages E12.5. Consistent with the failure to form junctions, the cadherin protein is not redistributed to the plasma membrane, such that at postnatal day 0 (P0), the cadherin protein accumulates at the perinuclear region (Figure 4-2). From these results, it is proposed that the aberrant corneal development observed in *Foxc1* mutant mice is a result of incomplete mesenchyme-endothelial transformation.

The present study provided a description of corneal endothelial development in mice and contributes towards the understanding of the mechanisms responsible for defects in corneal endothelial development. The exact role of *Foxc1* still remains unclear and studies are needed to identify target genes that act either upstream or downstream of this gene in regulating corneal endothelial development. It is likely that *Foxc1* is involved in mesenchyme-epithelial transformation since there is a failure of mesenchyme transformation when the gene is non-functional, for example in the kidney (as described earlier) and during corneal endothelial development (this study).

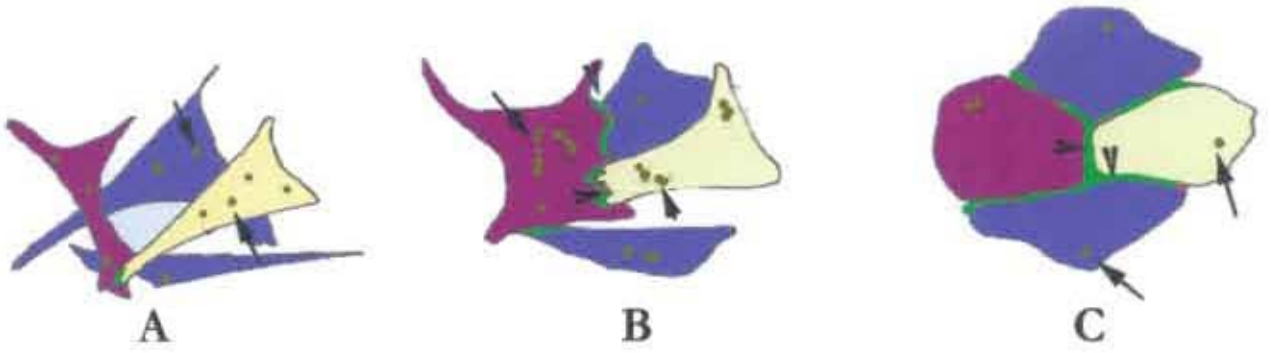

Figure 4-1. A proposed model of normal corneal endothelial morphogenesis and protein translocation to the cell membranes. As soon as the early migrating cells occupy the space between the lens and the corneal epithelium, they start to form a meshwork of irregularly arranged cells that overlap (E12.0 – E12.5). At this stage, N-cadherin protein forms a punctate distribution in the cytoplasm of cells (A, arrows). As the process of shuffling and lateral arm retraction begins, stable junctions begin to form and this is shown by the recruitment of cadherin protein to the cell junctions (E13.0-E14.5) (B, arrowheads), whilst new N-cadherin protein accumulates at the perinulcear region (B, arrows). Eventually a cobblestone monolayer in which all cells are interconnencted is formed (E17.5-adulthood). At this time, N-cadherin appears as intracellular vesicles near the cell membrane (C, arrows) and tight junctions have been established as marked by the presence of ZO-1 protein at the tight junction (C, arrowheads).

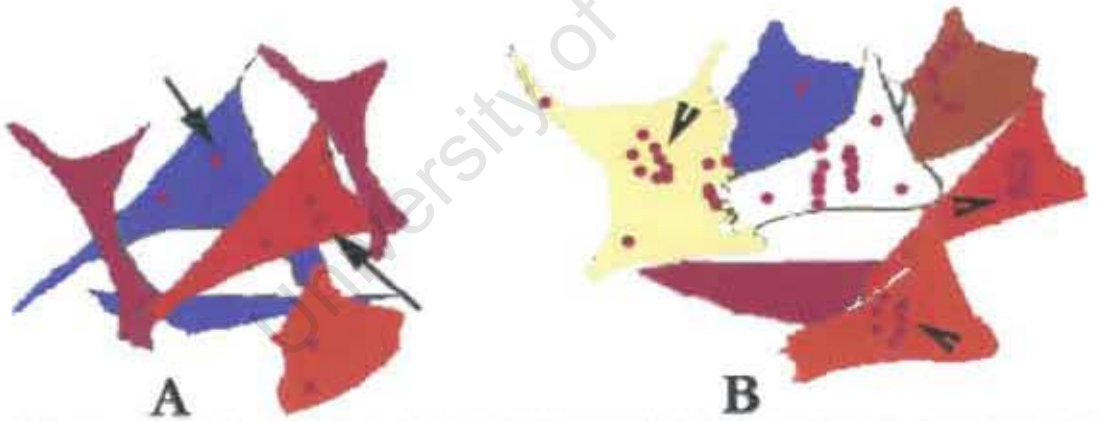

Figure 4-2. A proposed model of corneal endothelial morphogenesis and protein translocation to the cell membranes in *Foxc1* mutants. At E12.5, cells appear as an irregulary arranged meshwork expressing cadherin protein in a punctate pattern (A, arrows). Cells begin to flatten, but fail to completely seal the intercellular gaps. This is accompanied by the accumulation of cadherin protein in the perinuclear region (B, arrowheads) and failure to translocate the protein to the plasma membrane.

APPENDIX

Pilot experiments to monitor corneal endothelial development *in vivo*

At the start of these experiments, the intention was to culture whole corneas and monitor corneal endothelium development *in vitro*. It was envisioned that without intervention, the mutant cells would fail to form junctions as they do *in vivo*. One of the approaches was to culture whole or bisected mouse embryonic heads and ectopically transplant embryonic lenses in cranial mesenchyme outside the eye region. This approach would address two specific questions: (i) can corneal mesenchyme cells respond to signal from the lens by altering cell shape? (ii) Is the lens signal (s) sufficient on its own to induce mesenchyme transformation? The second approach was to co-culture cranial neural crest cells with embryonic lenses in hanging drops, an attempt to induce endothelial differentiation. A number of problems were encountered with all of these approaches.

Firstly, culture of whole eyes resulted in "thinning" of the cornea such that the development of the corneal endothelium could not be followed. Although development of organs progressed from the optic cup invagination stage to lens and corneal formation in cultured whole/bisected heads, the morphology of cells was abnormal and most cells were apoptotic (Fig. 5-1B and 5-1). In control eyes that were not cultured but processed for histological analysis at E12.5, the cornea was filled with presumptive corneal stroma and endothelial cells (Fig. 4-5-1A and 5-1C). The problem with whole eye cultures was confounded by the absence of corneal endothelial specific markers.

To explore the cranial neural crest-lens co-culture, it was necessary to establish the viability of embryonic lenses in hanging drop cultures over time. To begin to do this, lenses were assayed for proliferative capacity by using ^{3}H thymidine incorporation. Indeed lens cells were proliferative in culture and therefore presumed able to produce growth factors under these conditions. However, there was a problem in utilizing cranial neural crest cells due to absence of mouse neural crest specific markers. A suitable method was needed to investigate mesenchyme endothelium conversion and to investigate the dynamics of this process in both wildtype and mutant cells.

Adams, C. L., Chen, Y. T., Smith, S. J. and Nelson, W. J. (1998). Mechanisms of epithelial cell-cell adhesion and cell compaction revealed by high-resolution tracking of E-cadherin-green fluorescent protein. *J Cell Biol* **142**, 1105-19.

Akitaya, T. and Bronner-Fraser, M. (1992). Expression of cell adhesion molecules during initiation and cessation of neural crest cell migration. *Dev Dyn* **194**, 12-20.

Andrikopoulos, K., Liu, X., Keene, D. R., Jaenisch, R. and Ramirez, F. (1995). Targeted mutation in the col5a2 gene reveals a regulatory role for type V collagen during matrix assembly. *Nat Genet* **9**, 31-6.

Angres, B., Barth, A. and Nelson, W. J. (1996). Mechanism for transition from initial to stable cell-cell adhesion: kinetic analysis of E-cadherin-mediated adhesion using a quantitative adhesion assay. *J Cell Biol* **134**, 549-57.

Balda, M. S., Garrett, M. D. and Matter, K. (2003). The ZO-1-associated Y-box factor ZONAB regulates epithelial cell proliferation and cell density. *J Cell Biol* **160**, 423-32.

Balda, M. S. and Matter, K. (2000). Transmembrane proteins of tight junctions. *Semin Cell Dev Biol* **11**, 281-9.

Balda, M. S., Whitney, J. A., Flores, C., Gonzalez, S., Cereijido, M. and Matter, K. (1996). Functional dissociation of paracellular permeability and transepithelial electrical resistance and disruption of the apical-basolateral intramembrane diffusion barrier by expression of a mutant tight junction membrane protein. *J Cell Biol* **134**, 1031-49.

Baum, J. L., Niedra, R., Davis, C. and Yue, B. Y. (1979). Mass culture of human corneal endothelial cells. *Arch Ophthalmol* **97**, 1136-40.

Beebe, D. C. and Coats, J. M. (2000). The lens organizes the anterior segment: specification of neural crest cell differentiation in the avian eye. *Dev Biol* **220**, 424-31.

Behrens, J., Vakaet, L., Friis, R., Winterhager, E., Van Roy, F., Mareel, M. M. and Birchmeier, W. (1993). Loss of epithelial differentiation and gain of invasiveness correlates with tyrosine phosphorylation of the E-cadherin/beta-catenin complex in cells transformed with a temperature-sensitive v-SRC gene. *J Cell Biol* **120**, 757-66.

Bourne, W. M., Nelson, L. R. and Hodge, D. O. (1997). Central corneal endothelial cell changes over a ten-year period. *Invest Ophthalmol Vis Sci* **38**, 779-82.

Braga, V. (2000). Epithelial cell shape: cadherins and small GTPases. *Exp Cell Res* **261**, 83-90.

Canfield, P. E., Geerdes, A. M. and Molitoris, B. A. (1991). Effect of reversible ATP depletion on tight-junction integrity in LLC-PK1 cells. *Am J Physiol* **261**, F1038-45.

Cordenonsi, M., Mazzon, E., De Rigo, L., Baraldo, S., Meggio, F. and Citi, S. (1997). Occludin dephosphorylation in early development of Xenopus laevis. *J Cell Sci* **110 (Pt 24)**, 3131-9.

Crawford, K. M., Ernst, S. A., Meyer, R. F. and MacCallum, D. K. (1995). NaK-ATPase pump sites in cultured bovine corneal endothelium of varying cell density at confluence. *Invest Ophthalmol Vis Sci* **36**, 1317-26.

de Iongh, R. U., Lovicu, F. J., Overbeek, P. A., Schneider, M. D., Joya, J., Hardeman, E. D. and McAvoy, J. W. (2001). Requirement for TGFbeta receptor signaling during terminal lens fiber differentiation. *Development* **128**, 3995-4010.

Dunker, N. and Krieglstein, K. (2000). Targeted mutations of transforming growth factor-beta genes reveal important roles in mouse development and adult homeostasis. *Eur J Biochem* **267**, 6982-8.

Dunlevy, J. R., Beales, M. P., Berryhill, B. L., Cornuet, P. K. and Hassell, J. R. (2000). Expression of the keratan sulfate proteoglycans lumican, keratocan and osteoglycin/mimecan during chick corneal development. *Exp Eye Res* **70**, 349-62.

Engelmann, K., Drexler, D. and Bohnke, M. (1999). Transplantation of adult human or porcine corneal endothelial cells onto human recipients in vitro. Part I: Cell culturing and transplantation procedure. *Cornea* **18**, 199-206.

Farquhar, M. G. and Palade, G. E. (1963). Junctional complexes in various epithelia. *J Cell Biol* **17**, 375-412.

Ferreira-Cornwell, M. C., Veneziale, R. W., Grunwald, G. B. and Menko, A. S. (2000). N-cadherin function is required for differentiation-dependent cytoskeletal reorganization in lens cells in vitro. *Exp Cell Res* **256**, 237-47.

Fleming, T. P., Sheth, B. and Fesenko, I. (2001). Cell adhesion in the preimplantation mammalian embryo and its role in trophectoderm differentiation and blastocyst morphogenesis. *Front Biosci* **6**, D1000-7.

Fujimoto, K. (1995). Freeze-fracture replica electron microscopy combined with SDS digestion for cytochemical labeling of integral membrane proteins. Application to the immunogold labeling of intercellular junctional complexes. *J Cell Sci* **108 (Pt 11)**, 3443-9.

Furuse, M., Sasaki, H., Fujimoto, K. and Tsukita, S. (1998). A single gene product, claudin-1 or -2, reconstitutes tight junction strands and recruits occludin in fibroblasts. *J Cell Biol* **143**, 391-401.

Genis-Galvez, J. M. (1966). Role of the lens in the morphogenesis of the iris and cornea. *Nature* **210**, 209-10.

Gordon-Thomson, C., de Iongh, R. U., Hales, A. M., Chamberlain, C. G. and McAvoy, J. W. (1998). Differential cataractogenic potency of TGF-beta1, -beta2, and -beta3 and their expression in the postnatal rat eye. *Invest Ophthalmol Vis Sci* **39**, 1399-409.

Gottardi, C. J., Arpin, M., Fanning, A. S. and Louvard, D. (1996). The junction-associated protein, zonula occludens-1, localizes to the nucleus before the maturation and during the remodeling of cell-cell contacts. *Proc Natl Acad Sci U S A* **93**, 10779-84.

Green, M. C. (1970). The developmental effects of congenital hydrocephalus (ch) in the mouse. *Dev Biol* **23**, 585-608.

Hay, E. D. and Revel, J. P. (1969). Fine structure of the developing avian cornea. *Monogr Dev Biol* **1**, 1-144.

Hiemisch, H., Schutz, G. and Kaestner, K. H. (1998). The mouse Fkh1/Mf1 gene: cDNA sequence, chromosomal localization and expression in adult tissues. *Gene* **220**, 77-82.

Howarth, A. G., Hughes, M. R. and Stevenson, B. R. (1992). Detection of the tight junction-associated protein ZO-1 in astrocytes and other nonepithelial cell types. *Am J Physiol* **262**, C461-9.

Itoh, M., Yonemura, S., Nagafuchi, A. and Tsukita, S. (1991). A 220-kD undercoat-constitutive protein: its specific localization at cadherin-based cell-cell adhesion sites. *J Cell Biol* **115**, 1449-62.

Jesaitis, L. A. and Goodenough, D. A. (1994). Molecular characterization and tissue distribution of ZO-2, a tight junction protein homologous to ZO-1 and the Drosophila discs-large tumor suppressor protein. *J Cell Biol* **124**, 949-61.

Johnston, M. C., Noden, D. M., Hazelton, R. D., Coulombre, J. L. and Coulombre, A. J. (1979). Origins of avian ocular and periocular tissues. *Exp Eye Res* **29**, 27-43.

Joo, C. K., Pepose, J. S. and Fleming, T. P. (1994). In vitro propagation of primary and extended life span murine corneal endothelial cells. *Invest Ophthalmol Vis Sci* **35**, 3952-7.

Joyce, N. C. (2003). Proliferative capacity of the corneal endothelium. *Prog Retin Eye Res* **22**, 359-89.

Joyce, N. C., Harris, D. L. and Mello, D. M. (2002). Mechanisms of mitotic inhibition in corneal endothelium: contact inhibition and TGF-beta2. *Invest Ophthalmol Vis Sci* **43**, 2152-9.

Joyce, N. C., Harris, D. L. and Zieske, J. D. (1998). Mitotic inhibition of corneal endothelium in neonatal rats. *Invest Ophthalmol Vis Sci* **39**, 2572-83.

Joyce, N. C., Meklir, B., Joyce, S. J. and Zieske, J. D. (1996). Cell cycle protein expression and proliferative status in human corneal cells. *Invest Ophthalmol Vis Sci* **37**, 645-55.

Joyce, N. C. and Zieske, J. D. (1997). Transforming growth factor-beta receptor expression in human cornea. *Invest Ophthalmol Vis Sci* **38**, 1922-8.

Kanwar, Y. S., Wada, J., Lin, S., Danesh, F. R., Chugh, S. S., Yang, Q., Banerjee, T. and Lomasney, J. W. (2004). Update of extracellular matrix, its receptors, and cell adhesion molecules in mammalian nephrogenesis. *Am J Physiol Renal Physiol* **286**, F202-15.

Kaufman, P. L. and Alm, A. (2003). Adler's Physiology of the eye. Missouri, USA: Mosby.

Kidson, S. H., Kume, T., Deng, K., Winfrey, V. and Hogan, B. L. (1999). The forkhead/winged-helix gene, Mf1, is necessary for the normal development of the cornea and formation of the anterior chamber in the mouse eye. *Dev Biol* **211**, 306-22.

Kitamura, K., Miura, H., Miyagawa-Tomita, S., Yanazawa, M., Katoh-Fukui, Y., Suzuki, R., Ohuchi, H., Suehiro, A., Motegi, Y., Nakahara, Y. et al. (1999). Mouse Pitx2 deficiency leads to anomalies of the ventral body wall, heart, extra- and periocular mesoderm and right pulmonary isomerism. *Development* **126**, 5749-58.

Kottra, G. and Fromter, E. (1983). Functional properties of the paracellular pathway in some leaky epithelia. *J Exp Biol* **106**, 217-29.

Kume, T., Deng, K. and Hogan, B. L. (2000). Murine forkhead/winged helix genes Foxc1 (Mf1) and Foxc2 (Mfh1) are required for the early organogenesis of the kidney and urinary tract. *Development* **127**, 1387-95.

Kume, T., Deng, K. Y., Winfrey, V., Gould, D. B., Walter, M. A. and Hogan, B. L. (1998). The forkhead/winged helix gene Mf1 is disrupted in the pleiotropic mouse mutation congenital hydrocephalus. *Cell* **93**, 985-96.

Le, T. L., Yap, A. S. and Stow, J. L. (1999). Recycling of E-cadherin: a potential mechanism for regulating cadherin dynamics. *J Cell Biol* **146**, 219-32.

Leibowitz, H. M. and Waring III, G. O. (1998). Corneal Disorders: Clinical diagnosis and management. Pennslyvania, USA: W.B. Saunders Company.

Lines, M. A., Kozlowski, K. and Walter, M. A. (2002). Molecular genetics of Axenfeld-Rieger malformations. *Hum Mol Genet* **11**, 1177-84.

Linsenmayer, T. F., Fitch, J. M., Gordon, M. K., Cai, C. X., Igoe, F., Marchant, J. K. and Birk, D. E. (1998). Development and roles of collagenous matrices in the embryonic avian cornea. *Prog Retin Eye Res* **17**, 231-65.

Liu, C. Y., Birk, D. E., Hassell, J. R., Kane, B. and Kao, W. W. (2003). Keratocan-deficient mice display alterations in corneal structure. *J Biol Chem* **278**, 21672-7.

Liu, C. Y., Shiraishi, A., Kao, C. W., Converse, R. L., Funderburgh, J. L., Corpuz, L. M., Conrad, G. W. and Kao, W. W. (1998). The cloning of mouse keratocan cDNA and genomic DNA and the characterization of its expression during eye development. *J Biol Chem* **273**, 22584-8.

Marchant, J. K., Hahn, R. A., Linsenmayer, T. F. and Birk, D. E. (1996). Reduction of type V collagen using a dominant-negative strategy alters the regulation of fibrillogenesis and results in the loss of corneal-specific fibril morphology. *J Cell Biol* **135**, 1415-26.

Martin-Padura, I., Lostaglio, S., Schneemann, M., Williams, L., Romano, M., Fruscella, P., Panzeri, C., Stoppacciaro, A., Ruco, L., Villa, A. et al. (1998). Junctional

adhesion molecule, a novel member of the immunoglobulin superfamily that distributes at intercellular junctions and modulates monocyte transmigration. *J Cell Biol* **142**, 117-27.

Mary, S., Charrasse, S., Meriane, M., Comunale, F., Travo, P., Blangy, A. and Gauthier-Rouviere, C. (2002). Biogenesis of N-cadherin-dependent cell-cell contacts in living fibroblasts is a microtubule-dependent kinesin-driven mechanism. *Mol Biol Cell* **13**, 285-301.

Matter, K. and Balda, M. S. (2003). Signalling to and from tight junctions. *Nat Rev Mol Cell Biol* **4**, 225-36.

McNeill, H., Ryan, T. A., Smith, S. J. and Nelson, W. J. (1993). Spatial and temporal dissection of immediate and early events following cadherin-mediated epithelial cell adhesion. *J Cell Biol* **120**, 1217-26.

Mears, A. J., Jordan, T., Mirzayans, F., Dubois, S., Kume, T., Parlee, M., Ritch, R., Koop, B., Kuo, W. L., Collins, C. et al. (1998). Mutations of the forkhead/winged-helix gene, FKHL7, in patients with Axenfeld-Rieger anomaly. *Am J Hum Genet* **63**, 1316-28.

Monier-Gavelle, F. and Duband, J. L. (1995). Control of N-cadherin-mediated intercellular adhesion in migrating neural crest cells in vitro. *J Cell Sci* **108 (Pt 12)**, 3839-53.

Morita, K., Furuse, M., Fujimoto, K. and Tsukita, S. (1999). Claudin multigene family encoding four-transmembrane domain protein components of tight junction strands. *Proc Natl Acad Sci U S A* **96**, 511-6.

Morrison-Graham, K., Schatteman, G. C., Bork, T., Bowen-Pope, D. F. and Weston, J. A. (1992). A PDGF receptor mutation in the mouse (Patch) perturbs the development of a non-neuronal subset of neural crest-derived cells. *Development* **115**, 133-42.

Murphy, C., Alvarado, J., Juster, R. and Maglio, M. (1984). Prenatal and postnatal cellularity of the human corneal endothelium. A quantitative histologic study. *Invest Ophthalmol Vis Sci* **25**, 312-22.

Nayak, S. K. and Binder, P. S. (1984). The growth of endothelium from human corneal rims in tissue culture. *Invest Ophthalmol Vis Sci* **25**, 1213-6.

Nelson, G. A. and Revel, J. P. (1975). Scanning electron microscopic study of cell movements in the corneal endothelium of the avian embryo. *Dev Biol* **42**, 315-33.

Nishimura, D. Y., Swiderski, R. E., Alward, W. L., Searby, C. C., Patil, S. R., Bennet, S. R., Kanis, A. B., Gastier, J. M., Stone, E. M. and Sheffield, V. C. (1998). The forkhead transcription factor gene FKHL7 is responsible for glaucoma phenotypes which map to 6p25. *Nat Genet* **19**, 140-7.

Noden, D. M. (1975). An analysis of migratory behavior of avian cephalic neural crest cells. *Dev Biol* **42**, 106-30.

Noske, W., Stamm, C. C. and Hirsch, M. (1994). Tight junctions of the human ciliary epithelium: regional morphology and implications on transepithelial resistance. *Exp Eye Res* **59**, 141-9.

Osumi-Yamashita, N., Ninomiya, Y., Doi, H. and Eto, K. (1994). The contribution of both forebrain and midbrain crest cells to the mesenchyme in the frontonasal mass of mouse embryos. *Dev Biol* **164**, 409-19.

Padgett, R. W. (1999). Intracellular signaling: Fleshing out the TGFbeta pathway. *Curr Biol* **9**, R408-11.

Pei, Y. F. and Rhodin, J. A. (1970). The prenatal development of the mouse eye. *Anat Rec* **168**, 105-25.

Pellegata, N. S., Dieguez-Lucena, J. L., Joensuu, T., Lau, S., Montgomery, K. T., Krahe, R., Kivela, T., Kucherlapati, R., Forsius, H. and de la Chapelle, A. (2000). Mutations in KERA, encoding keratocan, cause cornea plana. *Nat Genet* **25**, 91-5.

Pollard, T. D. and Earnshaw, W. C. (2002). Cell Biology. Pennslyvania, USA: Saunders.

Pressman, C. L., Chen, H. and Johnson, R. L. (2000). LMX1B, a LIM homeodomain class transcription factor, is necessary for normal development of multiple tissues in the anterior segment of the murine eye. *Genesis* **26**, 15-25.

Radice, G. L., Ferreira-Cornwell, M. C., Robinson, S. D., Rayburn, H., Chodosh, L. A., Takeichi, M. and Hynes, R. O. (1997a). Precocious mammary gland development in P-cadherin-deficient mice. *J Cell Biol* **139**, 1025-32.

Radice, G. L., Rayburn, H., Matsunami, H., Knudsen, K. A., Takeichi, M. and Hynes, R. O. (1997b). Developmental defects in mouse embryos lacking N-cadherin. *Dev Biol* **181**, 64-78.

Rajasekaran, A. K., Hojo, M., Huima, T. and Rodriguez-Boulan, E. (1996). Catenins and zonula occludens-1 form a complex during early stages in the assembly of tight junctions. *J Cell Biol* **132**, 451-63.

Reneker, L. W. and Overbeek, P. A. (1996). Lens-specific expression of PDGF-A alters lens growth and development. *Dev Biol* **180**, 554-65.

Reneker, L. W., Silversides, D. W., Xu, L. and Overbeek, P. A. (2000). Formation of corneal endothelium is essential for anterior segment development - a transgenic mouse model of anterior segment dysgenesis. *Development* **127**, 533-42.

Rice, R., Rice, D. P., Olsen, B. R. and Thesleff, I. (2003). Progression of calvarial bone development requires Foxc1 regulation of Msx2 and Alx4. *Dev Biol* **262**, 75-87.

Riethmacher, D., Brinkmann, V. and Birchmeier, C. (1995). A targeted mutation in the mouse E-cadherin gene results in defective preimplantation development. *Proc Natl Acad Sci U S A* **92**, 855-9.

Ryeom, S. W., Paul, D. and Goodenough, D. A. (2000). Truncation mutants of the tight junction protein ZO-1 disrupt corneal epithelial cell morphology. *Mol Biol Cell* **11**, 1687-96.

Saika, S., Liu, C. Y., Azhar, M., Sanford, L. P., Doetschman, T., Gendron, R. L., Kao, C. W. and Kao, W. W. (2001). TGFbeta2 in corneal morphogenesis during mouse embryonic development. *Dev Biol* **240**, 419-32.

Saitou, M., Fujimoto, K., Doi, Y., Itoh, M., Fujimoto, T., Furuse, M., Takano, H., Noda, T. and Tsukita, S. (1998). Occludin-deficient embryonic stem cells can differentiate into polarized epithelial cells bearing tight junctions. *J Cell Biol* **141**, 397-408.

Sakakibara, A., Furuse, M., Saitou, M., Ando-Akatsuka, Y. and Tsukita, S. (1997). Possible involvement of phosphorylation of occludin in tight junction formation. *J Cell Biol* **137**, 1393-401.

Sanford, L. P., Ormsby, I., Gittenberger-de Groot, A. C., Sariola, H., Friedman, R., Boivin, G. P., Cardell, E. L. and Doetschman, T. (1997). TGFbeta2 knockout mice have multiple developmental defects that are non-overlapping with other TGFbeta knockout phenotypes. *Development* **124**, 2659-70.

Sarfarazi, M. (1997). Recent advances in molecular genetics of glaucomas. *Hum Mol Genet* **6**, 1667-77.

Sasaki, H. and Hogan, B. L. (1993). Differential expression of multiple fork head related genes during gastrulation and axial pattern formation in the mouse embryo. *Development* **118**, 47-59.

Schatteman, G. C., Morrison-Graham, K., van Koppen, A., Weston, J. A. and Bowen-Pope, D. F. (1992). Regulation and role of PDGF receptor alpha-subunit expression during embryogenesis. *Development* **115**, 123-31.

Semina, E. V., Reiter, R., Leysens, N. J., Alward, W. L., Small, K. W., Datson, N. A., Siegel-Bartelt, J., Bierke-Nelson, D., Bitoun, P., Zabel, B. U. et al. (1996). Cloning and characterization of a novel bicoid-related homeobox transcription factor gene, RIEG, involved in Rieger syndrome. *Nat Genet* **14**, 392-9.

Shields, M. B. (1983). Axenfeld-Rieger syndrome: a theory of mechanism and distinctions from the iridocorneal endothelial syndrome. *Trans Am Ophthalmol Soc* **81**, 736-84.

Smith, R. S., Zabaleta, A., Kume, T., Savinova, O. V., Kidson, S. H., Martin, J. E., Nishimura, D. Y., Alward, W. L., Hogan, B. L. and John, S. W. (2000). Haploinsufficiency of the transcription factors FOXC1 and FOXC2 results in aberrant ocular development. *Hum Mol Genet* **9**, 1021-32.

Srinivasan, Y., Lovicu, F. J. and Overbeek, P. A. (1998). Lens-specific expression of transforming growth factor beta1 in transgenic mice causes anterior subcapsular cataracts. *J Clin Invest* **101**, 625-34.

Stevenson, B. R., Siliciano, J. D., Mooseker, M. S. and Goodenough, D. A. (1986). Identification of ZO-1: a high molecular weight polypeptide associated with the tight junction (zonula occludens) in a variety of epithelia. *J Cell Biol* **103**, 755-66.

Stern P.D. and Holland P.W.H. (1993). In situ Hybridization. Oxford University Press. New York.

Stuart, R. O., Sun, A., Bush, K. T. and Nigam, S. K. (1996). Dependence of epithelial intercellular junction biogenesis on thapsigargin-sensitive intracellular calcium stores. *J Biol Chem* **271**, 13636-41.

Topczewska, J. M., Topczewski, J., Shostak, A., Kume, T., Solnica-Krezel, L. and Hogan, B. L. (2001). The winged helix transcription factor Foxc1a is essential for somitogenesis in zebrafish. *Genes Dev* **15**, 2483-93.

Trainor, P. A. and Tam, P. P. (1995). Cranial paraxial mesoderm and neural crest cells of the mouse embryo: co-distribution in the craniofacial mesenchyme but distinct segregation in branchial arches. *Development* **121**, 2569-82.

Tuft, S. J. and Coster, D. J. (1990). The corneal endothelium. *Eye* **4 (Pt 3)**, 389-424.

Vanderburg, C. R. and Hay, E. D. (1996). E-cadherin transforms embryonic corneal fibroblasts to stratified epithelium with desmosomes. *Acta Anat (Basel)* **157**, 87-104.

Vasioukhin, V. and Fuchs, E. (2001). Actin dynamics and cell-cell adhesion in epithelia. *Curr Opin Cell Biol* **13**, 76-84.

Walter, M. A., Mirzayans, F., Mears, A. J., Hickey, K. and Pearce, W. G. (1996). Autosomal-dominant iridogoniodysgenesis and Axenfeld-Rieger syndrome are genetically distinct. *Ophthalmology* **103**, 1907-15.

Wilson, S. E., Lloyd, S. A., He, Y. G. and McCash, C. S. (1993). Extended life of human corneal endothelial cells transfected with the SV40 large T antigen. *Invest Ophthalmol Vis Sci* **34**, 2112-23.

Winnier, G. E., Kume, T., Deng, K., Rogers, R., Bundy, J., Raines, C., Walter, M. A., Hogan, B. L. and Conway, S. J. (1999). Roles for the winged helix transcription factors MF1 and MFH1 in cardiovascular development revealed by nonallelic noncomplementation of null alleles. *Dev Biol* **213**, 418-31.

Wulle, K. G. and Lerche, W. (1969). Electron microscopic observations of the early development of the human corneal endothelium and Descemet's membrane. *Ophthalmologica* **157**, 451-61.

Yap, A. S., Brieher, W. M. and Gumbiner, B. M. (1997). Molecular and functional analysis of cadherin-based adherens junctions. *Annu Rev Cell Dev Biol* **13**, 119-46.

Yap, A. S., Niessen, C. M. and Gumbiner, B. M. (1998). The juxtamembrane region of the cadherin cytoplasmic tail supports lateral clustering, adhesive strengthening, and interaction with p120ctn. *J Cell Biol* **141**, 779-89.

Yue, B. Y., Sugar, J., Gilboy, J. E. and Elvart, J. L. (1989). Growth of human corneal endothelial cells in culture. *Invest Ophthalmol Vis Sci* **30**, 248-53.